Calhoun: The NPS Institutional Archive

DSpace Repository

Theses and Dissertations | 1. Thesis and Dissertation Collection, all items

1997-12

Comparative analysis of selected radiation effects in Medium Earth Orbits

Bolin, Jennifer A.

Monterey, California. Naval Postgraduate School

https://hdl.handle.net/10945/8105

This publication is a work of the U.S. Government as defined in Title 17, United States Code, Section 101. Copyright protection is not available for this work in the United States.

Downloaded from NPS Archive: Calhoun

http://www.nps.edu/library

Calhoun is the Naval Postgraduate School's public access digital repository for research materials and institutional publications created by the NPS community. Calhoun is named for Professor of Mathematics Guy K. Calhoun, NPS's first appointed -- and published -- scholarly author.

Dudley Knox Library / Naval Postgraduate School
411 Dyer Road / 1 University Circle
Monterey, California USA 93943

NPS ARCHIVE
1997.12
BOLIN, J.

NAVAL POSTGRADUATE SCHOOL
MONTEREY, CALIFORNIA

THESIS

COMPARATIVE ANALYSIS OF SELECTED RADIATION EFFECTS IN MEDIUM EARTH ORBITS

by

Jennifer A. Bolin

December 1997

Thesis Advisor: Vicente Garcia
Co-Advisor: Brij Agrawal

Approved for public release; distribution is unlimited.

Thesis
B6525

DUDLEY KNOX LIBRARY
NAVAL POSTGRADUATE SCHOOL
MONTEREY CA 93943-5101

REPORT DOCUMENTATION PAGE

Form Approved OMB No. 0704-0188

Public reporting burden for this collection of information is estimated to average 1 hour per response, including the time for reviewing instruction, searching existing data sources, gathering and maintaining the data needed, and completing and reviewing the collection of information. Send comments regarding this burden estimate or any other aspect of this collection of information, including suggestions for reducing this burden, to Washington Headquarters Services, Directorate for Information Operations and Reports, 1215 Jefferson Davis Highway, Suite 1204, Arlington, VA 22202-4302, and to the Office of Management and Budget, Paperwork Reduction Project (0704-0188) Washington DC 20503.

1. AGENCY USE ONLY *(Leave blank)*	2. REPORT DATE	3. REPORT TYPE AND DATES COVERED
	December 1997	Master's Thesis

4. TITLE AND SUBTITLE
COMPARATIVE ANALYSIS OF SELECTED RADIATION EFFECTS IN MEDIUM EARTH ORBITS

5. FUNDING NUMBERS

6. AUTHOR(S) Jennifer A. Bolin

7. PERFORMING ORGANIZATION NAME(S) AND ADDRESS(ES)
Naval Postgraduate School
Monterey CA 93943-5000

8. PERFORMING ORGANIZATION REPORT NUMBER

9. SPONSORING/MONITORING AGENCY NAME(S) AND ADDRESS(ES)

10. SPONSORING/MONITORING AGENCY REPORT NUMBER

11. SUPPLEMENTARY NOTES The views expressed in this thesis are those of the author and do not reflect the official policy or position of the Department of Defense or the U.S. Government.

12a. DISTRIBUTION/AVAILABILITY STATEMENT
Approved for public release; distribution is unlimited.

12b. DISTRIBUTION CODE

13. ABSTRACT *(maximum 200 words)*

Satellite design is well developed for the common Low Earth Orbit (LEO) and Geosynchronous Orbit (GEO) and Highly Elliptical Orbits (HEO), i.e.,Molniya, cases; Medium Earth Orbit (MEO) satellite design is a relatively new venture. MEO is roughly defined as being altitudes above LEO and below GEO. A primary concern, and a major reason for the delay in exploiting the MEO altitudes, has been the expected radiation environment and corresponding satellite degradation anticipated to occur at MEO altitudes. The presence of the Van Allen belts, a major source of radiation, along with the suitability of GEO and LEO orbits, has conventionally discouraged satellite placement in MEO. As conventional Earth orbits become increasingly crowded, MEO will become further populated.

This thesis investigates the major sources of radiation (geomagnetically trapped particles, solar particle events and galactic cosmic radiation) with respect to specific Naval Research Laboratory (NRL) designated MEO (altitudes between 3,000 nautical miles (nmi) and 9,000 nmi; inclination angle of 15 degrees). The contribution of each of these components to the total radiation experienced in MEO and the effects of the expected radiation on a representative spacecraft are analyzed in comparison to a baseline LEO orbit of 400 nmi and 70 degrees inclination. Dose depth curves are calculated for several configurations, and show that weight gains from necessary expected shielding are not extreme. The radiation effects considered include proton displacement dose and solar cell degradation.

14. SUBJECT TERMS Radiation, Medium Earth Orbit (MEO)	15. NUMBER OF PAGES 154
	16. PRICE CODE

17. SECURITY CLASSIFICATION OF REPORT	18. SECURITY CLASSIFICATION OF THIS PAGE	19. SECURITY CLASSIFICATION OF ABSTRACT	20. LIMITATION OF ABSTRACT
Unclassified	Unclassified	Unclassified	UL

NSN 7540-01-280-5500

Standard Form 298 (Rev. 2-89)
Prescribed by ANSI Std. 239-18 298-102

Approved for public release; distribution is unlimited.

COMPARATIVE ANALYSIS OF SELECTED RADIATION EFFECTS IN MEDIUM EARTH ORBITS

Jennifer A. Bolin
Lieutenant, United States Navy
B.S., United States Naval Academy, 1992

Submitted in partial fulfillment
of the requirements for the degree of

MASTER OF SCIENCE IN ASTRONAUTICAL ENGINEERING

from the

NAVAL POSTGRADUATE SCHOOL
December 1997

NPS Archive
1997.12
Bolin, J.

DUDLEY KNOX LIBRARY
NAVAL POSTGRADUATE SCHOOL
MONTEREY CA 93943-5101

ABSTRACT

Satellite design is well developed for the common Low Earth Orbit (LEO), Geosynchronous Orbit (GEO) and Highly Elliptical Orbits (HEO), i.e., Molniya, cases; Medium Earth Orbit (MEO) satellite design is a relatively new venture. MEO is roughly defined as being altitudes above LEO and below GEO. A primary concern, and a major reason for the delay in exploiting the MEO altitudes, has been the expected radiation environment and corresponding satellite degradation anticipated to occur at MEO altitudes. The presence of the Van Allen belts, a major source of radiation, along with the suitability of GEO and LEO orbits, has conventionally discouraged satellite placement in MEO. As conventional Earth orbits become increasingly crowded, MEO will become further populated.

This thesis investigates the major sources of radiation (geomagnetically trapped particles, solar particle events and galactic cosmic radiation) with respect to specific Naval Research Laboratory (NRL) designated MEO (altitudes between 3,000 nautical miles (nmi) and 9,000 nmi; inclination angle of 15 degrees). The contribution of each of these components to the total radiation experienced in MEO and the effects of the expected radiation on a representative spacecraft are analyzed in comparison to a baseline LEO orbit of 400 nmi and 70 degrees inclination. Dose depth curves are calculated for several configurations, and show that weight gains from necessary expected shielding are not extreme. The radiation effects considered include proton displacement dose and solar cell degradation.

TABLE OF CONTENTS

I. INTRODUCTION 1

A. THE SPACE RADIATION ENVIRONMENT 1

1. Geomagnetic Coordinates 2

B. THE EARTH RADIATION ZONE 2

C. THE AURORAL ZONE 2

D. THE INTERPLANETARY ZONE 3

E. RADIATION TYPES 3

1. Alpha Particle (α) 3
2. Beta Particle (β) 4
3. Electromagnetic Radiation 4
4. Photon 4
5. Bremsstrahlung 4
6. Cosmic Rays 4
7. Electron (e) 4
8. Gamma Rays (γ) 5
9. Proton (p) 5
10. X-Ray 5

F. OVERVIEW OF CHAPTER CONTENTS 5

1. Chapter II 5
2. Chapter III 6
3. Chapter IV 6
4. Chapter V 6
5. Chapter VI 6
6. Chapter VII 6
7. Chapter VIII 7

II. GEOMAGNETICALLY TRAPPED RADIATION 9

A. GENERAL COMPOSITION 9

B. TRAPPED PROTONS 13

C. Trapped Electrons 15
D. Orbital Integration 17
E. Summary 18

III. ADDITIONAL RADIATION SOURCES 19
A. Galactic Cosmic-Ray Radiation 19
B. Solar Flare Radiation 20
C. Summary 27

IV. SPACE RADIATION MODELING SOFTWARE 29
A. Introduction 29
B. Foundation Models 30
C. Space Radiation Additions to the Models 32
D. Space Radiation File Types 32
1. Orbital Trajectory 33
2. Geomagnetic Shielding 33
3. Spacecraft Shielding 34
4. Trapped Proton 34
5. Trapped Electron 35
6. Solar Proton 35
7. Energy Spectrum 36
8. LET Spectrum 36
9. Dose-Depth 37
E. Radiation Assessment Using Space Radiation 37
1. Specify Spacecraft Position or Trajectory 38
2. Define the Spacecraft Shielding 38
3. Calculate the Shielding Provided by Earth's Magnetic Field ... 38
4. Determine the Radiation Environment 39
5. Transport Radiation Components Through Shielding 40

6. Compute the LET Spectrum 41
7. Calculate Radiation Effects of Interest 41
D. Summary 42

V. PROTON DISPLACEMENT EFFECT 43

A. Introduction 43
B. Results 44
1. Galactic Cosmic Radiation 44
2. Geomagnetically Trapped Radiation 46
3. Solar Proton Radiation 48
4. Solar Energetic Particle Radiation 50
5. Composite (All Source) Radiation 52
C. Summary 53

VI. SOLAR CELL EFFECTS 55

A. Introduction 55
1. Effects on Solar Cells 56
2. Effects on Solar Cell Covers 58
3. Other Solar Cell Array Materials 58
4. Particulate and Ultraviolet Radiation Combined 59
B. Solar Cell Damage 59
1. Damage Equivalent 1-MeV Fluence 60
2. Electron Damage 61
3. Proton Damage 61
a. Low Energy Proton Damage 61
C. Radiation Damage Annealing 63
D. Photon Effects 63
E. Analysis of Damage Equivalent Radiation Dose to Solar Cells 65
F. Summary 73

VII. RADIATION DOSE 75

A. DOSE DEPTH CURVES 75

B. RESULTS 76

1. Baseline Orbit 76

2. Medium Earth Orbits 78

C. SUMMARY 85

VIII. SUMMARY AND CONCLUSIONS 87

LIST OF TERMS 89

LIST OF REFERENCES 95

APPENDIX A. ORBITAL GRAPHS 101

APPENDIX B. GRAPHICAL RESULTS FOR BASELINE ORBIT 105

APPENDIX C. DATA RESULTS 115

INITIAL DISTRIBUTION LIST 141

LIST OF FIGURES

Figure 2. 1 Motion of Charged Particles 10
Figure 2. 2 Regions of the Magnetosphere 11
Figure 2. 3 Charged Particle Distribution in the Magnetosphere 13
Figure 3. 1 Movement of Solar Flares 21
Figure 5. 1 Comparison of Galactic Cosmic Source Proton Displacement Doses at MEO Altitudes to Same Effect at Baseline Orbit 46
Figure 5. 2 Proton Displacement Dose from Galactic Cosmic Radiation at Various MEO Altitudes and Baseline Orbit 46
Figure 5. 3 Comparison of Trapped Proton Source Proton Displacement Doses at MEO Altitudes to Same Effect at Baseline Orbit 47
Figure 5. 4 Proton Displacement Dose from Trapped Protons at Various MEO Altitudes and Baseline Orbit 48
Figure 5. 5 Comparison of Solar Proton Source Proton Displacement Doses at MEO Altitudes to Same Effect at Baseline Orbit 49
Figure 5. 6 Proton Displacement Dose from Solar Protons at Various MEO Altitudes and Baseline Orbit 49
Figure 5. 7 Comparison of Solar Energetic Particle Source Proton Displacement Doses at MEO Altitudes to Same Effect at Baseline Orbit 51
Figure 5. 8 Proton Displacement Dose from Solar Energetic Particles at Various MEO Altitudes and Baseline Orbit 51
Figure 5. 9 Comparison of All Source Proton Displacement Doses at MEO Altitudes to Same Effect at Baseline Orbit 53
Figure 5. 10 Total Proton Displacement Dose (from All Sources) at Various MEO Altitudes and Baseline Orbit 53
Figure 6. 1 Damage to GaAs Solar Cells from Trapped Protons : No Coverglass 66
Figure 6. 2 Damage to Silicon Solar Cells from Trapped Protons: No Coverglass 67
Figure 6. 3 Damage to Silicon Solar Cells from Trapped Protons: I_{SC} 68
Figure 6. 4 Damage to Silicon 3 mils Coverglass Solar Cells from Trapped Protons: P_{MAX}, V_{OC} 68

Figure 6. 5 Damage to Silicon 3 mils Coverglass Solar Cells from Trapped Protons 69
Figure 6. 6 Damage to Silicon Solar Cells from Trapped Protons : P_{MAX}, ... 69
Figure 6. 7 Damage to GaAs 3mil coverglass Solar Cell from Solar Protons (JPL1991) 70
Figure 6. 8 Damage to Silicon Solar Cells from Solar Protons (JPL1991) 70
Figure 6. 9 Damage to GaAs Solar Cell from Trapped Electrons 71
Figure 6. 10 Damage to Silicon Solar Cells from Trapped Electrons 71
Figure 6. 11 Comparison of Silicon Solar Cells Degradation at MEO to Baseline 73
Figure 6. 12 Comparison of GaAs Solar Cell Degradation at MEO to Baseline 73
Figure 7. 1 Dose Depth Curve for Trapped Electrons: Baseline Orbit 77
Figure 7. 2 Dose Depth Curve for Trapped Protons : Baseline Orbit 77
Figure 7. 3 Dose Depth Curve for Solar Protons : Baseline Orbit 78
Figure 7. 4 Dose Depth Curves for Trapped Electrons : Various Altitudes ... 79
Figure 7. 5 Dose Depth Curves for Trapped Electrons : Close View 79
Figure 7. 6 Dose Depth Curves for Trapped Protons : Various Altitudes 80
Figure 7. 7 Dose Depth Curves for Trapped Protons : Close View 81
Figure 7. 8 Dose Depth Curves for Solar Protons : Various Altitudes 82
Figure 7. 9 Composite Dose Depth Curves : Various Altitudes 83
Figure 7. 10 Composite Dose Depth Curves : Close View 83

I. INTRODUCTION

This thesis investigates the effects of the radiation present in several Medium Earth Orbit (MEO) altitudes. The orbits analyzed were chosen with the guidance of the Naval Research Laboratory (NRL) in Washington, D.C. The radiation environment is described, the software used to evaluate the orbits and the corresponding radiation environment is explained, and then analysis of selected radiation effects is presented, and conclusions are drawn.

A. THE SPACE RADIATION ENVIRONMENT

The vastness of space is far from empty; the vacuum of space should imply no absence of environment. Radiation may be defined as the emission and propagation of energy through either space or a material medium. The space radiation environment is composed of cosmic rays, electromagnetic radiation, geomagnetically trapped radiation (the Van Allen belts), auroral particles, and solar flare particles. The radiation environment can be characterized by the earth radiation zone, where Van Allen belts are a major factor, the auroral zone, and the interplanetary zone. Radiation near the Earth consists of electrons and protons trapped in the geomagnetic field, corpuscular radiation associated with large solar flare activity, and to a lesser extent, galactic cosmic ray radiation. Near Jupiter an environment similar to the Earth's trapped particle radiation exists, but the intensity is far greater, due primarily to the large magnetic field. The following qualitatively describe the space radiation environment.

1. Geomagnetic Coordinates

Normally, it is convenient to plot the radiation intensity in the earth's radiation zone in geomagnetic rather than geographic coordinates. The origin of these coordinate systems coincide, but the geomagnetic axis is tilted by 11.5 degrees with respect to the axis of rotation of the earth.

B. The Earth Radiation Zone

The earth radiation zone is characterized by magnetically trapped electrons and protons. This zone, often referred to as the Van Allen belts, is made up of two concentric belts, the inner belt and the outer belt. The inner belt extends from approximately 300 to 6,400 km, with the intensity reaching a maximum at 2,900 to 3,200 km above the geomagnetic equator. The inner belt is sometimes referred to as the hard belt, and contains high energy protons of energies to 700 MeV, with electrons in the 20 keV to 1 MeV range. The outer belt extends from about 13, 000 to 21, 000 km; the region of high intensity is from 16,000 to 29, 000 km. This belt, called the soft belt, consists primarily of electrons from 20 keV to 5 MeV and some protons over 60 MeV.

C. The Auroral Zone

The auroral zone is located between approximately 60 and 65 degrees geomagnetic latitude. Low energy (less than 200 keV) electrons entering the atmosphere produce the auroral displays. Protons may also be present. The auroral particles are easily stopped.

D. The Interplanetary Zone

Radiation in interplanetary space consists of an energetic cosmic flux and pulses of radiation associated with solar flares. The largest flares, consisting of high energy protons, are extremely rare. The smallest flares occur as often as eight times per day. In addition to these sources of interplanetary radiation, there also exists a continuous ejection of low energy particles, primarily protons and electrons from the sun, known as the solar wind. The distribution of the solar wind particles is assumed to obey the inverse-square law with the sun acting as a point source.

Cosmic rays of galactic origin consist of protons (93 percent) and alpha particles (7 percent) along with smaller amounts of heavier elements. The energy of the protons is in the range of 5×10^8 eV to 2×10^{10} eV. Although energies are quite high, the free space flux of particles is 2.5 particles/sec • cm^2. Since this flux is small, radiation damage due to cosmic rays usually needs to be considered only on very long space flights.

E. Radiation Types

Radiation types may be generally classified as either electromagnetic (zero rest mass) or particulate (finite rest mass). Electromagnetic radiation includes ultraviolet light, X-rays, and gamma rays. Particulate radiation consists of electrons, protons, neutrons, alpha particles, and others. The more frequently encountered radiation types are defined as follows:

1. Alpha Particle (α)

A positively charged particle identical to all properties of the

nucleus of a helium atom, consisting of two protons and two neutrons.

2. Beta Particle (β)

A negatively or positively charged electron emitted from a nucleus with an energy range of approximately 1 Me V.

3. Electromagnetic Radiation

Radiation having wavelengths from approximately 10^{-7} to 10^{-11} cm. Generally this term refers to radiation types having no rest mass.

4. Photon

The generic term for the particular aspects of electromagnetic radiation. Photons of nuclear origin are called X-rays. Photons have wavelike properties, but occur as discrete energy quanta. The energy of a photon is inversely proportional to its wavelength.

5. Bremsstrahlung

The secondary radiation induced by high energy electrons which are detected by another charged particle such as a nucleus. The bremsstrahlung photons are X-rays having energies near that of high energy electrons, but which are more penetrating than the electrons themselves.

6. Cosmic Rays

High energy particles or electromagnetic radiation originating in interstellar space. Also called galactic cosmic radiation.

7. Electron (e)

An elementary particle of rest mass equal to 9.109×10^{-31} kg and a charge of 1.602×10^{-19} coulomb; its charge may be positive or negative. A negative electron is called a negatron, but the term electron is often

used. A positive electron is called a positron. Negative electrons occurring in space are designated by e.

8. Gamma Rays (γ)

Electromagnetic radiation having wavelengths from approximately 10^{-8} to 10^{-11} cm. Gamma rays are highly penetrating, and are emitted by a nucleus in its transition from a higher to a lower energy state.

9. Proton (p)

A positively charged particle of mass number 1 (having a mass of 1.672×10^{-27} kg) and a charge equal in magnitude to the electron (i. e., 1.602×10^{-19} coulombs). It is the nucleus of a hydrogen atom.

10. X-Ray

Electromagnetic radiation having wavelengths of approximately 10^{-8} cm. X rays are highly penetrating and are usually formed by bombarding a metallic target in a high vacuum with a particle. X-rays are also called roentgen rays.

F. Overview of Chapter Contents

This thesis is organized into eight chapters. The following section previews the remaining chapters.

1. Chapter II

Chapter II explains the geomagnetically trapped radiation in and characterizes the trapped electrons and trapped protons that compose this type of radiation. Models of geomagnetically trapped radiation are presented and research discussed. Orbital integration is also addressed.

3. Chapter III

Chapter III reviews radiation sources other than geomagnetically trapped radiation. It discusses the main components of radiation that originate outside the magnetosheath, in the Interplanetary Zone.

4. Chapter IV

Chapter IV explains the main radiation analysis tool used in this thesis, Space Radiation 4.0 software. The various file types are delineated, and the steps in using the software in radiation analysis are also discussed.

5. Chapter V

Chapter V introduces the analysis completed on the chosen orbits, beginning with the proton displacement effect. The importance of this effect is noted. The assumptions inherent in the analysis are pointed out and final data is presented.

6. Chapter VI

Chapter VI discusses the operation, characteristics of solar cells. Previous research on this topic is reviewed and some of the major findings are discussed. The chosen solar cell models are detailed and the assumptions made in this analysis are delineated and final data is presented.

7. Chapter VII

Chapter VII presents the last radiation effect analyzed. The use of dose depth curves is addressed and various dose depth curves are presented, for the components of radiation and their cumulative composite curve.

8. Chapter VIII

Chapter VIII reviews the highlights of this thesis and presents the final conclusions. It is followed by a list of terms used in the thesis, the refernce list and three appendices that included the data produced by the analysis.

II. GEOMAGNETICALLY TRAPPED RADIATION

The geomagnetic dipole field is responsible for the radiation belts near the Earth, holding the trapped charged particles for long periods of time. It is a plasma confined in an inhomogeneous magnetic field. The understanding of charge transport within the field, loss and capture mechanisms of charged particles has improved considerably over recent years. Models prepared to characterize the trapped radiation are continuously updated and now include solar cycle dependence.

A. GENERAL COMPOSITION

Geomagnetically trapped radiation may be either of natural or artificial origin, such as high-altitude nuclear explosions. Since a particle has to possess a charge to be trapped in a magnetic field, the energetic trapped particles are mainly electrons and protons. Regardless of their sources, particles with just the right momentum and pitch angle can be trapped in the field. The particles will then spiral about a geomagnetic field line with varying pitch angle (angle between magnetic field vector and velocity) and curvature in the nonhomogeneous field. They continue the motion until they reach the mirror (or reflection) point where the pitch angle becomes 90 degrees, then turn around and travel back along the field line into the other hemisphere. This is represented in Figure 2. 1 (after Stern and Ness, 1981).

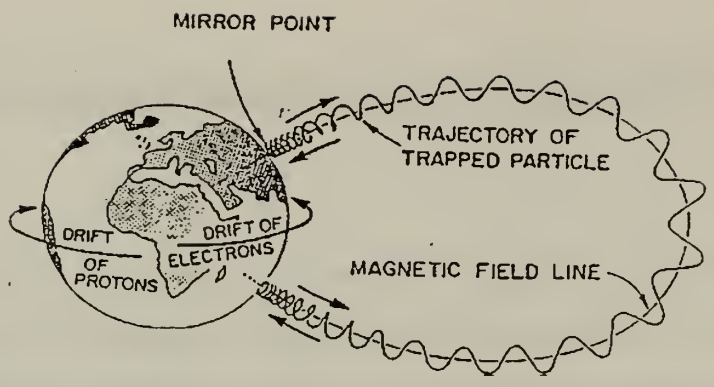

Figure 2. 1 Motion of Charged Particles (after Stern and Ness, 1981)

The particles continue to bounce back and forth between conjugate mirror points (latitudinal motion). At the same time the particles drift in the longitudinal direction as the result of forces due to the gradient of field strength and the curvature of field lines. During a quiescent state (periods of normal solar activity) the trapped particles can be characterized by three periodic motions:

a). circulation about the field line with cyclotron (Larmor) frequency,

b). latitudinal motion between mirror points, and

c). longitudinal drift.

The direction of longitudinal drift motion for electrons is eastward, opposite that of protons (westward) because of their opposite charge. The resultant charge separation produces a ring current. Particles whose mirror points are in the upper atmosphere collide with gas molecules, gradually losing their energy and changing trajectory until they are lost in the lower atmosphere.

At some distance from the Earth the field is distorted by the solar wind as shown in Figure 2. 2 (after Singley and Vette, 1972). The solar

wind is a plasma flowing outward from the sun and is dominated by protons with an average energy of approximately one keV and a density on the order of 10 particles/cm^2. The solar wind interacts with the geomagnetic field, resulting in the formation of a shock wave. This in turn forms and shapes the magnetosphere. As the solar plasma passes the shock wave, the random speeds of the particles increase, producing turbulence in the magnetic field. This turbulent region, the magnetosheath, extends inward from the shock front to the magnetopause, which is the outer boundary of the more regular field region associated with the earth.

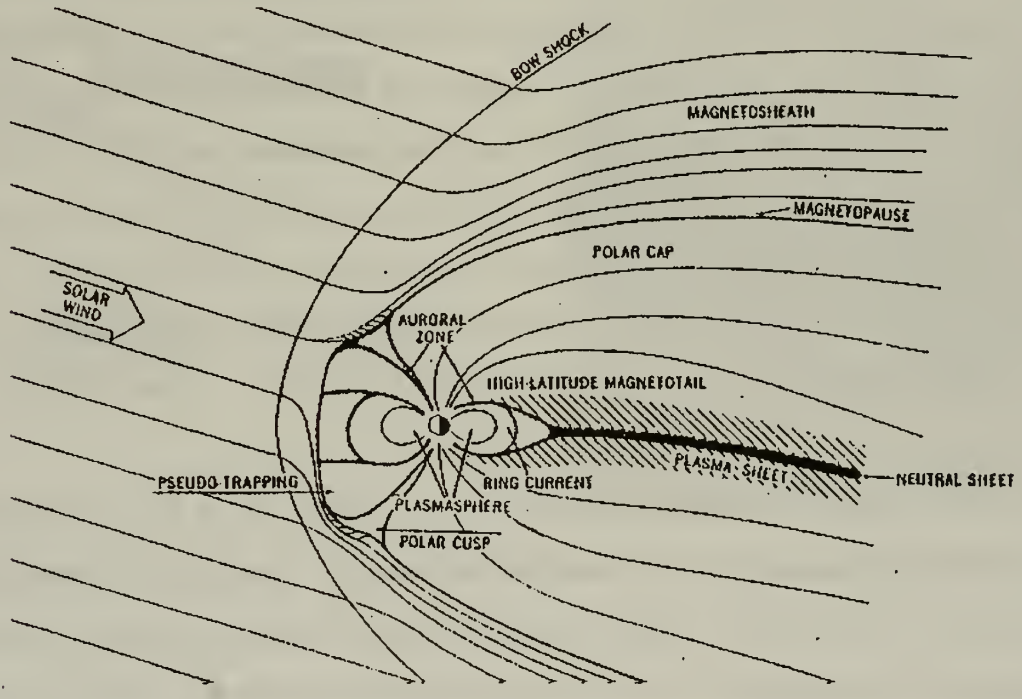

Figure 2. 2 Regions of the Magnetosphere (after Singley and Vette, 1972)

The geomagnetic field lines just inside the magnetopause are qualitatively similar to those associated with the simple dipole model and trap corpuscular radiation as described above. During quiescence a

relatively steady flow of solar wind blows the field away from the sun, contributing to an asymmetric shape of the radiation belt, compressed on the sun's side and forming the neutral sheet and magnetotail extending away from the Earth in the antisolar direction.

McIlwain in 1961 proposed a coordinate system consisting of the magnetic field B and the integral invariant I, which can adequately relate measurements made at different geographic locations. The quantity I is the length of the field line between mirror points weighed by a function of the magnetic field along the line and is an adiabatic invariant of the motion. He introduced the magnetic shell parameter, L. L = function(B,I) and is analogous to a physical distance in a dipole field (which reduces to the equatorial radius of a field line in the case of a dipole field), thus reducing the number of variables needed to describe the physical situation of trapped charged particles and presenting field data in a manner which facilitates its physical interpretation. For a radial distance of R and a dipole moment of M, the transformation using the dipole relation is expressed as follows:

$$B = M/R^3 \cdot [4 - (3R/L)]^{1/2}$$

where the magnetic shell parameter $L = R\ (\cos\lambda)^2$, M is the geomagnetic dipole moment, and λ is the magnetic latitude. In order to apply this concept to the Earth's field, which is not a simple dipole, McIlwain expanded the parameter L into a polynomial function of a variable which is a function of I, B, and M and elegantly represented trapped particle phenomena using two dimensions (B and L) instead of three.

Since its introduction, numerous particle field data were presented in this (B, L) coordinate system. Stassinopoulos, Vette and co-workers, at the National Space Science Data Center in Greenbelt, Maryland, have concentrated efforts on the compilation of particle field

data reported by numerous investigators and continue to construct and update models of the radiation environment. The strong dependence of trapped particle fluxes on altitude and latitude is best expressed in terms of the L parameter. The distribution of the charged particles in the magnetosphere is illustrated in Figure 2. 3 (after Stassinopoulos, 1980).

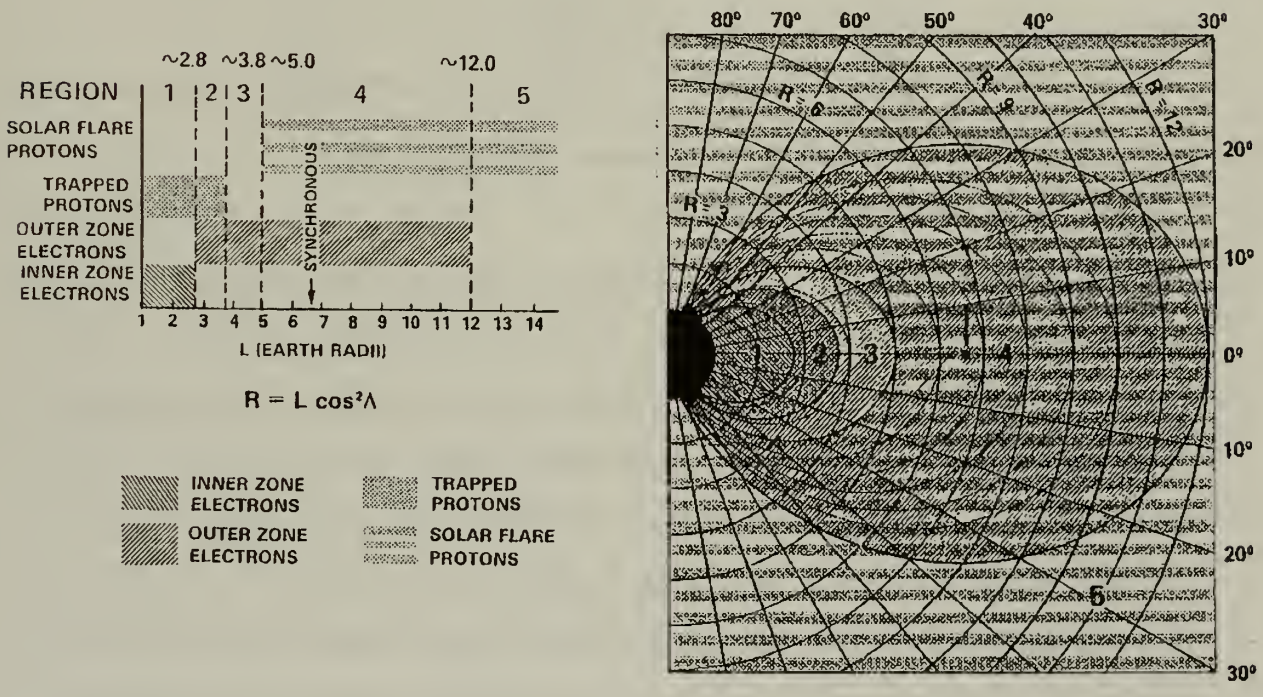

Figure 2. 3 Charged Particle Distribution in the Magnetosphere (after Stassinopoulos, 1980)

B. TRAPPED PROTONS

The largest concentration of protons at intermediate energies is near the Earth within a L value of four (geocentric) Earth radii, peaked at about two Earth radii. The high energy protons concentrate even closer to Earth, peaking at 1.5 Earth radii (R_E), whereas the distribution of the lower energy protons extends nearly to synchronous altitude (L = 6.6 R_E).

Generally speaking, the energy spectrum becomes softer as the L-value increases. At synchronous altitude the spectrum is so soft that practically no protons with energies greater than 2 MeV exist.

The former time-averaged models for trapped protons are as shown in Table 2. 1:

Energy Model Designation	Radiation Zone	Energy Range (MeV)
AP1	Inner Belt	30 - 50
AP5	Outer Belt	< 4
AP6	Inner Belt	4 – 30
AP7	Inner Belt	> 50

Table 2. 1 Trapped Proton Models

In 1976, a single trapped proton model, the AP8, replaced several older models (e.g. AP5, AP6, AP7), each of which was valid only over a specific energy range. The new AP8 describes the entire energy spectrum in a coherent, uniform, and continuous way. It was issued in two versions: the AP8-MAX and the AP8-MIN, relating, respectively, to average solar maximum and solar minimum conditions. In this case there is good theoretical reasoning for solar cycle effects which have been verified by experimental observations. Trapped protons are affected by solar cycle variations only in the vicinity of the atmospheric cutoff regions. No changes of consequence have been observed in the heart of the proton trapping domain or at synchronous altitudes since the observed temporal variations are in most cases of no greater extremes than the precision obtained between measurements by detectors on different satellites.

C. TRAPPED ELECTRONS

Electrons in the earth's radiation belts are trapped by the geomagnetic field. Trapped electrons with energies of a few hundred keV extend to the outer boundary of the magnetosphere, which fluctuates at 8 to 10 Earth radii. There are two intense regions: an inner one covers the L-values in the range of $1.2 < L < 2.5$ and peaks about 1.4 Earth radii, whereas the outer zone ranges between $3 < L < 11$ and peaks at around 4 to 5 Earth radii with the flux about 10^7 electrons/cm^2-sec for both zones with energies $E \geq 250$ KeV.

The outer zone is a very dynamic region of space where some particles are stably trapped but others are considered to be pseudo-trapped because the lifetimes are shorter than the drift time around the Earth. However, strong external (e.g., galactic and solar) sources supply electrons to this region of space and thus substantial fluxes are always present. In this zone, the flux has large short-term temporal variations related to the local time as well as a long-term change in average flux associated with a solar cycle. In as much as the geomagnetic field is continually varying during day-night cycles and due to solar activity, the flux density and energy spectrum at a given point in space also varies continually. Time-averaged values of flux have been prepared and are known as Trapped Radiation Belt Models. The former models for electrons were as follows in Table 2. 2:

Energy Model Designation	Radiation Zone	Energy Range (MeV)
AE4	Outer Belt	> 0.04
AE5	Inner Belt	> 0.04

Table 2. 2 Trapped Electron Models

The other models which describe the outer zone electrons (L ~ 2.8) are AEI7-HI and AEI7-LO. The "HI" version favors Vampola's fits to the enhanced OVI-19 data, while the "LO" version is representative of more quiescent times averaged over longer time periods. These are interim models replacing the older solar min and max versions of AE-4. However, they do not reflect solar cycle variations.

Stassinopoulos (1980) has pointed out that the radiation experienced by a spacecraft in a geosynchronous orbit is dependent on its longitude. This is because the geomagnetic coordinate system is tilted and displaced from the geographic coordinate system on which the satellite orbits are based. Thus, a measurement of L vs. longitude at geosynchronous altitude would yield a periodic curve with two maxima and two minima. The highest maxima occurs at a longitude of 70 degrees W with an L of 7.02 and the lowest minima occurs at 160 degrees W with an L of 6.6. This results in the trapped electron fluence with energies > 3 MeV having an intensity at 160 degrees W about an order of magnitude larger than at 70 degrees W. Careful assessments of the interaction of solar panels with the trapped electrons at synchronous altitude must take this longitude effect into account. It is not a problem at any other altitude because in general the spacecraft sweeps through all longitude and the effect is averaged out.

In the inner zone, the effect of geomagnetic storms on the average flux is significant at high L values and higher energies. A long-term increase in the inner zone flux is correlated with an increase in solar activity. Past sources of temporal variations include the decay of residual electrons from the high altitude "Starfish" nuclear test, but present data indicate these electrons are no longer present. These temporal variations are accommodated in the compilation of data and

publications on the AE model sequence by Vette, et al, two of which (the versions AE5 and AP6) are appropriate near solar minimum and solar maximum, respectively.

D. Orbital Integration

Vette and co-workers have time integrated both the trapped proton and electron environments for convenient energy ranges, and have tabulated the average daily fluence for circular orbits having specific altitudes and inclinations. There are two forms of spectra in his data: one is of the form of integral flux, the other of difference flux. (The latter should not be confused with the differential flux.)

If $\phi(E)$ is a differential flux at energy E in NeV, normally expressed in terms of particles/cm^2-sec-MeV, and $\Phi(>E)$ is an integral flux with an energy greater than E, expressed in particles/cm^2-sec, the relationship of these two quantities is:

$$\Phi(>E) = \int_{\infty}^{E} \phi(E)\, dE = \sum_j (E_j) \Delta E_j$$

On the other hand, the difference fluence is simply :

$$\Delta\Phi_j = \phi(>E_j) - \phi(>E_j + \Delta E_j)$$

For spacecraft trajectories other than circular orbits the radiation environment encountered by the spacecraft must be determined by some other method. The most accurate way to determine the environment is to make use of the physically significant coordinate system (B,L) so that uncertainties and inaccuracies attributable to the geographic coordinate system are eliminated. The geographic coordinates are then transformed into geomagnetic shell coordinates (B,L) on which isoflux contour maps are plotted.

E. SUMMARY

Geomagnetically trapped radiation is a significant contributor to the radiation environments at MEO altitudes and must be carefully modeled. Although complex, the actions of geomagnetically trapped radiation has received a significant amount of study and is understood relatively well. This eases the burden of modeling this component of the environment.

III. ADDITIONAL RADIATION SOURCES

Geomagnetically trapped radiation is not the only radiation sources experienced by satellites in orbit. While Medium Earth Orbit (MEO) altitudes share the same region of space with geomagnetically trapped radiation, other sources can have significant effects. Interplanetary spacecraft are not the only objects that experience the effects of distant radiation sources.

A. GALACTIC COSMIC-RAY RADIATION

Galactic cosmic rays are a highly penetrating radiation originating beyond the solar system. Many possess energies greater than 1 BeV and are capable of extraordinary interactions with matter in the upper atmosphere such as spallation, fission, fragmentation, and the subsequent secondary processes. The local cosmic-ray radiation in the atmosphere contains protons, neutrons, pi-mesons, mu-mesons, electrons, photons, and strange particles. Near the upper limits of the atmosphere, the primary radiation, consisting of 79 percent protons and 20 percent alpha particles, predominates over the products of nuclear reactions and the decay products; thus the components change with altitude.

If a galactic cosmic ray approaches Earth in the plane of the equator, the Earth's magnetic filed will bend the particles in the ray back to space or to the polar regions, depending upon its initial direction and energy. Consequently, the Earth's magnetic filed effectively shields the lower altitude and inclination orbit from some of the galactic cosmic rays.

One remarkable characteristic of cosmic rays is their isotropy. The average diurnal effect is very small. There is a definite relationship between the fluctuation and solar activity in general; 27-day effects, an 11-year fluctuation cycle, and the Forbush decrease associated with the magnetic storms are examples. Although the energy is very high, the flux is negligibly small compared with other environments considered; however, single event effects are a main result of galactic cosmic rays.

B. Solar Flare Radiation

Solar flares are eruptions of the sun that are associated with optical phenomena (called sun spots) and with the emission of energetic particles (called solar proton events). Solar flares occur in the neighborhood of sunspots, very seldom emit white light, and cause a sudden increase in intensity of the hydrogen alpha line (wavelength 656 nm). After its inception the flare rapidly expands over an area of a few million to a billion km^2 of the solar disk, reaching a peak intensity and gradually decaying and completely disappearing within several minutes to several hours, depending on the size of the flare. This can be seen in Figure 3. 1 (after Mcdonald, 1963).

Within half an hour or more following the appearance of large solar flares, energetic particles, consisting mostly of protons, are detected at the Earth, particularly within the auroral zones around the geomagnetic poles. The radiation dies away with a time constant of one to three days. The constituent particles are electrons, protons, alpha particles, and very small numbers of nuclei having intermediate masses (C, N and 0). The ratio of protons to alpha particles and of protons to medium nuclei vary considerably between solar events, whereas the ratio of alpha particles to medium nuclei remains relatively constant.

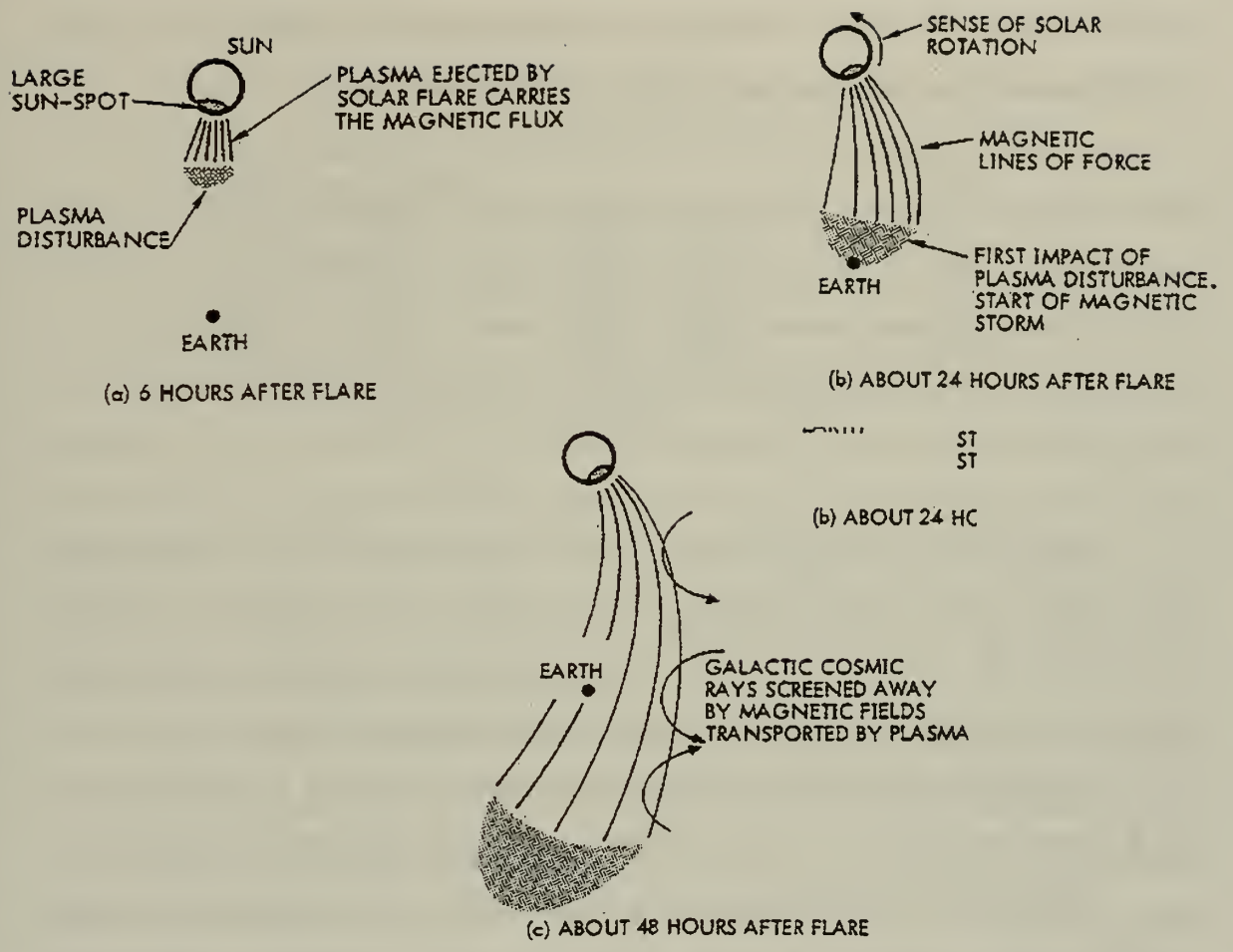

Figure 3. 1 Movement of Solar Flares (after Mcdonald, 1963)

As with most naturally occurring phenomena, the solar proton events show a range of distributions. During August 1972, and again in October 1989, there were two extremely large solar proton events. To classify the size of a solar proton event, the flare models are typically used. The ordinary model represents an average flare, the worst-case model is the 90% confidence level flare, and the anomalously large flare, based upon the August 1972 flare, is the absolute worst care model.

The frequency with which sunspots occur increases to a maximum

and decreases again during the approximately 11-year long solar cycle. The duration of solar maximum is approximately 7 years. The solar cycles of current interest are defined as follows in Table 3. 1:

Solar Cycle No.	Period of Cycle	Duration of Maximum Activity
19	1953 – 1964	1955 - 1961
20	1964 - 1975	1965 - 1972
21	1975 - 1986	1977 - 1983
22	1986 - 1997	1988 - 1994

Table 3. 1 Recent Solar Cycles

Sun spot cycles have been observed and recorded for more than 200 years but emitted energetic particles have been observed only since approximately 1954 during the nineteenth and twentieth solar cycles. Most of the solar flare protons that damage solar cells occur in one (or a few) anomalously large flares that seem to occur during a time span of 3 to 4 years centered around the middle of the solar maximum activity.

Although the fluctuation in flux intensity is much more severe and random than those of galactic cosmic rays, the following phenomena have been observed:

a). there may be an ll-month cycle in the peak number of events;

b). there is a semiannual variation which has maxima in March and September, near the equinoxes;

c). the maximum number of events occurs on the average near the September equinox and the minimum during December or January;

d). the number of flares varies with the ll-year solar cycle; and

e). there is a definite tendency for flare events producing a large proton fluence to occur during the increase or decrease of

sunspot activity rather than during the maximum. (Tada, 1982)

These findings suggest that reasonable predictions of damage due to solar flares can be made only over reasonably long periods (at least 1 year). Many solar flare proton models have been developed. Two solar proton flux models for the twenty-first solar cycle that have found widespread acceptance in satellite systems specifications, denoted here as the Aerospace and Intelsat V models. The Aerospace Model applies an arbitrary safety factor of 1 - 5 to the average of the flux observed during the nineteenth and twentieth cycle (actually to the average of the two nineteenth-cycle curves and the twentieth-cycle curve) whereas the Intelsat V model is a straight-line approximation to the higher flux observed during the nineteenth cycle.

Most of the total proton flux during the past two solar cycles has occurred during one (or a few) anomalously large solar proton events. Solar flare proton measurements were made only during the last two solar cycles and only in the energy range from 10 to 100 MeV. The observed data was compiled by Stassinopoulos and King. This data has been extrapolated to energies lower than 10 MeV and forms the basis for predicting the flux for the next (twenty-first) solar cycle. The number of these events is too small to warrant a meaningful statistical analysis for predicting the time of occurrence of anomalously large events. According to this data, the annual relative solar flare proton flux was approximately:

a). 1966-1971 5 percent per year

b). 1972 70 percent per year

Therefore, a small degradation due to ordinary flare protons should be allowed for during the entire active solar period, even if no anomalously large flare events occur in some years.

Customarily, this is expressed in terms of the characteristic rigidity R_o as follows:

$\Phi(>R)$ = integral flux having rigidity greater than R

$\Phi(>R) = \Phi(>R_o) \cdot (e^{1 - R/R_o})$

R = rigidity (v or Mv)

$R = pc/zq = [\, E^2 - (m_oc^2)^2 \,]^{1/2}/[zq] = [\, T\,(T + 2m_oc^2) \,]^{1/2}/[zq]$

E = total energy (MeV)

T = kinetic energy (MeV)

P = momentum (MeV/c)

m_oc^2 = rest mass energy (938 MeV per nucleon)

zq = atomic charge

The characteristic rigidity R_o varies not only with each event but within the spectrum of an event. The R_o computed for the annual flux is smaller during the years near sunspot maximum (50 to 70 MV), but the total annual fluence is higher during these years. (Tada, 1982)

For the purpose of predicting the size and spectrum of solar flare proton events, many statistical analyses have been made on proton events observed near or on the Earth. Unfortunately, the correlation between the prediction and observations has been rather poor. A Poisson distribution may be appropriate for sunspot numbers and solar flares on the sun, but not for solar flare proton events. The flares which are large enough to emit a large number of energetic particles and further satisfy the requirements of protons to reach the Earth obviously belong to a special class of solar flare events. Phenomena observed during solar cycle 19 are enumerated below for review: particular emphasis be placed on those which

appear to be dependent on solar activity.

a). The flares capable of producing large proton events tend to occur when the rate of change in annual sunspot number becomes greater.

b). The characteristic rigidity of solar flare protons is randomly distributed throughout an ll-year cycle, but both the annual expectation value and variance are not. During a period of increasing or decreasing sunspot activity, the R_E becomes larger on the average than that during the maximum, and the variance becomes smaller during the solar maximum. That is to say, the solar flare proton events are relatively steady and confined in a smaller rigidity range during the solar maximum, whereas the size and spectrum become erratic when the rate of change in sunspot activity becomes severe.

c). The size of each event, as measured by an integral proton flux of energy greater than 30 MeV, is almost randomly distributed over an ll-year cycle, but a line connecting the successive annual fluence plotted against sunspot number is not a single-valued function.

King made a probabilistic study of solar proton fluence level based on 1966-1972 data. The probability with which any given solar proton fluence level will be exceeded was computed for the active phase of the current cycle (1977-1983). The probability is a function of fluence level, proton energy threshold, and mission duration. He assumed that fluences of all anomalously large (AL) events have a spectrum given by the August 1972 event, and fluences of the ordinary (OR) events obey a log normal distribution. A spectrum softer than the August 1972 event

is used for the latter model and the annual fluence level is scaled according to the solar activity as measured by smoothed sunspot number.

Since solar flare particle fluxes are rich in low rigidities, a strong cutoff phenomenon is expected. During the quiescent state, the cutoff rigidity at low latitude is a strong function of direction as well as of latitude approximately proportional to $\cos^4\Lambda$, for large geomagnetic latitudes), and hence of L. Galactic cosmic rays follow this normal Stormer cutoff as do flare particles just before the plasma cloud hits the geomagnetic field. After the impact of the plasma front from the flare event the geomagnetic field is disturbed, resulting in a magnetic storm. This disturbance is in such a manner that a field due to a time-dependent ring current appears to superimpose on the normal geomagnetic dipole field. This causes the disturbed line of force to stretch farther out from the Earth at a given latitude. As a result, the particle rigidity necessary to penetrate at a given latitude is greatly reduced and the cutoff energy becomes time dependent. Satellite observations have indicated that the cutoff energy at synchronous altitude seems to be much less than expected, and flare protons with energy as low as a few hundred keV were observed during the storm. If this is indeed the case, the cutoff energy due to the geomagnetic field becomes insignificant at this altitude, because the cutoff due to solar cell cover shield is normally far greater than the magnetic cutoff during a storm. If both altitude and latitude are low, the field perturbation due to the storm may be insignificantly small compared with that of the quiescent state and the Stormer cutoff approximation may prevail. It is evident that orbit inclination is a significant factor for spacecraft at low altitude.

For unmanned missions of a year or longer the ordinary (OR) solar flare fluence may be insignificant because there is a high probability that an anomalously large (AL) solar flare event will occur. This AL event will expend all its fluence in a relatively short time, 2 to 4 days, and totally overshadow all the OR events. Neither the AL event itself nor its time of occurrence can be predicted, but statistically an AL event will occur sometime during a solar cycle. The prediction of solar flare proton fluxes becomes a function of mission duration and a confidence level Q through a modified type of Poisson statistics. Missions of short duration are less subject to AL events and more subject to OR events, but this does not preclude the possibility of an AL event occurring during a short mission.

C. SUMMARY

While synchronous orbits do not experience a significant amount of geomagnetic shielding for cosmic rays of solar or galactic origin of energy E>10 MeV, geomagnetic shielding is a necessary factor to consider at MEO altitudes. Therefore, spacecraft in geostationary orbit will receive 100% exposure of unattenuated interplanetary solar flare proton intensities of all energies above 10 MeV. (and to a first approximation this exposure is omnidirectional and isotropic), but the same statement does not hold true for MEO. MEO calculations require a detailed computation of the orbital path and the corresponding geomagnetic filed strengths to yield accurate estimations.

IV. SPACE RADIATION MODELING SOFTWARE

This chapter explains the main tool used in the radiation analysis discussed in following chapters. The models included in the software are discussed, the different file types created by the software are delineated, and the steps in using the software in radiation analysis are addressed.

A. INTRODUCTION

Space Radiation is a comprehensive software tool for modeling the space and atmospheric environment and radiation effects in spacecraft and aircraft systems. Version 4.0 of the Space Radiation software was used for the calculations included in this thesis. Natural sources of radiation include solar flares, galactic cosmic radiation, the Van Allen belts, and neutrons in the atmosphere. The software simulates spacecraft exposure to protons, neutrons, electrons, and heavy ions on any trajectory. After correction for attenuation in the Earth's magnetosphere, Space Radiation 4.0 transports the particle environment through spacecraft structure to a point of interest, for example, the site of a sensitive electronic component. Finally, it computes a number of radiation effects including total dose, single-event upsets induced by protons and by heavy ions, proton displacement damage, and biological dose equivalent.

Space Radiation 4.0 is used principally by engineers who need to assess the risks that radiation, and other environmental factors, pose to space and aircraft onboard systems. These risks include bit errors and damage to semiconductor components including digital electronics, charge-coupled devices, and solar cells. Some examples are single-event upsets (random, non-destructive bit errors), latchup, permanent

degradation of silicon dioxide insulating structures, and creation of traps in charge-coupled device materials.

The radiation codes have been tested extensively and are in wide use today. Space Radiation 4.0 software combines these codes into a single user environment with a windows-based user interface, includes on-line help, supplies database storage of intermediate results, provides procedures for complete documentation of results, and includes a variety of extensions which increase the utility of the codes.

B. FOUNDATION MODELS

Space Radiation is based primarily on public-domain models that are well-documented in the literature. The term model here refers to mathematical formulas and numerical tabulations representing some aspect of the environment or a radiation effects simulation. It does not refer to computer code. Space Radiation 4.0 consists almost entirely of original computer code copyrighted by Space Radiation Associates of Eugene, Oregon. It is carefully designed for accuracy, reliability, and efficiency. Recent examples of well-documented, public-domain models upon which Space Radiation draws include JPL 1991 (see more below), HICUP (Sandia), and MACREE (Boeing). A full listing of models used for this thesis is included in the List of References.

The AP-8 trapped proton and AE-8 trapped electron models were developed by Donald M. Sawyer and James I. Vette of the National Aeronautics and Space Administration (NASA). These models contain estimates of the trapped particle intensity at any point within the Earth's magnetosphere. The AP-8 and AE- 8 models are currently distributed by the National Space Science Data Center in Greenbelt, Maryland. The ALLMAG, GDALMG, and LINTRA computer programs perform a rapid computation of the Earth's magnetic field at any geographical location

based on coefficients of a spherical harmonic expansion. The programs also trace magnetic field lines and are used in combination with the INVAR program which provides B and L coordinates required by the AP-8 model. The ALLMAG program was developed by E.G. Stassinopoulos and colleagues at the NASA Goddard Space Flight Center in Greenbelt, Maryland. The INVAR program was developed by McIlwain and colleagues at NASA.

The SHIELDOSE code was developed by Steven M. Seltzer at the National Bureau of Standards (NBS). This model contains code for transporting electron spectra through aluminum and computing the radiation dose in various materials. The code takes into account both direct ionization and bremsstrahlung production. The SHIELDOSE model is currently distributed by the Radiation Shielding Information Center at Oak Ridge National Laboratory.

Models of individual solar flares have been developed by J.H. King at NASA (August 1972 event); and H.H. Sauer, R.D. Zwickl, and M.J. Ness at the National Oceanic and Atmospheric Administration (NOAA) (Events in 1989). A statistical model of solar flare frequency and intensity (JPL 1991) has been developed by J. Feynman, G. Spitale, J. Wang, and S. Gabriel at the Jet Propulsion Laboratory (JPL). It is based on King's work.

Of particular importance are the geomagnetic field models. The Van Allen belt particle models require a geomagnetic field model used to determine B and L values at each location on the orbit. A wide selection of geomagnetic field models is supplied with Space Radiation. The first line is a description of the model. The second line contains the degree (n) of the model, the value of Earth's radius used in the expansion, and the epoch of the model. There are (n+1)(n+2)/2 remaining lines each containing a degree and order, the values (g and h), the derivatives (dg/dt

and dh/dt), and the second derivatives (d^2g/dt^2 and d^2h/dt^2) of the spherical harmonic coefficients.

C. Space Radiation Additions to the Models

Space Radiation combines these models into one system and provides a consistent environment for space radiation effects estimates. The Space Radiation user interface is based on Microsoft Windows. This interface simplifies the computational effort while at the same time improving accuracy. Space Radiation provides the engineer or scientist with a versatile and easy- to-use code for assessing the risk of ionizing radiation in space systems. Space Radiation is based on well-tested, public-domain software which is widely used in the aerospace engineering community.

The parameters defining each Space Radiation computation are stored in a database for further use. Reports may be generated from the database to provide complete documentation. The parameters may be reexamined and changed whenever necessary. Space Radiation provides a variety of options which are not found in other programs. The program augments CREME by computing radiation dose, dose equivalent, and empirical single event upset computations with funneling. It offers many different spacecraft and device materials, not just aluminum and silicon. Shielding may be modeled as a single thickness or a distribution. User-defined trajectories, shielding distributions, and proton spectra are accepted. Thicknesses, times, and doses may be expressed in any of several units.

D. Space Radiation File Types

Analysis using Space Radiation 4.0 utilizes many different file types, each having specific characteristics. Usage of the file in further

computations is restricted depending upon file type. Each file type created in this analysis using the Space Radiation 4.0 software is discussed in the below section.

1. Orbital Trajectory

Orbital Trajectory files contain the geographical position of a spacecraft (or other vehicle) at one or more times. The file is used in subsequent calculations to integrate over various features of the environment. Actual environment calculations are performed only at the points listed in the Orbital Trajectory file. For example, in low-earth orbit all proton dose is picked up in occasional brief South Atlantic Anomaly (SAA) passages. Orbital Trajectory files are identified by the ORB file extension.

2. Geomagnetic Shielding

Geomagnetic Shielding files contain information defining how particles from outside the Earth's magnetic field are attenuated as they pass through the field and contain the geomagnetic transmission function. This function quantifies what fraction of galactic cosmic radiation and solar flare particles can penetrate the Earth's magnetic field and reach the spacecraft. The level of penetration depends on particle rigidity, a combination of momentum and charge. Higher speed and lower charge particles pass straight through the magnetic field and can access spacecraft more easily.

These files are necessary to work with solar protons, solar heavy ions, and galactic cosmic radiation. They are not needed to work with trapped proton, trapped electron, and neutron environments. Geomagnetic Shielding files are generally created by evaluating the geomagnetic cutoff at each point on an orbit, or they may also specify a file with a single fixed cutoff. A fixed cutoff of zero is recommended for

analysis of geostationary orbits and for determining orbit-independent upper limits on environments. Geomagnetic Shielding files are identified by the GEO file extension.

3. Spacecraft Shielding

Spacecraft Shielding files specify the effective thickness and composition of structural shielding between the environment and systems within a spacecraft. Structural material usually helps to shield against radiation. The actual contents of the file are a shielding distribution tabulating the fraction of rays (or solid angle) emanating from a point within a spacecraft which pass through each thickness range. Each thickness in the distribution represents the actual thickness used in a transport computation. The fraction represents the number of rays with that effective thickness. The total fraction is normally one.

Spacecraft Shielding files are used in transport and radiation effects calculations. More rays and finer thickness intervals require more radiation transport time, but yield more accurate results. More rays are used to represent the geometry more accurately. Finer bin intervals represent the transport more accurately. Spacecraft Shielding files are identified by the SHD file extension.

4. Trapped Proton

Trapped Proton files contain a flux (or fluence) of protons over a range of energies. Spectra may be in integral or histogram (binned) form. They are used in transport and radiation effects computations, including dose-depth curves and proton-induced single event upsets. Trapped Proton files can contain the spectrum of protons encountered during passages of the spacecraft through the radiation belts. In this case, they are derived from Orbital Trajectory files and may contain either the

mission-integrated fluence, average flux or peak flux on the trajectory. Any proton spectrum, from any source whatsoever, can be utilized within Space Radiation after importing it as a Trapped Proton file. Trapped Proton files are identified by the TRP file extension.

5. Trapped Electron

Trapped Electron files contain a flux (or fluence) of electrons over a range of energies. Spectra may be in integral or histogram (binned) form. They are used in transport and radiation effects computations including dose-depth curves. Trapped Electron files can contain the spectrum of electrons encountered during passages of the spacecraft through the radiation belts. In this case, they are derived from Orbital Trajectory files and may contain either the mission-integrated fluence, average flux or peak flux on the trajectory.

6. Solar Proton

Solar Proton files contain a flux (or fluence) of protons over a range of energies. They contain proton spectra arriving at Earth from outside the magnetosphere, normally protons associated with solar flares. Spectra may be in integral or histogram (binned) form. They are used in transport and radiation effects computations, including dose-depth curves and proton-induced single event upsets. Solar protons are attenuated by the Earth's magnetic field. The Solar Proton file contains the proton intensity outside the magnetosphere. It is consequently always used in conjunction with a Geomagnetic Shielding file. The Geomagnetic Shielding file attenuates the protons to an actual spacecraft orbit. Solar Proton files may contain either the event-integrated fluence, average mission or event flux, or peak event or mission flux. Solar Proton files are identified by the SEP file extension.

7. Energy Spectrum

Energy Spectrum files contain a flux (or fluence) of particles as a function of energy. They are designed to contain the spectrum heavy ions in the environment. However, they may also contain the same information as a Trapped Proton, Trapped Electron, Neutron, or Solar Proton files. Energy Spectrum files originally contained proton and heavy ion fluxes within a spacecraft, that is, after transport through spacecraft shielding. The files may also contain energy spectra in the environment, that is, prior to transport through shielding. Furthermore, energy spectrum files can be used as input and output, allowing spectra through layers of shielding.

Energy Spectrum files are used in a variety of radiation effects calculations, including proton-induced single event upsets and proton displacement damage. They are also used to create LET Spectrum files, which in turn are used for single-event upset, radiation dose, and dose equivalent calculations. Energy Spectrum files contain far more information than other spectrum files. Typically, they contain data on 92 particle species at 500 energies. Compare with Trapped Proton files which contain data on 1 particle species (protons) at 20 energies. For this reason, Energy Spectrum files are stored as very compact binary files. Energy Spectrum files are identified by the FLX file extension.

8. LET Spectrum

LET Spectrum files contain the flux (or fluence) of protons and heavy ions as a function of LET. The LET spectrum file is used in a variety of radiation effects computations including heavy-ion induced single event upsets. LET spectra are used because they store essential information (energy loss rate) about a large number of particle types in a single function. Typically an LET spectrum contains the fluence for all

particle species combined into one function containing 1000 data points. Compare with nearly 50,000 points for an Energy Spectrum file. LET Spectrum files are identified by the LET file extension.

9. Dose-Depth

Dose-Depth files contain the total dose (rads or Gray) or dose rate at the center of shells of various thicknesses. This gives an indication of the reduction in absorbed dose accomplished by adding shielding. The Dose-Depth files may be used as is or may be convoluted with a Spacecraft Shielding file to get dose inside a complex shielding geometry. Dose-Depth files are identified by the KER file extension.

E. Radiation Assessment Using Space Radiation

Normally radiation assessment should consider at least four sources of radiation:

a). Galactic Cosmic Radiation

b). Solar Flare Particles

c). Trapped Protons

d). Trapped Electrons

The first two sources originate outside the magnetosphere. As they pass into the magnetosphere, low energy particles are deflected away. A cutoff rigidity can be calculated at each point on the orbit. Particles below the cutoff do not arrive at that point. At another point, the same particles or particles of the same energy may penetrate the magnetosphere because they are above the cutoff. The trapped particles are confined within the magnetosphere and are not shielded by the geomagnetic field.

A radiation assessment in Space Radiation consists of a number of steps that produce a sequence of files. Each file, as described below, contains a portion of the modeling information, either problem definition, intermediate results, or final results.

1. Specify Spacecraft Position or Trajectory

Define the spacecraft orbit within the Trajectory menu. Space Radiation needs this information to establish the radiation environment which depends on position. This step can be deleted only if the spacecraft is outside the magnetosphere. In that case, a fixed cutoff of 0 GV is used. All the Medium Earth Orbits altitudes in this thesis reamin within the magnetosphere.

2. Define the Spacecraft Shielding

Spacecraft structural materials attenuate radiation, in this case, electrons, protons, and heavy ions in space. Use the Shielding menu options to describe the thickness and type of material making up the spacecraft structure.

3. Calculate the Shielding Provided by Earth's Magnetic Field

Galactic cosmic radiation and solar flare particles come from outside the magnetosphere and are shielded by the magnetic field. These radiation transport modules require a Geomagnetic Shielding file. (Van Allen belt protons and electrons are trapped within the geomagnetic field but are not attenuated. Transport of these environments does not require a Geomagnetic Shielding file.)

Geomagnetic shielding files contain a representation of the shielding effect of the magnetosphere. Normally these files contain an orbit average of the vertical cutoff called the geomagnetic transmission function. This file is used to compute mission-average galactic cosmic radiation environments. A modification of cutoffs occurs during geomagnetic storms (often associated with large solar flares). The cutoffs are lower so that a larger fraction of particles penetrate to any point in the magnetosphere. Such an enhancement is visible in the intensity of

the aurora borealis (northern lights) during geomagnetic storms. Some modeling tasks require the worst-case (minimum cutoff) point on an orbit for galactic cosmic radiation or solar flare particles. Selecting worst case causes that point to be found. The computed geomagnetic transmission function is appropriate for that worst-case point.

The Earth itself shields spacecraft in Low Earth Orbit (LEO) from almost one-half of external radiation, thus Earth's shadow is an important inclusion in the modeling. While the effect is not as pronounced in MEO, it is important to include. Usually calculations are performed using the vertical geomagnetic cutoff, that is, the cutoff for particles arriving from the zenith. In fact the cutoff is angle dependent and a different transmission function is obtained if integration is over all those angles taking into account all arrival directions and the Earth's shadow (if necessary).

4. Determine the Radiation Environment

Use the Environment menu to calculate Van Allen belt (trapped) proton and electron intensities, or describe models of solar proton events. This step may be skipped for galactic cosmic radiation environments and some solar particle environments which are precalculated in Space Radiation. The environment menu contains procedures for defining radiation environments. These environments include galactic cosmic ray electrons, protons and heavy ions, trapped protons and electrons in the Van Allen belts, solar protons and heavy ions, atmospheric neutrons, and arbitrary user-defined proton, electron, and neutron spectra. The menu also contains environment grid modules, which compute various environmental features on a grid of points, and environment path modules, which compute the same quantities at each point on an orbit.

5. Transport Radiation Components Through Shielding

The Transport menu combines the radiation environment, geomagnetic shielding, and spacecraft shielding files that have been created. They provide an estimate of the particle environment inside the spacecraft. The transport menu contains procedures that transport radiation inside a spacecraft. Radiation transport through shielding account for energy losses encountered by particles as they pass through materials.

Other selections on the menu supply Space Radiation format files containing the spacecraft orbit, the radiation environment in the vicinity of the spacecraft, and the radiation shielding provided by the Earth's magnetic field and the spacecraft structure. The Transport selection utilizes these files to assess the radiation environment at the site of a microelectronic component or system inside the spacecraft. The transport modules create either an Energy Spectrum file, an LET Spectrum file, or a Dose-Depth file.

Energy Spectrum files contain a flux (or fluence) of particles as a function of energy. They are designed to contain the spectrum heavy ions in the environment. However, they may also contain the same information as a Trapped Proton, Trapped Electron, Neutron, or Solar Proton files. The files may now contain energy spectra in the environment, that is, prior to transport through shielding. They are also used to create LET Spectrum files, which in turn are used for single-event upset, radiation dose, and dose equivalent calculations. Energy Spectrum files contain far more information than other spectrum files. Typically, they contain data on 92 particle species at 500 energies. Compare with Trapped Proton files which contain data on 1 particle species (protons) at 20 energies. For this reason, Energy Spectrum files

are stored as very compact binary files. Energy Spectrum files are identified by the FLX file extension.

6. Compute the LET Spectrum

The LET spectrum is used for radiation effects computations with heavy ions, including single-event upsets and total dose. LET spectra are used because they store essential information (energy loss rate) about a large number of particle types in a single function. Typically an LET spectrum contains the fluence for all particle species combined into one function containing 1000 data points. Compute an LET file as part of the Transport or Effects step.

7. Calculate Radiation Effects of Interest

Radiation effects computations are based on an LET or energy spectrum calculated in the radiation transport section. (The electron radiation dose includes transport and is calculated directly from a Trapped Electron file.) Note that many radiation effects calculations yield only a single number result, not a file.

Single-event upsets (SEUs) occur when highly charged particles pass through the sensitive region near a memory bit on a chip. The charge deposition can change the state of the bit without causing permanent damage. SEUs can be caused either directly by the passage of a cosmic-ray heavy ion, or indirectly when a proton causes the recoil of a substrate atom. There are several methods available for computing the direct SEU rate. The best is to use a file containing the upset cross section as a function of LET. If a complete cross section vs. LET file is not available, a slightly more conservative result may be calculated using the LET threshold (1.5 MeV/(mg/cm^2)) and asymptotic upset cross section (0.045 cm^2) for the device.

Displacement damage arises from non-ionizing interactions of radiation. When a charge particle passes through material it can lose energy in two ways. The primary energy loss mode is ionization. Electrons are stripped from atoms and sent on their way with relatively small amounts of energy transferred from the incident particle. The other type of energy loss, non-ionizing, occurs when the incident particle has essentially a mechanical collision with an atom in the lattice. In this way the lattice gets damaged and absorbs energy from the incident particle. Non-ionizing energy loss is closely correlated with radiation effects such as gain degradation in bipolar transistors, and damage to CCDs and solar cells.

F. SUMMARY

This chapter detailed the spacefications and operation of the Space Radiation 4.0 software. A powerful analysis tool, Space Radiation 4.0 greatly assisted in the analysis completed in this thesis. Understanding of the limitations of the software is necessary for a full comprehension of the results included in the following chapters.

V. PROTON DISPLACEMENT EFFECT

The first radiation effect discussed in proton displacement effect. It is explained in the introduction and the results of the analysis conducted are presented.

A. INTRODUCTION

Proton displacement damage is a concern to internal components of spacecraft, and must be considered as seriously as other types of radiation damage. The magnitude of this effect in Medium Earth Orbits (MEO) is considered in this chapter.

The displacement damage function is the energy deposited per unit mass of material by lattice displacement, a non-ionizing effect. This quantity is often closely correlated with radiation damage to charge-coupled devices (CCDs) and solar cells. It is based on a model developed by Burke. This calculation convolutes the proton spectrum with an energy-dependent conversion factor (flux-to-dose). The flux conversion function is provided in file (DAMAGE.DAT), included in Appendix C. This option computes non-ionizing radiation dose, or displacement damage, using an Energy Spectrum file containing proton intensities inside a spacecraft.

The result of this computation is the energy deposition rate, reported in Radiation Absorbed Dose (rad) per day. Normally the unit rad refers to ionizing radiation. Here it refers to the smaller, non-ionizing, component of radiation which causes damage to transistors, CCDs, and solar cells. To convert rad units to 1-MeV proton equivalent (protons/cm^2), divide the result here by 9.9×10^{-10}. To convert rad units

to 1-MeV neutron equivalent (neutrons/cm^2), divide the result here by 2.6×10^{-11}.

The calculations were conducted using a spherical model spacecraft, with two shell thicknesses of 100 mils and 300 mils. The rates were found at the center of the sphere, which had a 10 inch inner radius. The calculation was made for the Low Earth Orbit (LEO) baseline orbit of 400 nautical mile (nmi) and was repeated for each altitude, in one thousand nmi increments, from three thousand nmi to nine thousand nmi. All orbits were circular.

Several sources of proton displacements effects were considered. Through use of the galactic cosmic radiation energy spectrum, the trapped proton energy spectrum, and the solar energetic (CREME model) particle energy spectrum evaluated at each altitude, the contributions of these various sources to proton displacement effects were considered. The target material designated was silicon.

B. Results

The following graphs represent the results of this analysis. The first section of graphs are a comparison of the proton displacement effect at the various MEO altitudes to the baseline LEO orbit of 400 nmi. This was simply accomplished by dividing the MEO altitude dose rate by the baseline orbit dose rate. The resulting number, termed the multiplicative factor, was plotted against the respective MEO altitude.

1. Galactic Cosmic Radiation

Galactic cosmic radiation (GCR) includes protons and heavy ions originating outside the solar system. It is the main source of radiation effects outside of the radiation belts when the sun is not active. GCR is attenuated by the solar wind as it moves through the solar system. This analysis was calculated for solar minimum activity; the GCR is then

maximum because the solar wind has less attenuating effect. At solar maximum activity, the GCR is minimum.

Military hardness specifications generally stipulate modeling with the 90% worst-case environment when characterizing SEU sensitivity; however, the solar minimum model is an adequate representation of long-term, worst-case galactic cosmic ray environment. The 90% worst-case environment includes solar flares and specifies a level of activity which is exceeded in only 1 out of 10 six-hour periods during a mission. If the mission duration exceeds a day or two, there is no likelihood of encountering the 90% worst-case environment continuously. Additionally, the analysis considers solar flare activity separately (see below), and thus solar flares are excluded in the galactic cosmic radiation analysis portion.

As can be seen in Figure 5. 1, the proton displacement rate from galactic cosmic radiation increases by a fairly constant magnitude with increasing altitude. Galactic cosmic radiation is significantly different at the MEO altitudes than at the baseline orbit, varying from a factor of 0.55 that of the baseline orbit (i.e., the dose from galactic cosmic radiation at three thousand nmi is about one-half the amount at the baseline orbit) to a high factor of 2.4679 for the nine thousand nmi altitude orbit. Figure 5. 2 shows the actual calculated values for the various MEO altitudes with a reference line plotted with stars showing the baseline orbit value. The crossover altitude, when radiation dose equals the baseline reference value, occurs at approximately 4500 nmi.

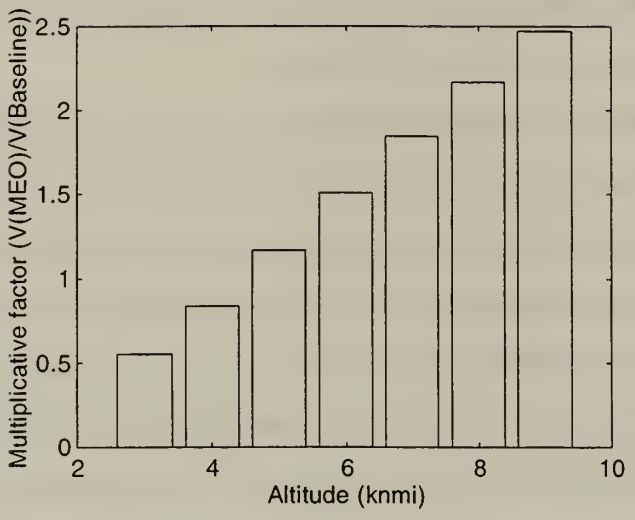

Figure 5. 1 Comparison of Galactic Cosmic Source Proton Displacement Doses at MEO Altitudes to Same Effect at Baseline Orbit

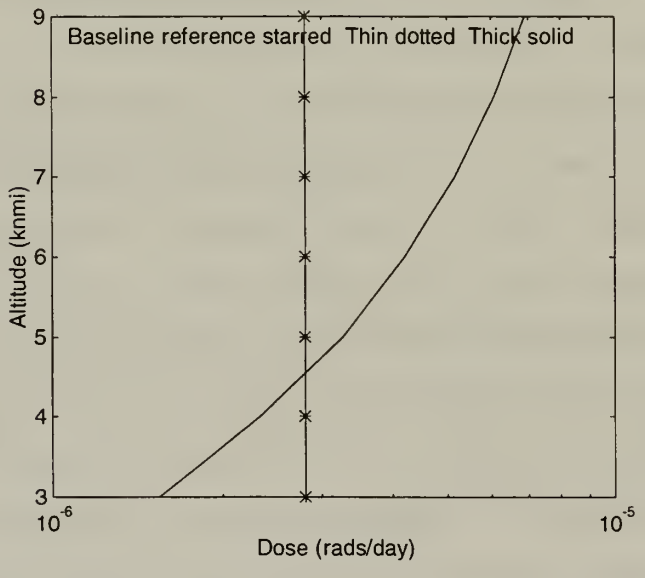

Figure 5. 2 Proton Displacement Dose from Galactic Cosmic Radiation at Various MEO Altitudes and Baseline Orbit

2. Geomagnetically Trapped Radiation

The contribution of trapped protons to proton displacement is plotted in Figure 5. 3. These values show a decreasing effect with increasing altitude, and exhibit an exponential characteristic in the multiplicative factor. For altitudes greater than seven thousand nmi, the

estimation of the proton displacement dose from trapped protons was zero. The dotted lines represent the data from the 100 mils thick sphere; the solid line is the 300 mils thick sphere. The additional shielding added by the thicker shell significantly reduces the proton displacement dose received at the center of the sphere (at three thousand nmi, the thin shell receives approximately 5.5 times more radiation dosage than the thick shell, and 337 times that of the baseline orbit). The actual calculated values of radiation dose due to trapped protons for the various MEO altitudes with a reference line plotted with stars showing the baseline orbit value are shown in Figure 5. 4.

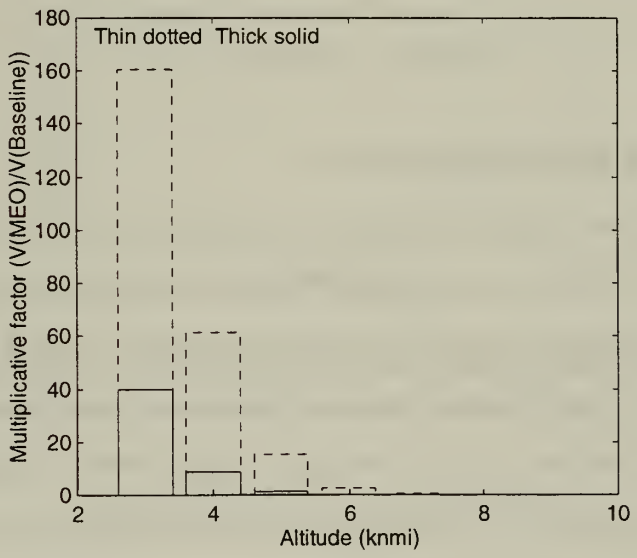

Figure 5. 3 Comparison of Trapped Proton Source Proton Displacement Doses at MEO Altitudes to Same Effect at Baseline Orbit

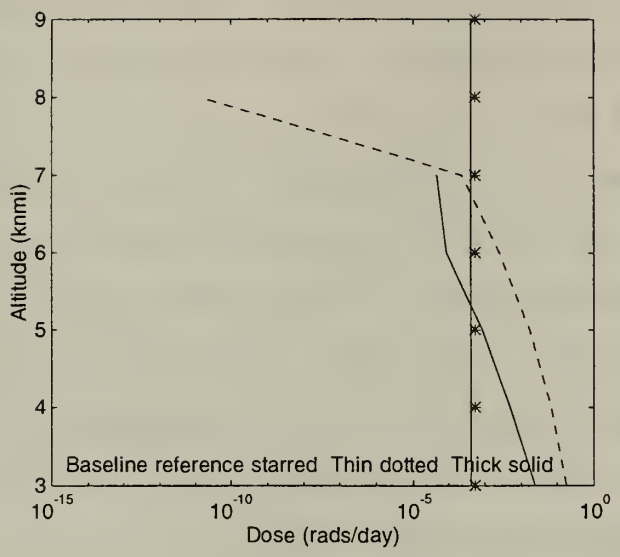

Figure 5. 4 Proton Displacement Dose from Trapped Protons at Various MEO Altitudes and Baseline Orbit

3. Solar Proton Radiation

The analysis was conducted using the JPL (Jet Propulsion Laboratory) 1991 model, a statistical model of solar proton fluences. It is based on an analysis of solar flare events between 1963 and 1991. This model is superior to previous models because it is based on a uniform data set and includes a wide energy range from 1 MeV to 60 MeV. Included in the data are the August 1972 event and several major events occurring in the 1989-1991 period.

In its published form, the JPL 1991 model defines five functions P[i](F,t), one for each energy E[i] = 1, 4, 10, 30, and 60 MeV. These functions are the probability that a solar proton event will occur with integrated fluence exceeding the threshold fluence, F(>E[i]), on a mission of duration, t. The form of the model presented in Space Radiation has been converted such that the functions, P[i](F,t), are now in the form, F[i](C,t). The new functions describe the solar proton fluence level, F[i](>E[i]), that will not be exceeded at a given confidence level,

C[i] (= 1 - Pi), on a mission of duration, t. The confidence level used in this analysis was 95%. The mission duration was one year.

The results are shown in Figure 5. 5 and Figure 5. 6. The dotted lines represent the data from the 100 mils thick sphere; the solid line is the 300 mils thick sphere; the reference line plotted with stars shows the baseline orbit value.

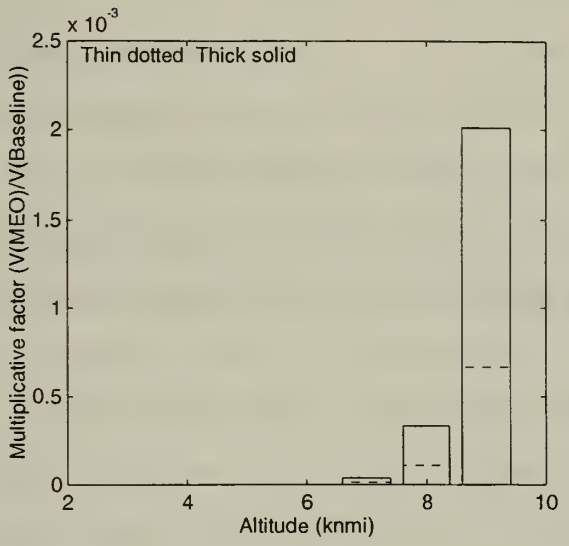

Figure 5. 5 Comparison of Solar Proton Source Proton Displacement Doses at MEO Altitudes to Same Effect at Baseline Orbit

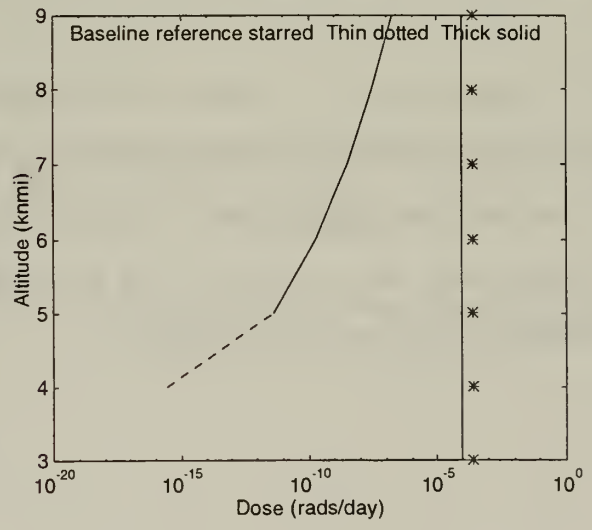

Figure 5. 6 Proton Displacement Dose from Solar Protons at Various MEO Altitudes and Baseline Orbit

The lower expected values can be attributed to the smaller inclination angle of the MEO orbits as compared to the baseline orbit (with a high inclination of 70°).

4. Solar Energetic Particle Radiation

Solar Energetic Particle (CREME) environments include protons and heavy ions originating in the sun. They are ejected in intense, but infrequent, solar flare events. Solar energetic particles typically have lower energy than cosmic radiation and trapped protons. Several solar energetic particle environments are defined in the Space Radiation software. Each event model generates the peak flux, or peak particle intensity, during a given flare event. Peak intensity is maintained for only a fraction of the event, i.e., an hour or two. The ordinary environment, which refers to a typical solar flare, was used in this analysis. The M values for the solar energetic particle models from CREME are indicated; however, there is a slight difference in treatment between Space Radiation and CREME. CREME adds the cosmic ray model at solar minimum (M=1) to each solar flare model. Space Radiation separates the two components. The ordinary model used here is (M5/M6 - M1).

As Figure 5. 7 and Figure 5. 8 show, the differences between the MEO orbits and the baseline orbit are quite small. The MEO orbits are actually expect to experience slightly less radiation effect due to solar energetic particles and solar flare protons, due to their lower inclination and the larger shielding effect near the equator.

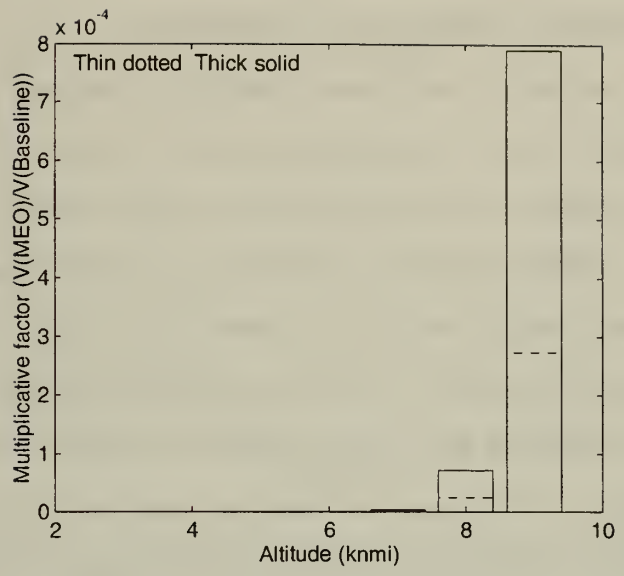

Figure 5. 7 Comparison of Solar Energetic Particle Source Proton Displacement Doses at MEO Altitudes to Same Effect at Baseline Orbit

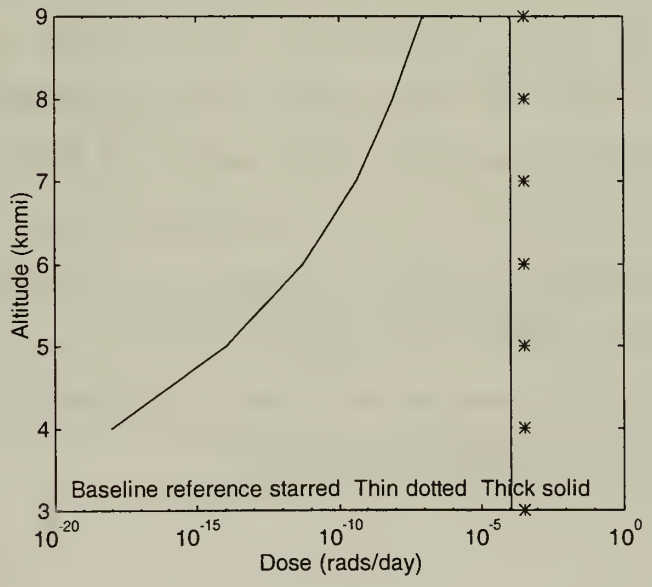

Figure 5. 8 Proton Displacement Dose from Solar Energetic Particles at Various MEO Altitudes and Baseline Orbit

5. Composite (All Source) Radiation

Once each separate case was analyzed, the data was combined to create a composite proton displacement effect dose. The resultant all-source radiation dose was then analyzed in the same manner as each component case. This composite radiation is not an absolute worst-case scenario, because each component was not taken to the extreme; however, it is biased towards a heavy radiation environment due to the solar minimum modeling and the inclusion of both solar flare and solar energetic particles. It is clear, as can be seen in Figure 5. 9, that the composite radiation dose strongly follows the trapped proton component.

The total proton displacement dose at higher MEO altitudes is evaluated as being significantly smaller than the baseline orbit proton displacement dose. This is primarily due to the difference in inclination between the two orbit schemes with the baseline orbit having an inclination of 70° and the MEO orbits having inclinations of 15°. The reduction in radiation dose experienced within the MEO schemes can be attributed to the distance from the Van Allen belts, a major source of geomagnetically trapped radiation. Figure 5. 10 illustrates the values for the thick and thin cases at the MEO altitudes and also includes a reference line for the baseline orbit thick shielding case (plotted with circles) and thin case (plotted with stars).

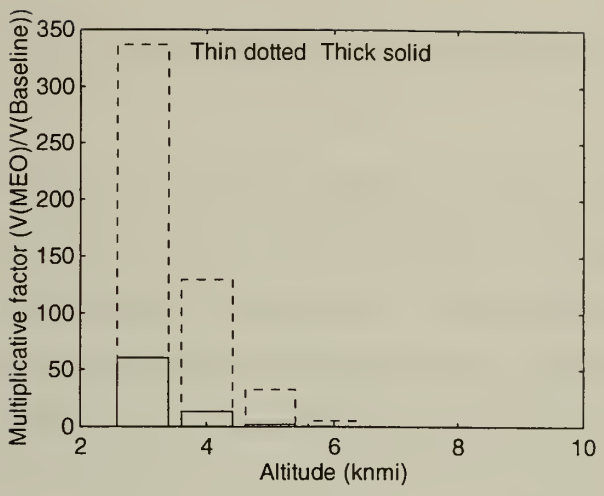

Figure 5. 9 Comparison of All Source Proton Displacement Doses at MEO Altitudes to Same Effect at Baseline Orbit

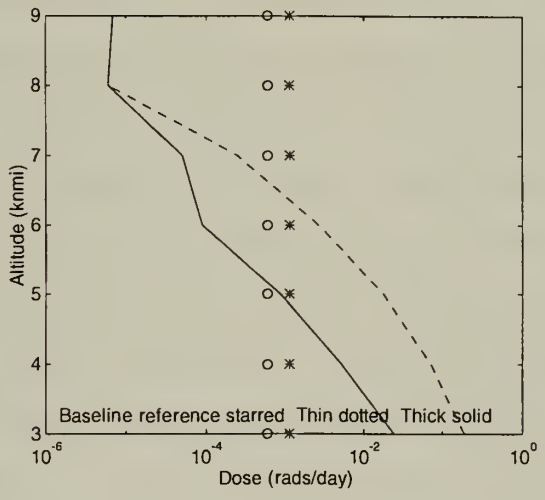

Figure 5. 10 Total Proton Displacement Dose (from All Sources) at Various MEO Altitudes and Baseline Orbit

C. SUMMARY

Proton displacement effect showed interesting characteristics. As can be seen the final figure of the chapter, Figure 5. 10, the higher MEO altitudes analyzed experience a more benign environment with respect to proton displacement damage than the baseline orbit. The fact that the orbits vary in inclination as well as in altitude should be remembered when considering this result.

VI. SOLAR CELL EFFECTS

Solar cell arrays are the most common power sources for satellites in orbit today. This fact makes all impacts upon the operation and lifetimes of solar cells of prime importance. This chapter discusses solar cell characteristics, reviews some important past research and presents the results of analysis using Space Radiation 4.0.

A. INTRODUCTION

If a photon of the proper frequency enters an n-p semiconductor, the photon may be absorbed by an atomic electron, which will then have sufficient kinetic energy to escape the electrical attraction to its nucleus. For silicon, the intrinsic ionization potential is 3.6 eV, which corresponds to a wavelength of 0.345 μm. Consequently, a solar cell can be viewed simply as an n-p or p-n semiconductor, called a photodiode.

Exposing a solar cell to the sun's visible radiation produces a number of ionizations per unit volume. Blue light is 99 percent absorbed within 0.2 microns of the surface of the solar cell, in the n-type material thickness (assuming a n-p type solar cell). Red light must travel about 200 microns, into the p-type material thickness before being 99 percent absorbed. Once the photon energy has been used to ionize atoms in the material, the resulting electrons act as free charge carriers and can contribute to the current flow. The majority of the electrons are liberated deep within a cell and diffuse through the material until they are either recaptured by an ionized atom or reach the n-p junction. If the electron is recaptured, the energy used to generate it is lost and appears as heat. If the electron reaches the junction, however, it is accelerated into the n-type material. Because the n-type material has relatively few atoms

capable of capturing the electron, the electron will continue to move toward the surface of the cell. If electrical leads are placed on the surface, this flow of electrons can be drawn off as current flow, which can be used to power a spacecraft.

As previously mentioned, a single cell generates a potential difference of about 1 volt and a current of a few mA. By connecting the cells in series, a potential difference of a desired voltage can be generated; by increasing the number of strings (serially connected cells) placed in parallel, additional current is produced. Typical efficiencies of silicon solar cells are about 12 percent, gallium arsenide efficiencies are about 15 percent. So, roughly 85 percent of the incident solar energy is lost in the form of heat.

As radiation interacts with a solar cell it will produce ionizations and atomic displacements. If an orbital electron in the coverglass becomes ionized, it may diffuse through the coverglass and become trapped by an impurity atom to form charge defect called a color center. As a result, the transparent material becomes darkened. If an ambient atom is displaced by the radiation, the structure of the lattice is altered and the average distance that an electron can diffuse before being deflected by the lattice defect is decreased. As the diffusion length, the mean free path, decreases, fewer electrons can make it from the interior of the cell to the n-p junction. Consequently, the current, voltage, and power produced by the cell are decreased. The effects of radiation on solar cells, solar cell covers, and other array materials are briefly discussed in the following paragraphs.

1. Effects on Solar Cells

Solar cell radiation damage does not constitute a mechanical damage, but rather a nearly permanent degradation of the cell's energy

conversion efficiency capability. Solar cells in orbit are damaged mainly due to irradiation with electrons and protons. In lower earth orbits both geomagnetically trapped electrons and protons may be of significance, while at higher altitudes (such as at or near synchronous altitude) during periods of high solar activity solar flare protons may add significantly to the total cell-damaging fluence. The radiation environments are responsible for solar cell degradation both during transfer orbits and on-station orbits.

The radiation particles of significance to solar damage have approximately the following energy ranges when they impinge on the solar cell covers:

a). Electrons - 0. 2 to 1 MeV

b). Protons - 4 to 40 MeV

The actual radiation environments seen by the solar cells differ from the naturally existing environment because of the following:

a). The energy-flux spectra of the natural radiation environments are modified by the solar cell radiation shields.

b). Cells receive radiation both through the front shield (coverglass) and the back shield (substrate), i.e., the radiation environment seen by the solar cells is in part design related.

A distinctly different and separate damage mechanism from the bulk damage mechanism discussed above may occur due to low energy protons (having energies in the order of hundreds of keV) impinging on small solar cell areas that are not adequately protected by glass, adhesive, or metallization. This so-called low-energy proton damage may be severe.

2. Effects on Solar Cell Covers

Solar cell covers are discolored (darkened) by particulate radiation, thereby absorbing some of the sunlight. This increased light absorption reduces solar cell output by two mechanisms:

a). Loss in illumination of the cell

b). Increased array operating temperature and hence a decrease in cell efficiency.

The loss in illumination and, hence, power output due to earth' s charged particle radiation can be estimated for circular orbits by first using the environmental data (converted into deposited energy in fused silica) and then consulting the cover transmission loss data.

It is important to note that test data from radiation exposure in the presence of air and in a vacuum environment indicates that radiation damage is reduced considerably in vacuum. This is explained by the fact that the presence of an oxidizer in the environment causes oxidation of ionized polymers which results in greater alteration of the molecular structure than in a chemically inert (vacuum) environment. Inert atmospheres available in the laboratory having an oxygen content as high as 1 part per million may be insufficiently pure for such tests. Vacuum of less than 10^{-6} torr (1.3×10^4 N/m^2) is usually mandatory. (Tada, 1982)

3. Other Solar Cell Array Materials

Solar cell array materials and components in addition to solar cells and covers which of special interest to radiation damage studies (in regard to both mechanical and electrical characteristics) include:

a). Electrical insulation of wires, terminals, connectors, and between the solar cells and a metallic substrate

b). Adhesives, both exposed and lightly shielded

c). Blocking diodes, shadow bypass diodes, Zener diodes, and temperature transducers.

4. Particulate and Ultraviolet Radiation Combined

In most practical satellite orbits, corpuscular and ultraviolet radiation exists simultaneously. Divergent views exist regarding the effect of such combined radiation on solar cell assemblies. One view, supported by ground testing is that ultraviolet exposure bleaches some of the darkening induced by corpuscular radiation. The other view, supported by comparing ground test data with orbital data, holds that the simultaneous combined exposure causes greater darkening than each exposure alone. However, the data of the very few ground tests which have been performed is in question, orbital data analysis is not very accurate, and the darkening mechanism is not fully understood at this time.

B. Solar Cell Damage

Irradiation of solar cells with electrons, protons, neutrons, and other particles causes permanent mechanical damage at the atomic level within the solar cell. Generally, protons and neutrons cause greater degradation in the cell power and voltage output capabilities than electrons. This damage impacts most solar cell parameters. Degradation is found in:

a). Short-circuit current output

b). Open-circuit voltage output

c). Maximum power output

d). Energy conversion efficiency

e). Spectral response (at the long wavelengths).

Changes in other parameters are found to affect temperature coefficients, series resistance and the I-V curve shape.

The magnitude of the I-V curve degradation with radiation, in general, depends upon the following:

a). Solar cell wafer thickness and presence or absence of electric drift fields in the cell

b). Solar cell minority carrier lifetime (initial and after irradiation)

c). Solar cell base resistivity and silicon material parameters, (initial)

d). Particle type (mass and charge)

e). Particle kinetic energy (usually expressed in units of electron-volts)

f). Cell temperature (while being irradiated)

g). Cell temperature/time profile during which damage annealing may take place

h). Previous exposure to radiation (accumulated-fluence or damage

i). Illumination level during or after irradiation (photon-induced damage).

1. Damage Equivalent 1-MeV Fluence

For analytical and test convenience, the concept of "damage-equivalent, normally-incident (DENQ), monoenergetic, 1-MeV Fluence," or in brief, 1-MeV fluence, has been developed. The actual damage produced in solar cells by electrons of various energies is related to the damage produced by 1-Me V electrons by the damage coefficients for electrons. Similarly, the damage produced by protons of various energies is related to the damage produced by 10-MeV protons by the damage coefficients for protons. The damage produced by 10-MeV protons is, in turn, related to the damage produced by 1-MeV electrons by a single

damage conversion factor. One 10-MeV proton does approximately the same damage as 3,000 1-MeV electrons (numbers ranging from 2,000 to 7,000 have been used, but this thesis preserves the first convention).

2. Electron Damage

Electrons damage solar cells such that a single value of equivalent 1-MeV fluence can be used to describe the degradation of cell currents and voltages.

3. Proton Damage

Protons (and other heavy particles) damage solar cells such that two different values of equivalent 1-MeV fluence must be used; one value is used to describe the degradation of cell currents and another value is used to describe the degradation of cell voltages.

a. Low Energy Proton Damage

Low energy proton damage is as being restricted to that damage mechanism which causes shunting of the p-n junction; thereby the low energy proton damage mechanism can be treated separately from and becomes independent of minority carrier lifetime considerations. Low energy proton damage can occur in one of two ways:

a). From medium or higher energy protons having sufficient energy to just penetrate the solar cell covers or contact metallizations

b). From lower energy protons incident directly on the solar cells in small gap areas that are not protected by the solar cell covers or contacts.

The number of protons that can be expected to penetrate solar cell covers is usually of no significance in most orbits except in those which are in the radiation belts. However, the number of low energy protons

that can potentially damage solar cells directly are available in great abundance not only in the radiation belts, but also above them and at synchronous altitude. The proton energy levels of concern are in the 100 to 500 keV range when incident on the silicon front surface, and up to approximately 5 MeV when incident on the front of coverglass.

Protons which come to rest (i. e., lose all their energy) near the solar cell p-n junction introduce shunt paths across the junction. These shunts cause the cell output to degrade significantly more than the ratio of the damaged cell area to the total cell area may indicate. The shunt defect induced by low energy protons has a diode-like current-voltage characteristic that leads to a relatively small loss in I_{SC} and to progressively larger losses toward P_{MAX} and V_{OC}.

The low energy proton damage mechanism was discovered on several satellites in synchronous orbit, and was verified by extensive ground testing. Excessive orbital degradation due to low energy proton damage had been as large as approximately 20 percent. The results of numerous investigations with regard to low energy proton damage in geosynchronous orbit can be summarized for design purposes as follows:

a). Even small unprotected areas (on the order of 1 percent) can lead to excessive output degradation (on the order of 10 percent at P_{MAX})

b). Small unprotected strips of cell area parallel to the n-contact collector bar are several times more damaging than unprotected strips away from the n-contact.

c). The entire active cell area not covered by metallic contacts should be protected by the coverglass. (Tada, 1982)

C. Radiation Damage Annealing

In general, the crystalline damage and associated electrical degradation sustained by a solar cell during exposure to corpuscular radiation is not totally stable. Two phenomena have been observed on irradiated cells: damage annealing and further degradation during exposure to sunlight.

Damage annealing occurs only at temperatures above approximately 20°C, and tends to be more significant for proton and neutron irradiated cells than for electron irradiated cells. The observed magnitude in recovery of the solar cell power output after 1 MeV electron irradiation ranges from zero to a few percent (typically less than 5 percent). Higher annealing temperatures (up to approximately 100°C) accelerate the annealing process, but do not appear to change the amount of possible recovery. Analysis of orbital flight has verified that a part of the solar cell output lost due to solar flare proton events is regained after some time. This effect was not modeled in this thesis.

D. Photon Effects

Solar cells that have sustained electrical degradation during irradiation with electrons may either degrade further or recover during subsequent long-term illumination (photon irradiation). A further electrical degradation can be expected in all solar cells fabricated from float-zone refined silicon that was typically used in Europe during the 1960's and early 1970's. The discovery of the photon degradation mechanism is credited to Crabb (1972); he found the following photon degradation after 1-MeV electron irradiation:

a). After 6×10^{13} e/cm^2 : 3.7 percent I_{sc} degradation

b). After 2.2×10^{15} e/cm^2 : 8.5 percent I_{sc} degradation

Comparative, controlled experiments by Fischer and Pschunder (1973) verified the photon degradation process in float- zone silicon cells and found a damage annealing process in crucible-grown silicon cells. Furthermore, these experiments identified both reversible and irreversible instability problems in both unirradiated and irradiated solar cells, which may have an impact on the ultimate solar cel1 calibration accuracy than can be achieved. The conclusions are:

a). Light (photon) induced degradation occurs in 1 ohm-cm, crucible grove n-on-p silicon cell after 12 hours at one solar constant (before particle irradiation) as follows:

1). I_{SC} degradation: l. 8 percent

2). V_{OC} degradation: l. 3 percent

3). P_{MAX} degradation: 3. 2 percent

b). Because the 1 ohm cm, crucible-grown silicon cells are unstable, they should not be used as standard solar cells.

c). The light (photon) induced degradation in the output of 1 ohm-cm and 10 ohm- cm float-zone silicon and of 10 ohm-cm crucible-grown silicon cells (before particle irradiation) is typically less than 1 percent.

d). The photon degradation causes a loss in both the minority carrier lifetime and the cell's red response. This leads to the conclusion that lifetime is not a constant material property as heretofore assumed. but rather depends strongly on thermal and light exposure history of the material.

e). Photon irradiation immediately after 1-MeV electron irradiation to a fluence of 1×10^{15} e/cm^2 resulted in the further degradation of 10 ohm-cm float-zone and 1 ohm-cm crucible grown silicon cells, but led to recovery of the 10

ohm-cm crucible-grown and 1 ohm-cm float-zone silicon cells.

E. Analysis of Damage Equivalent Radiation Dose to Solar Cells

For convenient calculation of solar cell performance degradation in a corpuscular radiation environment and simplified laboratory radiation test methods, the concept of "normally incident damage equivalent 1-MeV fluence" was used. Particulate radiation damage to solar cells is dependent on the energy and type of the particle. Conversion into 1-MeV fluence utilizes equivalent damage coefficients. Solar cell damage coefficients for silicon (Si) and gallium arsenide (GaAs) were computed.

Fused silica coverglass thicknesses of 3 mils and 6 mils, as well as the case of no coverglass at all, were investigated. The nominal density of fused silica was taken as 2.2 g/cm^2. Both trapped proton and trapped electron exposure were found. Also considered was the probability and resulting exposure to a large solar proton event (JPL 1991). Proton damage depends on the operational state of the solar cells. Short-circuit current (I_{SC}), open-circuit voltage (V_{OC}), and maximum power (P_{MAX}) results are reported.

Exposure of both sides of the solar cell to radiation must be factored in the total radiation exposure. The backside exposure is computed by estimating the thickness of aluminum (or other materials) shielding the back of the panel. The total solar cell damage coefficient is the sum of the front and back exposures. As this analysis is comparative, and the effects of backshielding would cancel out, assuming each cell was mounted on the same type of substrate, backside exposure was not considered in these calculations.

The calculations are based on data from the JPL Green Book containing 1 MeV electron/proton equivalents for electrons/protons of various energies behind several coverglass thicknesses and were executed using Space Radiation 4.0.

The first several figures show the damage in 1-MeV fluence from trapped protons at the various MEO altitudes on gallium arsenide and silicon solar cells. All three effects (upon V_{OC}, P_{MAX}, and I_{SC}) of gallium arsenide solar cells can be seen in Figure 6.1. A corresponding plot for the unprotected silicon cell is shown in Figure 6. 2.

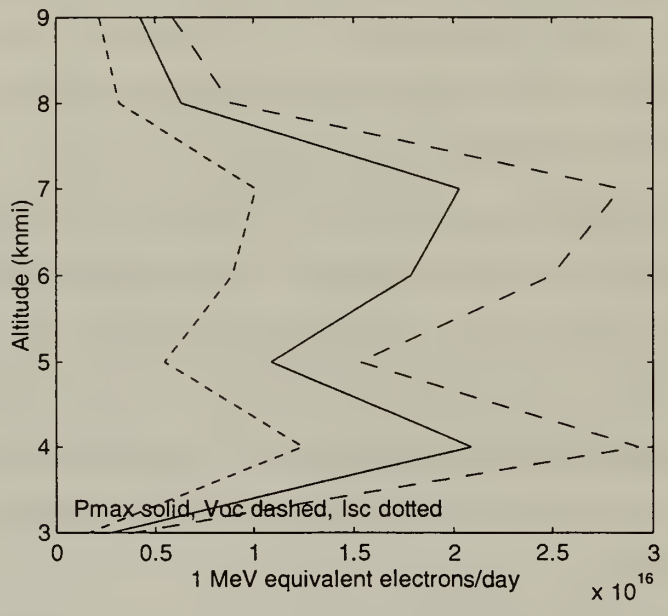

Figure 6.1 Damage to GaAs Solar Cells from Trapped Protons : No Coverglass

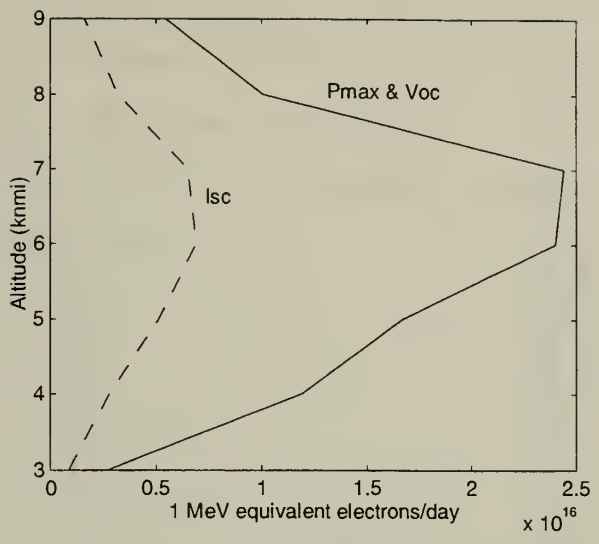

Figure 6. 2 Damage to Silicon Solar Cells from Trapped Protons: No Coverglass

In Figure 6. 3, the effect on I_{SC} of all three configurations of silicon solar cells (no coverglass, fused silica coverglass of three mils thickness, and fused silica coverglass of six mils thickness) are plotted. The benefits of coverglass can be seen easily in this graph (note the semilogarithmic axes). The red reference line is the same effect on GaAs solar cells without coverglass (i.e., the far left line in Figure 6.1). The effects upon P_{MAX} and V_{OC} are shown in Figure 6. 4, again with a red gallium arsenide reference line; the yellow reference line is the silicon unprotected solar cell I_{SC} effect.

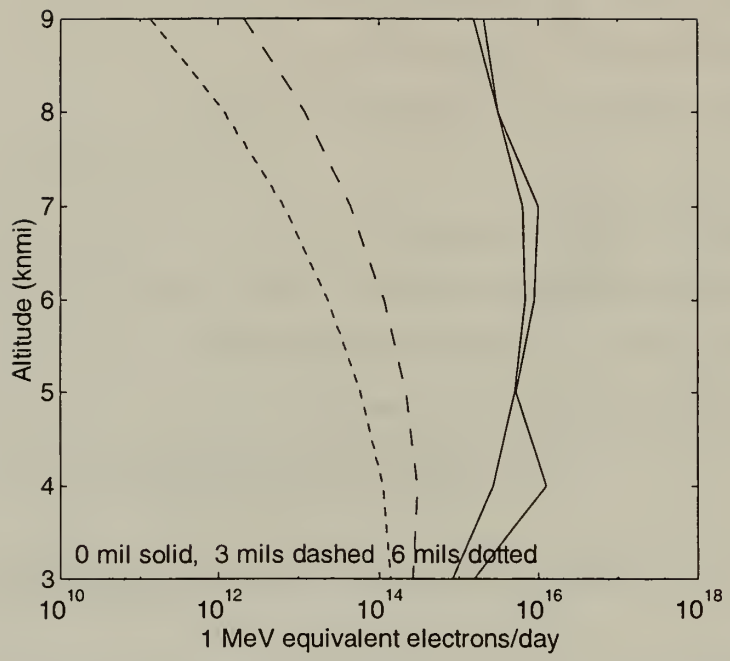

Figure 6. 3 Damage to Silicon Solar Cells from Trapped Protons : Isc

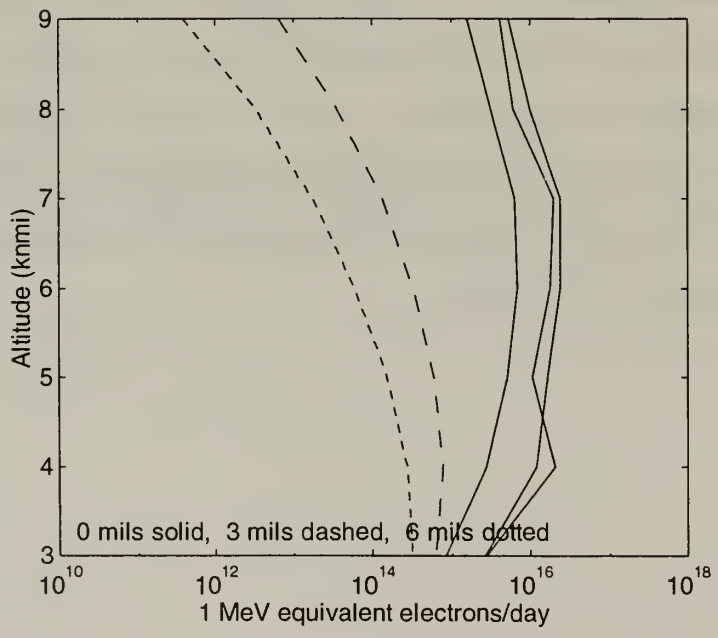

Figure 6. 4 Damage to Silicon Solar Cells from Trapped Protons : P_{MAX}, V_{OC}

The difference between the responses of V_{OC}, P_{MAX}, and I_{SC} in silicon solar cells can be seen in Figure 6. 5. The next figure, Figure 6. 6, clearly illustrates the effectiveness of the additional three mils of fused silica coverglass, especially at the lower MEO altitudes where the inner Van Allen belt is a concern.

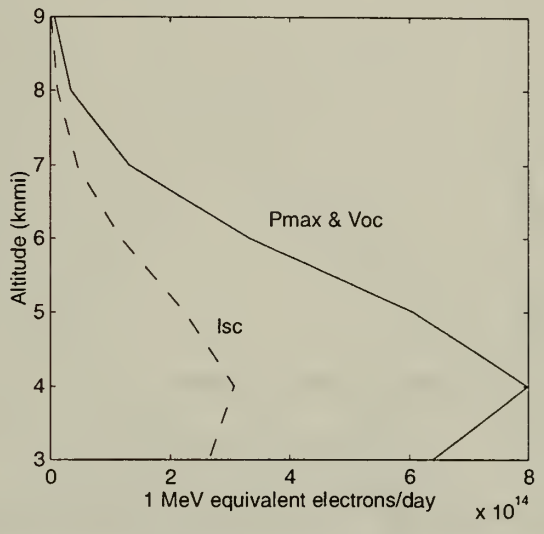

Figure 6. 5 Damage to Silicon 3 mils Coverglass Solar Cells from Trapped Protons

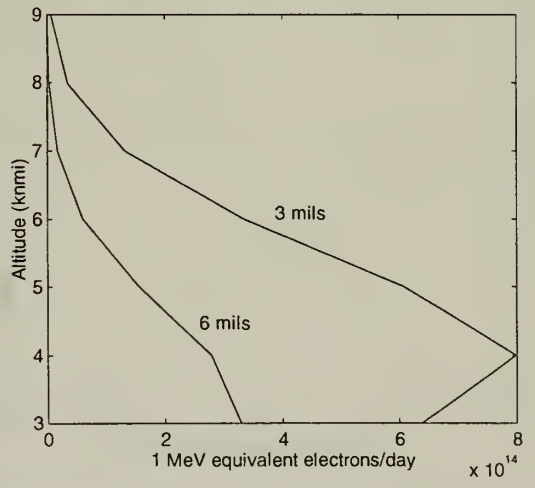

Figure 6. 6 Damage to Silicon Solar Cells from Trapped Protons: P_{MAX}

The interesting responses of the gallium arsenide solar cell's parameters, V_{OC}, P_{MAX}, and I_{SC}, to a solar proton event (the JPL 1991

model) are plotted in Figure 6. 7. Note the logarithmic scale of the radiation axis. A similar plot for silicon cells, all three configurations, is presented in Figure 6. 8, which demonstrates the relative ineffectiveness of coverglass against solar protons.

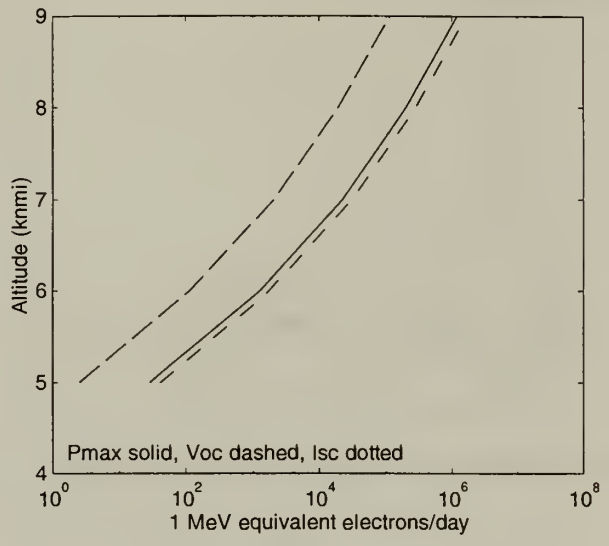

Figure 6. 7 Damage to GaAs 3mil coverglass Solar Cell from Solar Protons (JPL1991)

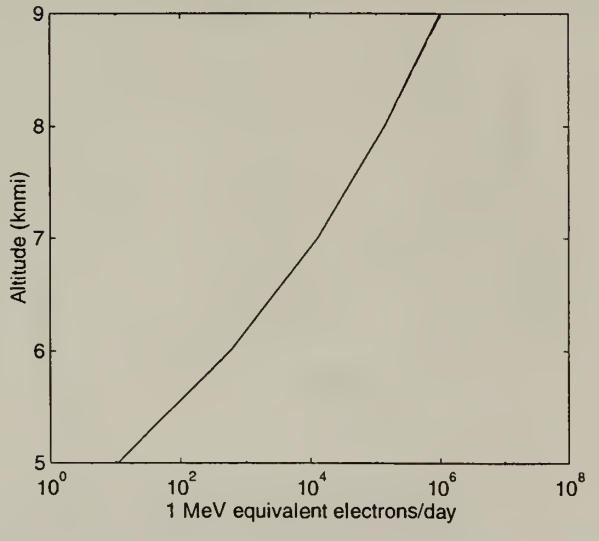

Figure 6. 8 Damage to Silicon Solar Cells from Solar Protons (JPL1991)

Trapped electrons' effects on solar cell parameters are plotted in Figure 6. 9 and Figure 6. 10, for gallium arsenide and silicon,

respectively. The greater damage from electrons to silicon solar cells as compared to gallium arsenide solar cells, as well as the advantage of coverglass, are obvious in these graphs. The green reference line (far right) in Figure 6. 9 is the effect upon silicon solar cells.

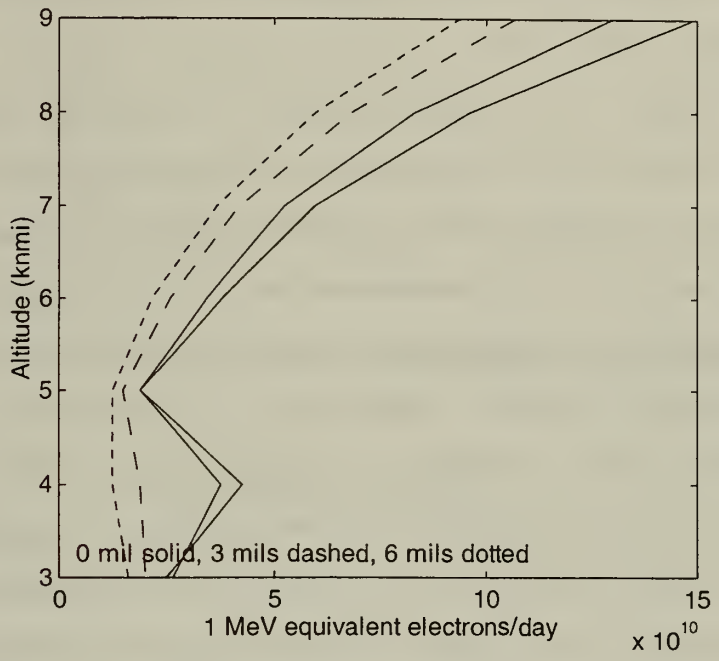

Figure 6. 9 Damage to GaAs Solar Cell from Trapped Electrons

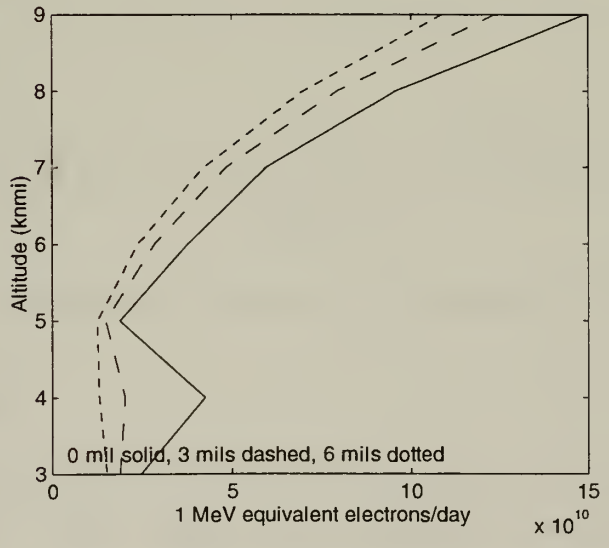

Figure 6. 10 Damage to Silicon Solar Cells from Trapped Electrons

The following graphs represent the results of the analysis of the composite solar cell degradation. The graphs are a comparison of the degradation at the various Mid Earth Orbit (MEO) altitudes to the baseline orbit of 400 nmi. This was simply accomplished by dividing the MEO altitude composite solar cell degradation dose rate by the baseline orbit composite dose rate. The resulting number, termed the multiplicative factor, was plotted against the respective MEO altitude. Figure 6. 11 shows the comparison of unprotected silicon solar cell degradation rates, for P_{MAX} and V_{OC} and I_{SC} with a reference line plotted for gallium arsenide, no coverglass solar cell degradation. Gallium arsenide degradation is significantly less than degradation of silicon, as expected. Gallium arsenide degradation, of unprotected, three mils coverglass and six mils coverglass configurations, is further illustrated in Figure 6. 12. Each degradation was divided by the corresponding case at baseline: please note that the results do not indicate that gallium arsenide unprotected solar cells have lower degradation than the three mils coverglass solar cells; instead, the degradation of the unprotected solar cells is of a closer magnitude to the baseline case than the six mils coverglass case.

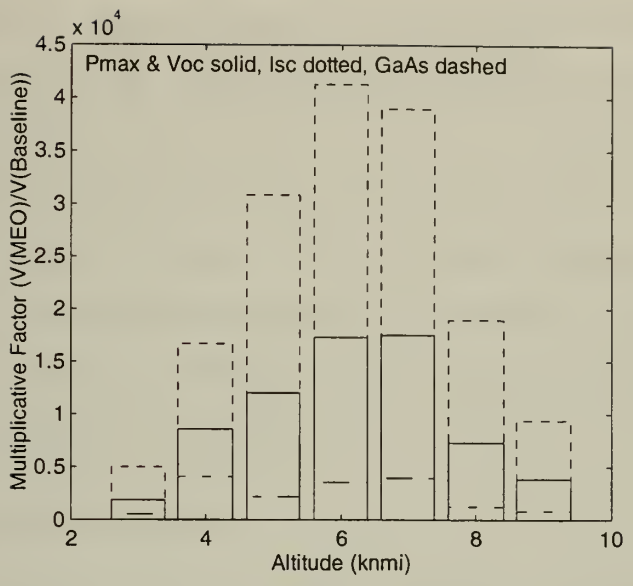

Figure 6. 11 Comparison of Silicon Solar Cell Degradation at MEO to Baseline

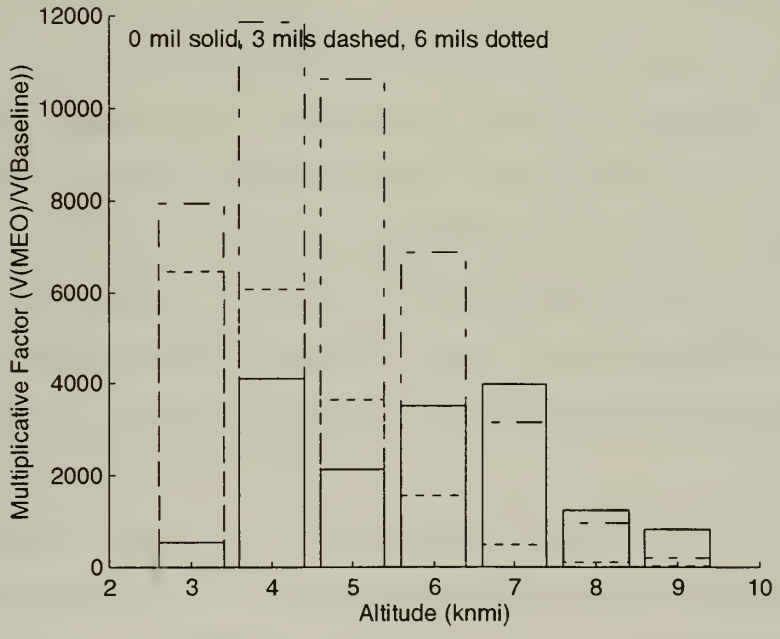

Figure 6. 12 Comparison of GaAs Solar Cell Degradation at MEO to Baseline

F. SUMMARY

This chapter discussed the theory of solar cells and reviewed past research on the topic and then presented results. The results demonstrate that solar cell degradation remains a major concern, with

significantly higher values than the baseline orbit. The improvement to be gained by using gallium arsenide solar cell, generally accepted as more radiaiton tolerant, was proven through this analysis.

VII. RADIATION DOSE

This chapter discusses the uses of dose depth curves and the importance of radiation dose. The necessary amount of shielding to reach a desired internal radiation dose is presented. The baseline orbit and the MEO cases are developed in a component fashion, and then combined for a total radiation dose.

A. DOSE DEPTH CURVES

Intense radiation environments degrade electronic systems and materials by ionization. Total dose is the energy deposited per unit mass of material by particle ionization. It is closely correlated with permanent degradation of microelectronic components. Typical irradiations are thousands of high-energy particles per square centimeter per second. A single high-energy particle initiates thousands of bond-breaking molecular collisions. Electron secondaries from these collisions cause additional disruption. In these environments, one may imagine that electron collisions occur uniformly over a small material volume. The ultimate effect of these collisions is conveniently characterized by the energy deposited in that volume.

Radiation dosage can be expressed either in terms of the exposure dose, which is a measure of the radiation to which a material is exposed, or in terms of the absorbed dose, which is a measure of the energy absorbed by the radiated material. Radiation dose is used here following the second definition. The most commonly used units of dose are rads; the official SI units are Gray (Gy).

a). $1 \text{ rad} = 6.24 \times 10^7 \text{ MeV/g}$.

b). $1 \text{ Gy} = 6.24 \times 10^{12} \text{ MeV/kg}$.

Total dose damage can often be mitigated by radiation shielding. Shielding can absorb much of the energy of incoming particles. This is particularly true in environments with steep energy spectra. A dose-depth curve gives us much of the information about the effectiveness of shielding for radiation protection.

B. RESULTS

First the results for the baseline orbit will be presented direcdtly as output from the Space Radiation 4.0 software; then, the results from the analysis of the baseline orbit as compared to the MEO cases are presented.

1. Baseline Orbit

The following graphs, Figure 7. 1, Figure 7. 2, and Figure 7. 3, show the baseline orbit dose depth curves; these graphs are plotted in depth units of millimeters Aluminum (mm Al) and a dose rate of rads/day. They were calculated taking into account geomagnetically trapped radiation as well as solar proton radiation environments. Each component has been separated for these dose depth curves.

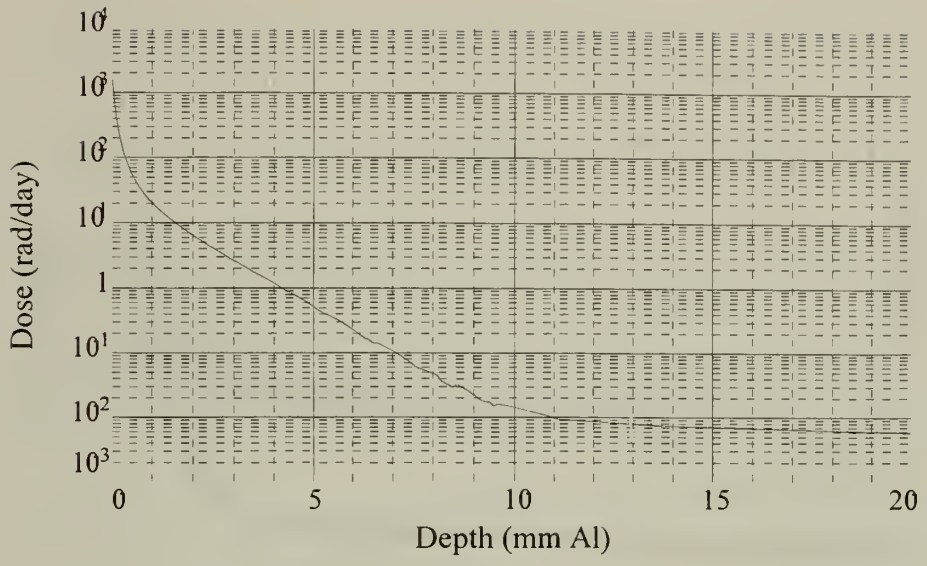

Figure 7. 1 Dose Depth Curve for Trapped Electrons: Baseline Orbit

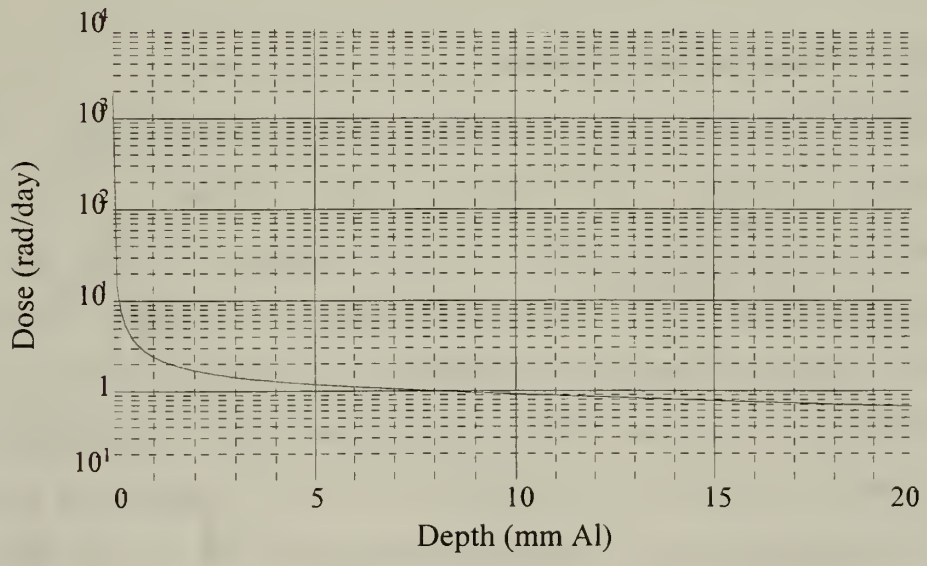

Figure 7. 2 Dose Depth Curve for Trapped Protons : Baseline Orbit

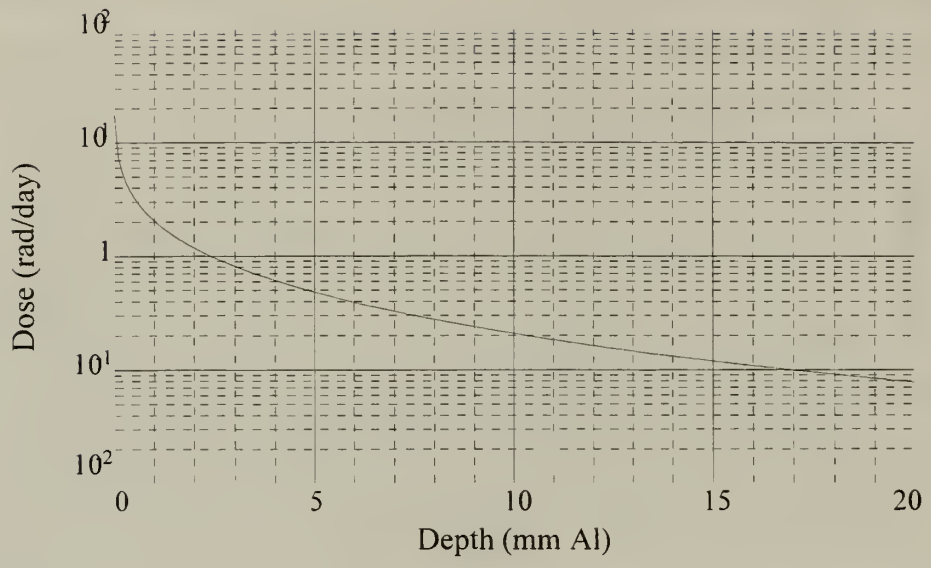

Figure 7. 3 Dose Depth Curve for Solar Protons : Baseline Orbit

2. Medium Earth Orbits

The MEO orbits analyzed remain the same as previously. They are a family of circular, 15° inclined orbits stationed in 1,000 nmi increments, beginning at 3,000 nmi and ending at 9,000 nmi. The following graphs are coded with the following convention. The starred line is the reference line for the baseline orbit values. Solid lines are even thousand nmi altitude MEO orbit values, and dotted lines are the odd thousand nmi altitude MEO orbit values. The data is now plotted in depth units of grams/cm^2 of Aluminum; dose remains in rads/day.

Figure 7. 4, and its companion close view found in Figure 7. 5, shows the dose depth curves for radiation resulting from the electron component of the geomagnetically trapped radiation. The higher altitude lines are plotted closer to the top of the graph. It is easily seen that the predicted radiation dose for the MEO orbits is significantly higher than the baseline orbit, and even with a correspondingly larger amount of shielding, the higher radiation level would persist.

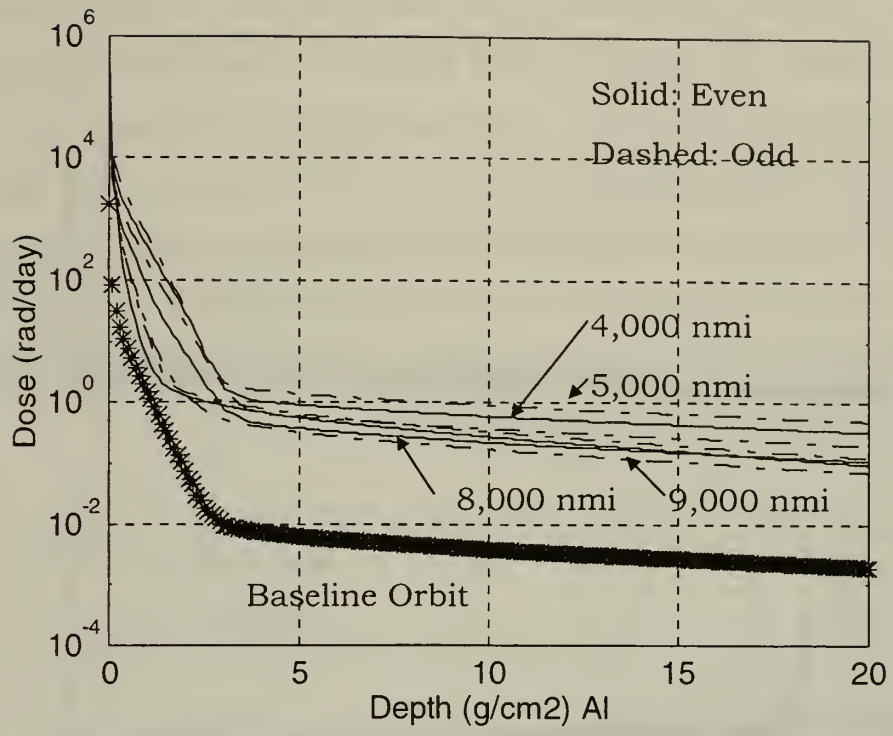

Figure 7. 4 Dose Depth Curves for Trapped Electrons : Various Altitudes

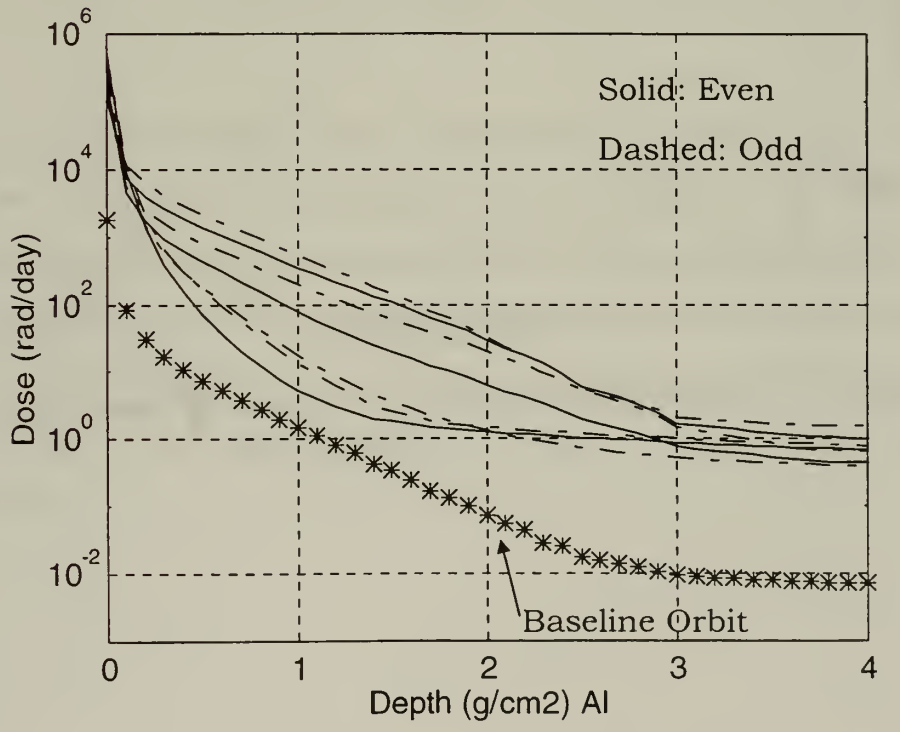

Figure 7. 5 Dose Depth Curves for Trapped Electrons : Close View

The trapped proton dose depth curve shows a slightly different predicted result. In Figure 7. 6 and Figure 7. 7, the lower altitudes plot nearer the tops of the graphs. It can be observed that the trapped proton environment drops off precipitously in the 9,000 nmi through 6,000 nmi altitudes, with correspondingly less shielding necessary at a certain dose level. The lower MEO altitudes, however, experience worse radiation than the baseline orbit and would necessitate more shielding to reach an equivalent dose level to the baseline orbit.

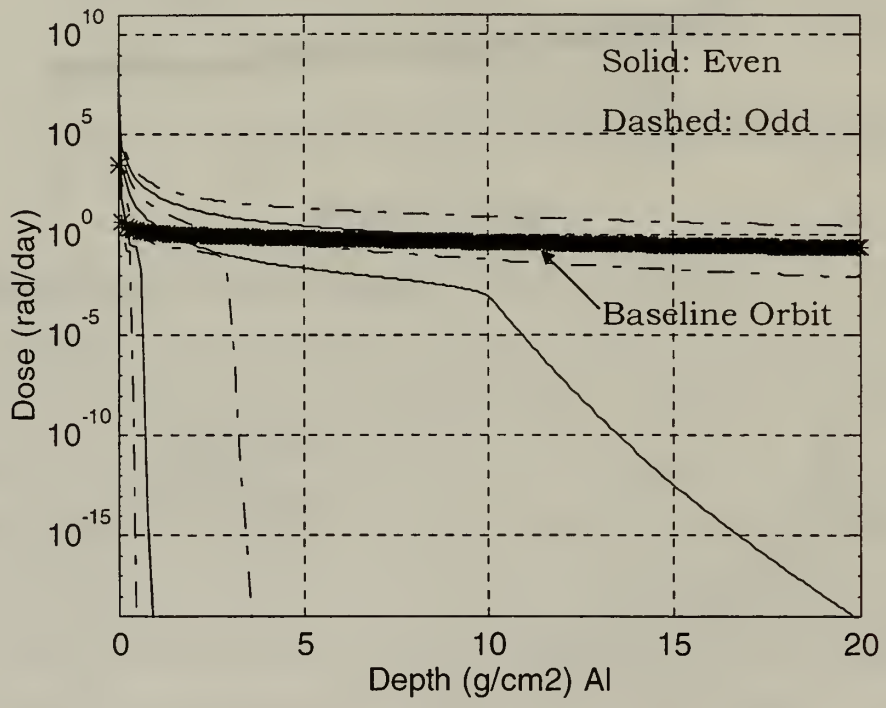

Figure 7. 6 Dose Depth Curves for Trapped Protons : Various Altitudes

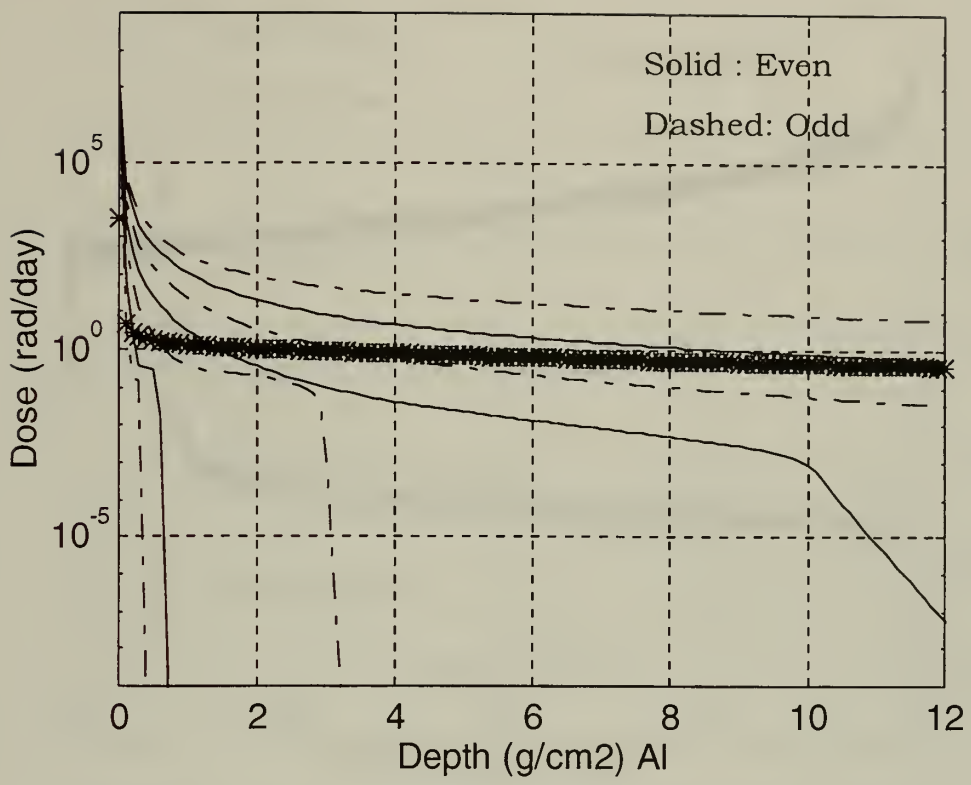

Figure 7. 7 Dose Depth Curves for Trapped Protons : Close View

The graph for solar proton radiation dose depth curves, Figure 7. 8, shows the effects of the equatorial shielding on the MEO orbits. Despite their higher altitudes, the MEO orbits experience lower effects than the baseline orbit, which has a solar radiation intensive inclination of 70°. The magnitude of the solar radiation components is much smaller than the geomagnetically trapped radiation (by orders of magnitude).

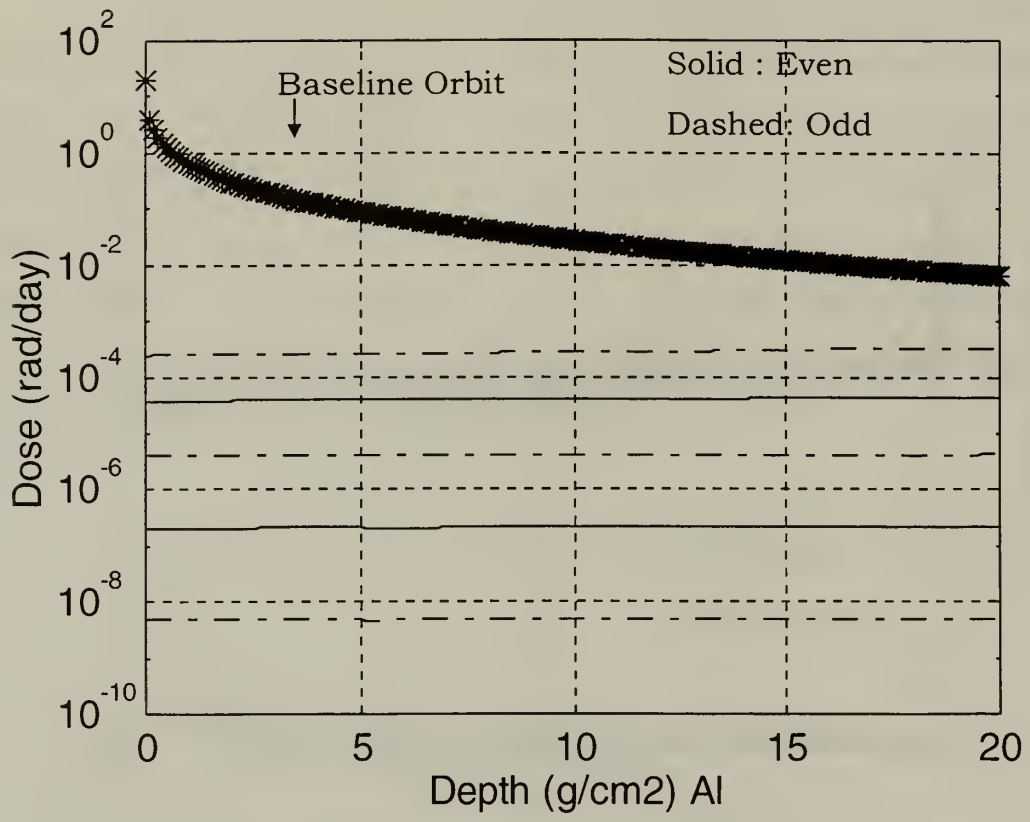

Figure 7. 8 Dose Depth Curves for Solar Protons : Various Altitudes

The data from the above three components-- geomagnetically trapped radiation, both electron and proton, and solar proton radiation-- were compiled into a total dose depth curve. This predicted composite dose depth curve closely follows the trapped electron curve, which is the largest component.

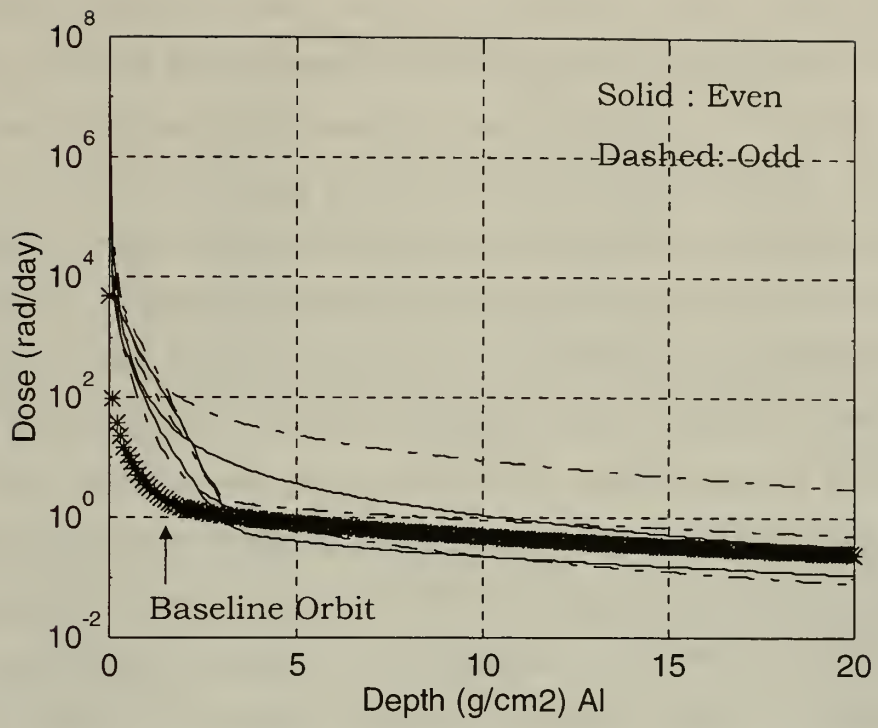

Figure 7. 9 Composite Dose Depth Curves : Various Altitudes

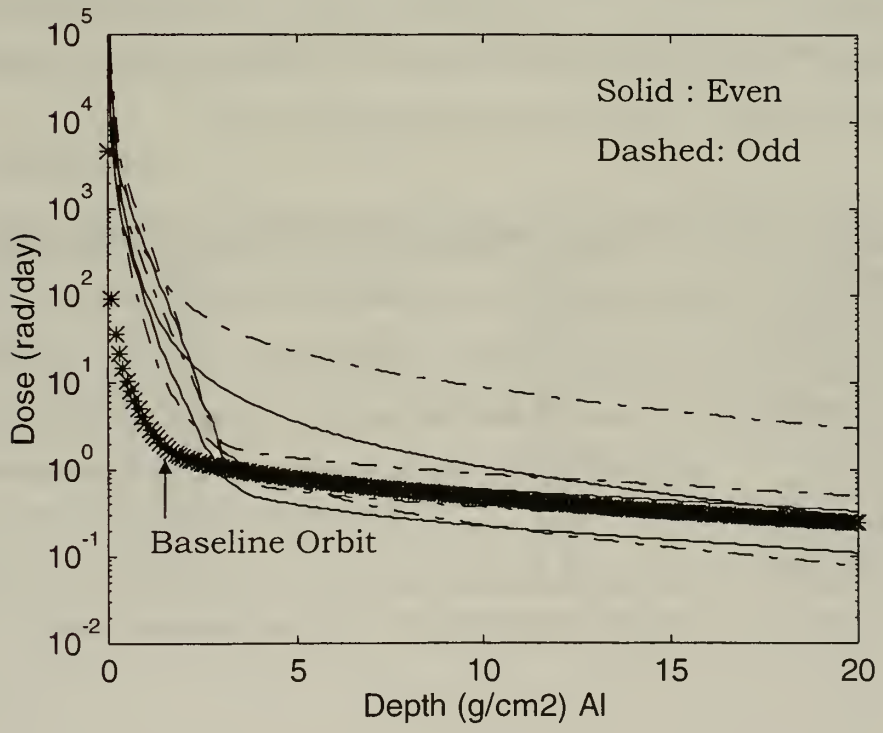

Figure 7. 10 Composite Dose Depth Curves : Close View

The depth units expressed in g/cm^2 allow weight comparisons among the orbits to be made easily. For example: if a desired radiation dose rate is set as 1 rad/day, the corresponding shielding dose depth necessary to reach that level of radiation is given by Table 7. 1. This simplified calculation shows that in most MEO orbits, more shielding is necessary to reach an equivalent level of internal radiation environment. It also demonstrates that some orbits would require less shielding to achieve the 1 rad/day radiation dose rate, and these orbits can be thought of as a more benign environment than the baseline orbit. The level of 1 rad/day is quite low, and most satellites would not need to meet such stringent requirements. Table 7. 2 and Table 7. 3 (both after Tribble, 1995) lists total dose tolerances for several technologies. For a mission life of 10 years, the total radiation dose received at a rate 1 rad/day would be only on the order of 3×10^3 rads, a level which many components can tolerate. Thus, a more specific analysis would need to be conducted to figure the actual values of added shielding necessary. The values in Table 7. 1 are only comparatively valid.

Orbit	Mass Required ($g/cm^{2)}$	Percentage of Baseline
Baseline	3.2	100 %
3,000 nmi	20	625 %
4,000 nmi	10.4	325 %
5,000 nmi	3.8	119 %
6,000 nmi	2.9	91 %
7,000 nmi	3.4	106 %
8,000 nmi	4.2	131 %
9,000 nmi	8.4	263 %

Table 7. 1 Mass Comparisons for 1rad/day Radiation Level

Technology	Total Dose Rate (rads Si)
CMOS	10^3 - 10^6
MNOS	10^3 - 10^6
NMOS	10^2 - 10^4
PMNOS	10^3 - 10^5
ECL	10^7
I^2L	10^5 - 10^6
TTL/STTL	>10^6

Table 7. 2 Total Dose Thresholds for Various Electronic Technologies (from Tribble, 1995)

Material	Usable Dose	Limited Use Dose
Teflon	2 x 10^4	3 x 10^4
Nylon	3 x 10^5	5 x 10^5
Polyethylene	1 x 10^7	6 x 10^7
PVC	1 x 10^7	1 x 10^8
Mylar	3 x 10^6	7 x 10^7
Kapton	2 x 10^8	2 x 10^9
Polystyrene	7 x 10^8	3 x 10^9

Table 7. 3 Total Dose Effects on Aerospace Polymers (from Tribble, 1995)

C. SUMMARY

The radiation effect demonstrated by the dose depth curves is again, not an insurmountable factor. While most of the MEO cases exhibited a worse environment, which would necessitate a heavier amount of shielding to reach a desired internal radiation dose, it is not so extreme that it would make a mission impossible.

VIII. SUMMARY AND CONCLUSIONS

This thesis compared selected effects of radiation upon spacecraft in Medium Earth Orbit (MEO). Radiation effects in MEO of 15 degrees inclination at altitudes from 3,000 nautical miles (nmi) to 9,000 nmi were investigated and the results compared to the same effects at baseline Low Earth Orbit (LEO) of 400 nmi altitude and 70 degrees inclination. The calculations in this thesis were completed using the software programs MATLAB and Space Radiation 4.0.

The radiation sources included solar proton events (SPE) or solar flares, galactic cosmic radiation, and geomagnetically trapped radiation (the Van Allen belts). One effect of the radiation investigated was proton displacement damage, a measure of degradation of electrical components such as charge-coupled devices (CCD) and other microelectronic equipment. The effects considered also included solar cell degradation, both to silicon solar cells and gallium arsenide solar cells, with various thicknesses of fused silica coverglass. Additionally, dose depth curves were calculated for the internal environment of a spherical model spacecraft. Each component source of radiation was considered separately and a composite curve was also produced.

For many applications, MEO provides a good compromise between GEO and LEO. MEO satellite constellations, only recently attempted, will become more common as it becomes further recognized that MEO altitudes are an exploitable area of space. The radiation from the Van Allen belts remains a concern, but the effects of other radiation sources on spacecraft are mitigated by the position of the spacecraft within the

shielding effects of the Earth's magnetic field. The radiation experienced by a spacecraft at a MEO altitude can be overcome through the use of shielding and redundancy.

LIST OF TERMS

The terms listed below are provided in order to clarify their use in this thesis. Several of these terms follow definitions found in Space Radiation 4.0 software.

Altitude

The altitude is the radial distance from the center of the earth minus the mean radius of the earth (6371.2 km).

Charge

The atomic number of an element. This term is used elements in the radiation environment are usually fully ionized and therefore have a charge equal to the number of protons in the nucleus.

Differential spectrum

A function, f(x), describing the number of particles between x and x+dx divided by the interval dx. The independent variable x may represent either energy or LET. The integral of this function between any two energies is the number of particles in that energy range. The differential spectrum is minus the derivative of the integral spectrum, i.e., -dF(x)/dx.

Displacement damage

Permanent damage to a semiconductor lattice caused by energetic particle interactions.

Dose

The energy deposited by radiation (per unit mass) when it passes through materials. Also called total dose. Usually quoted in rads or gray (= 100 rads).

Energy spectrum

A function representing the distribution of energies of any particle type. Spectra may be integral or differential.

Fluence

The total number of particles passing through a unit area. Units are particles/m^2 for an integral fluence. Units are particles/m^2/MeV for a differential energy fluence. A directional fluence includes /sr (steradian).

Flux

The rate at which particles pass through a unit area. Units are particles/m^2/s for an integral flux. Units are particles/m^2/s/MeV for a differential energy flux. A directional flux includes /sr (steradian).

Galactic cosmic radiation

Protons and heavy ions coming from outside the solar system. These particles are very energetic and can penetrate thick shielding. Also called cosmic radiation.

Geomagnetic cutoff

An effect caused when charged particle trajectories are bent in Earth's magnetic field preventing them from reaching some points on a spacecraft orbit. The geomagnetic cutoff is the minimum particle rigidity (momentum divided by charge) that can reach a point. The vertical cutoff is the geomagnetic cutoff for particles arriving from the zenith only.

Geomagnetic transmission function

This function specifies the fraction of particles at each energy which penetrate the Earth's magnetic field and arrive at the spacecraft. Those charged particles which do not arrive at the spacecraft are deflected away when their trajectories bend in the magnetic field.

Heavy ion

The nucleus of an atom other than a proton. Heavy ions are very energetic and emit strong electric fields.

L shell parameter

A special coordinate used in conjunction with the magnetic field strength (B) to map trapped particle intensities. The parameter labels a group of magnetic field lines forming a surface (shell). A trapped particle tends to remain within a shell while it spirals around a field line and drifts from one field line to the next.

LET

Linear energy transfer. The rate that a charged particle loses energy in matter.

LET spectrum

A function containing charged particle intensities organized according to the rate that they lose energy ion matter. This function is a compact way of representing the energy spectra of many types of charged particles

LET threshold

The minimum LET required to cause a single-event upset in a memory element. Particle is assumed to be normally-incident on the chip. Units are usually MeV/(mg/cm^2).

Magnetosphere

The region of space above the atmosphere that is dominated by Earth's magnetic field and the Van Allen belts.

MeV/n

MeV per nucleon. The kinetic energy of a nucleon divided by the atomic weight (number of nucleons).

Quantities derived from the geomagnetic field models:

Magnetic field (gauss): The magnitude of the magnetic field vector, i.e., the magnetic field strength.

L-shell parameter: The McIlwain L parameter as defined in his paper.

Magnetic deviation (degrees): The deviation of the magnetic field direction from true north. Angle is measured east of north.

Magnetic dip angle (degrees): The angle of the magnetic field vector relative to the horizon. Positive values are above the horizon; negative values are below the horizon.

Radial component of B (gauss): The component of the magnetic field directed outward from the center of the Earth. Negative values represent inward pointing components.

N-S component of B (gauss): The component of the magnetic field pointing north. Negative values represent south pointing field components. The magnetic field vectors are directed from the south pole to the north pole.

E-W component of B (gauss): The component of the magnetic field pointing east. Negative values represent west pointing field components.

Rad

From Radiation (or Roentgen) Absorbed Dose. A measure of the dose actually absorbed by a specific object in terms of the energy transferred to it. 1 rad absorbed = 10 mJ/kg of energy deposited in the substance by ionizing radiation. Thus: one rad in silicon = equivalent expressions

Particles	of Energy	of Fluence
electrons	3 MeV	$4 \times 10^{11}/m^2$
protons	1 MeV	$1 \times 10^{10}/m^2$
nuetrons	1 MeV	$3 \times 10^{13}/m^2$
photons	1 MeV	$2 \times 10^{13}/m^2$

Rigidity

Momentum divided by charge. Used to predict the bending of charged particles trajectories in magnetic fields. Megavolts (MV) and gigavolts (GV) are commonly used units.

Roentgen (R)

A measure of exposure. 1 R = the exposure that would deliver 8.78 mJ to one kg of dry air.

South Atlantic Anomaly (SAA)

A location near Brazil where the Van Allen belt protons are closest to Earth. The point arises because the geomagnetic field is not aligned with Earth's rotational axis and is not centered at Earth's center.

Single-event upset (SEU)

A random bit error occurring in a semiconductor memory element when a single charged particle passes through it.

Solar flare

A storm event on the sun. Often associated with intense emission of charged particles, x-rays, and gamma rays

Solar particle event

A solar flare event where charged particles are emitted. Also called a solar proton event because protons are the most abundant charged particles emitted. Heavy ion components are often not measured or modeled, but may have important engineering consequences.

Trapped particle

A proton or electron which is confined to the Earth's magnetic field. There are trapped heavy ions in radiation belts around Earth and Jupiter.

Van Allen belts

Two regions of the magnetic field around Earth which contain energetic charged particles. The inner belt contains protons and electrons; the outer belt contains only electrons.

LIST OF REFERENCES

This List of References is first organized alphabetically by the name of the models which are referenced and used as an integral part of the Space Radiation 4.0 software; then, references to other works are organized alphabetically by the author of the work cited.

Model References

ALLMAG

E.G. Stassinopoulos and G.D. Mead, *ALLMAG, GDALMAG, LINTRA: Computer Programs for Geomagnetic Field and Field-Line Computations*, NASA-TM-X-65844 (1972).

AUG72

J.H. King, "Solar Proton Fluences for 1977-1983 Space Missions," *Journal of Spacecraft & Rockets*, 11, 401 (1974).

AE-8

J.I. Vette, "The AE-8 Model", pp. 4.19-4.28, in: *Development of Improved Models of the Earth's Radiation Environment*, Technical Note 1: Model Evaluation, European Space Agency, ESTEC Contract No. 8011/88/NL/MAC, Noordwijk, The Netherlands (1989).

M.J. Teague, K.W. Chan, and J.I. Vette, *AE-6: A Model Environment of Trapped Electrons for Solar Maximum*, NASA NSSDC/WDC-A-R&S 76-04 (1976).

AP-8

D.M. Sawyer and J.I. Vette, *AP-8 Trapped Proton Environment for Solar Maximum and Solar Minimum*, NSSDC 76-06 [NASA-TM-X-72605] (1976).

CREME

J.H. Adams, Jr., R. Silberberg, and C.H. Tsao, *Cosmic Ray Effects on Microelectronics, Part I: The Near-Earth Particle Environment*, NRL Memorandum Report 4506 (1981).

J.H. Adams, Jr., J.R. Letaw, and D.F. Smart, *Cosmic Ray Effects on Microelectronics, Part II: The Geomagnetic Cutoff Effects*, NRL Memorandum Report 5099 (1983).

C.H. Tsao, R. Silberberg, J.H. Adams, Jr., and J.R. Letaw, *Cosmic Ray Effects on Microelectronics, Part III: Propagation of Cosmic Rays in the Atmosphere*, NRL Memorandum Report 5402 (1984).

J.H. Adams, Jr., *Cosmic Ray Effects on Microelectronics, Part IV*, NRL Memorandum Report 5901 (1986).

Galactic Cosmic Ray Electrons

J.R. Letaw, *Interplanetary Ionizing Radiation Environment on the Mars Observer Mission*, SCC Report 88-03, Severn Communications Corporation (30 June 1988).

Geomagnetic Field Models

IGRF I[illegible]rnational Geomagnetic Reference Field Revision 1985, *Journal of Geo[illegible]gnetism and Geoelectricity*, vol. 37, 1157-1163 (1985).

Jensen & Cain (1962) D.C. Jensen and J.C. Cain, "An Interim Geomagnetic Field," *Journal of Geophysical Research*, vol. 67, 3568 (1962).

GSFC (9/65) S.J. Hendricks and J.C. Cain, Magnetic Field Data for Trapped-Particle Evaluation, J. Geophys. Res. 71, 346 (1966).

GSFC (12/66) J.C. Cain, S.J. Hendricks, R.A. Langel, and W. Hudson, "A Proposed Model for the International Geomagnetic Reference Field," 1965, *Journal of Geomagnetism and Geoelectricity*, vol. 19, 335 (1967).

GSFC (12/83) R.A. Langel and R.H. Estes, "The Near-Earth Magnetic Field at 1980 Determined from MAGSAT Data," *Journal of Geophysical Research*, vol. 90, 2495 (1985).

GSFC (11/87) R.A. Langel, J.R. Ridgway, M. Sugiura, and K. Maezawa, "The Geomagnetic Field at 1982 from DE 2 and other Magnetic Field Data," *Journal of Geomagnetism and Geoelectricity*, vol. 40, 1103 (1988).

POGO (10/68) J.C. Cain and S.J. Hendricks, *The Geomagnetic Survey by the Polar-Orbiting Geophysical Observatories OGO 2 and OGO 4 1965-67*, Goddard Space Flight Center, Report X- 612-68-502, Greenbelt, Maryland (1968).

POGO (8/69) J.C. Cain and R.E. Sweeney, "Magnetic Field Mapping of the Inner Magnetosphere," *Journal of Geophysical Research,* vol. 75, 4360 (1970).

POGO (8/71) R.A. Langel, "Near- Earth Disturbances in Total Field at High Latitudes: 1. Summary of Data from OGO 2, 4, and 6," *Journal of Geophysics Research*, vol. 79, 2363 (1974).
IGS (1975) D.R. Barraclough, "A Model of the Geomagnetic Field of Epoch 1975," *Geophysics Journal of the Royal Astronomy Society*, vol. 43, 645 (1975).

AWC (1975) N.W. Peddie and E.B. Fabiano, A Model of the Geomagnetic Field for 1975 (AWC/75), *Journal of Geophysical Research*, vol. 81, 2539 (1976).

MGST (6/80) R.A. Langel, R.H. Estes, G.D. Mead, E.B. Fabiano, and E.R. Lancaster, Initial Geomagnetic Field Model from MAGSAT Vector Data, Geophysics Research Letter 7, 793 (1980).

MGST (4/81) R.A. Langel, J. Berbert, T. Jennings, and R. Horner, *MAGSAT Data Processing: A Report for Investigators*, NASA TM-82160, Washington, DC (1981).

INVAR
A. Hassitt and C.E. McIlwain, *Computer Programs for the Computation of B and L*, National Space Science Data Center, NSSDC 67-27 (1967).

SHIELDOSE
S.M. Seltzer, SHIELDOSE: Code System for Space Shielding Radiation Dose Calculations, *ORNL/RSIC CCC-379* (1984).

JPL 1991
J. Feynman, G. Spitale, J. Wang, and S. Gabriel, "Interplanetary Proton Fluence Model: JPL 1991," *Journal of Geophysical Research*, vol. 98, 13281-13294 (1993).

L shell
C.W. McIlwain, "Coordinates for Mapping the Distribution of Magnetically Trapped Particles", *Journal of Geophysical Research*, vol. 66, 3681-3691 (1961).

OCT89
H.H. Sauer, R.D. Zwickl, and M.J. Ness, *Summary Data for the Solar Energetic Particle Events of August through December 1989*, NOAA Space Environment Laboratory Report (21 Feb 1990).

Solar Cells

H.Y. Tada, J.R. Carter, Jr., B.E. Anspaugh, and R.G. Downing, *The Solar Cell Radiation Handbook, 3rd Edition*, NASA/JPL Publ. 82-69 (1 Nov 1982).

Author References

Burke, E. A., "Energy Dependence of Proton-Induced Displacement Damage in Silicon," *IEEE Transactions on Nuclear Science*, NS-33, 1276-1281 (1986).

Crabb, R.L., "Photon Induced Degradation of Electron Irradiated Silicon Solar Cells," Records of the 9th IEEE Photovoltaic Specialists Conference (1972).

Feynman, J., G. Spitale, J. Wang, and S. Gabriel, "Interplanetary Proton Fluence Model: JPL 1991," *Journal of Geophysical Research*, vol. 98, 13281-13294 (1993).

Fischer, H. and W. Pschunder, "Invetigation of Photon and Thermal Induced Changes in Silicon Solar Cells," Records of the 10th IEEE Photovoltaic Specialists Conference (1973).

King, J.H., "Solar Proton Fluences for 1977-1983 Space Missions," *Journal of Spacecraft & Rockets*, vol. 11, 401 (1974).

McIlwain, C.W., "Coordinates for Mapping the Distribution of Magnetically Trapped Particles", *Journal of Geophysical Research*, 66, 3681-3691 (1961).

Rauschenbauch, H.S., ed., *Solar Cell Array Design Handbook, Volume 1*, JPL SP-43-38, Jet Propulsion Laboratory, California Institute of Technology, Pasadena, CA (1976).

Sawyer, D.M. and J.I. Vette, *AP-8 Trapped Proton Environment for Solar Maximum and Solar Minimum*, NSSDC 76-06 [NASA-TM-X-72605] (1976).

Stassinopoulos E.G., "The Geostationary Radiation Environment," *Journal of Spacecraft & Rockets* , vol. 17, 145 (1980).

Tada, H. Y.J.R. Carter, Jr., B.E. Anspaugh, and R.G. Downing, *The Solar Cell Radiation Handbook, 3rd Edition*, NASA/JPL Publ. 82-69 (1 Nov 1982).

Tribble, A.C., *The Space Radiation Environment: Implications for Spacecraft Design*, Princeton Press (1995).

APPENDIX A. ORBITAL GRAPHS

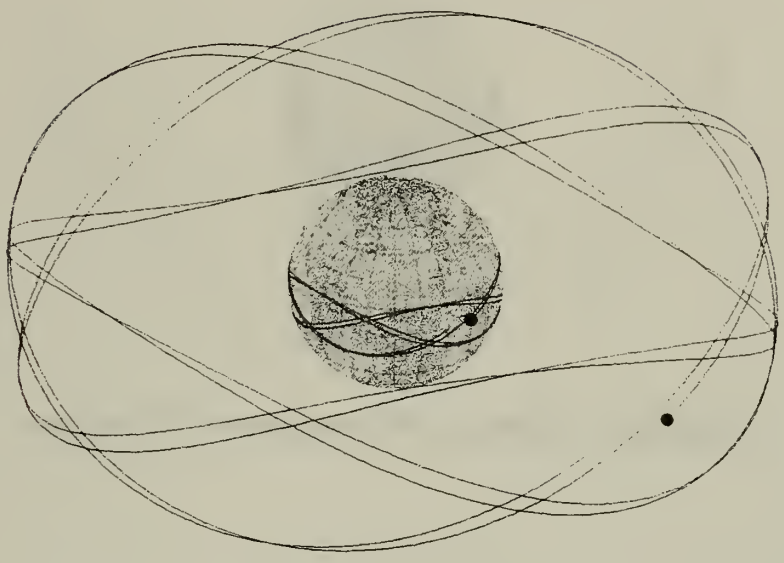

Figure A. 1 **Orbit of Nine Thousand nmi, 15° inclination**

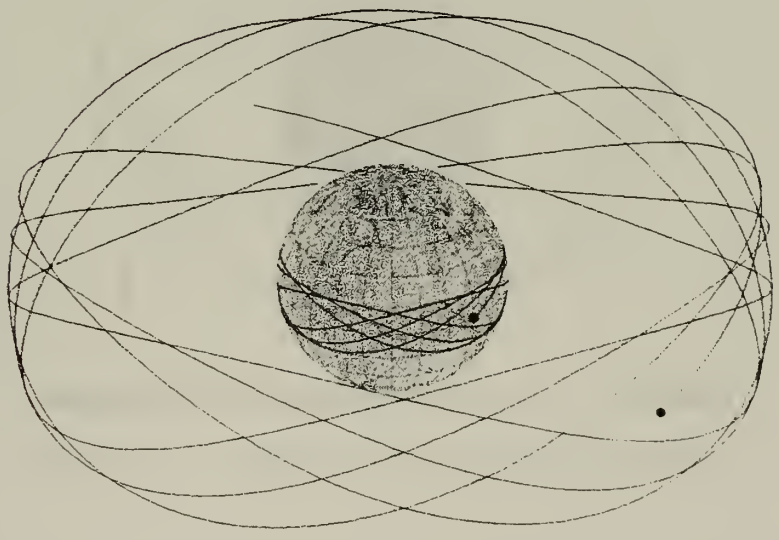

Figure A. 2 **Orbit of Eight Thousand nmi, 15° inclination**

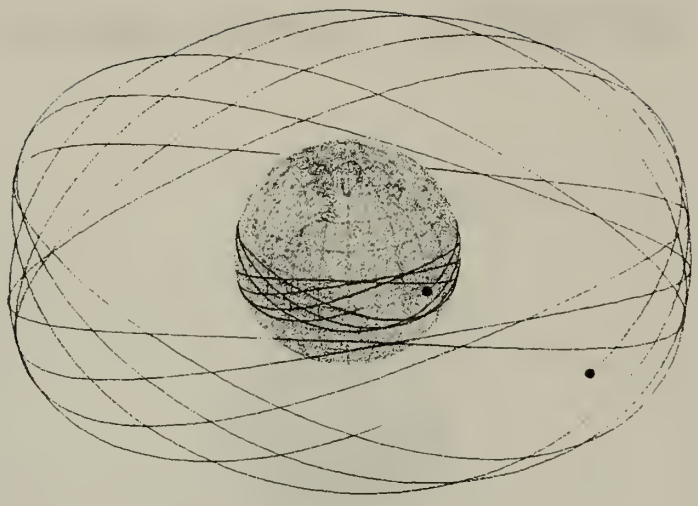

Figure A. 3 Orbit of Seven Thousand nmi, 15° inclination

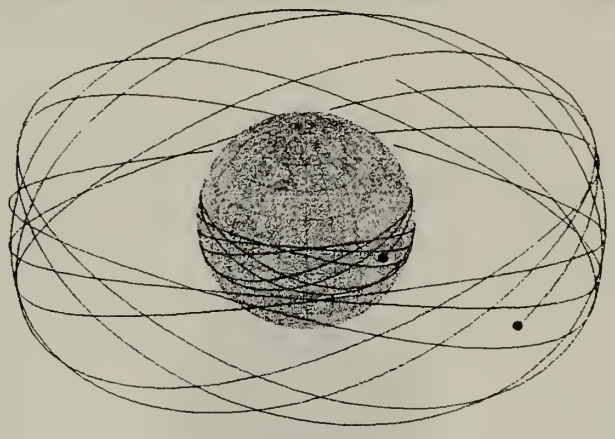

Figure A. 4 Orbit of Six Thousand nmi, 15° inclination

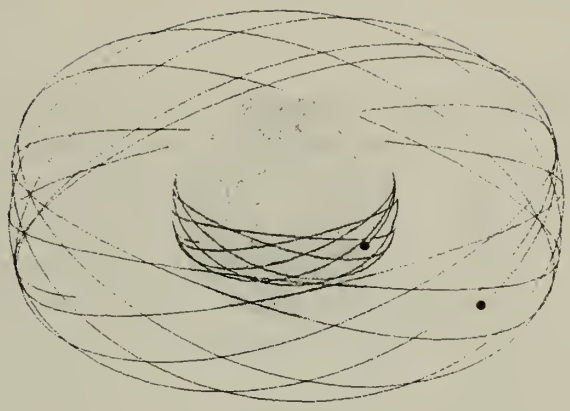

Figure A. 5 Orbit of Five Thousand nmi, 15° inclination

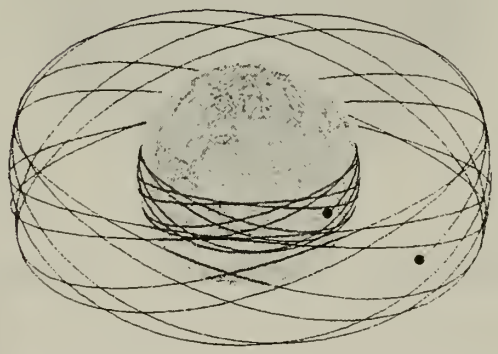

Figure A. 6 Orbit of Four Thousand nmi, 15° inclination

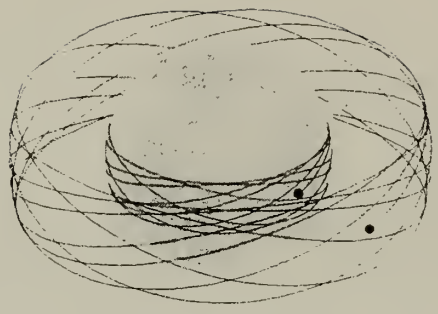

Figure A. 7 Orbit of Three Thousand nmi, 15° inclination

APPENDIX B. GRAPHICAL RESULTS FOR BASELINE ORBIT

Included in this appendix are the results for the baseline orbit shown in Figure B. 1, having the following parameters:

a) Apogee: 740.8 km
b) Perigee: 740.8 km
c) Inclination: 70 degrees
d) Mission Duration: 5283.333 orbits
e) Step Size: 103.5 points/orbit
f) Longitude of Ascending Node: 0 degrees
g) Ascending Node to Perigee: 0 degrees
h) Perigee to Spacecraft: 0 degrees
i) Precession: Yes

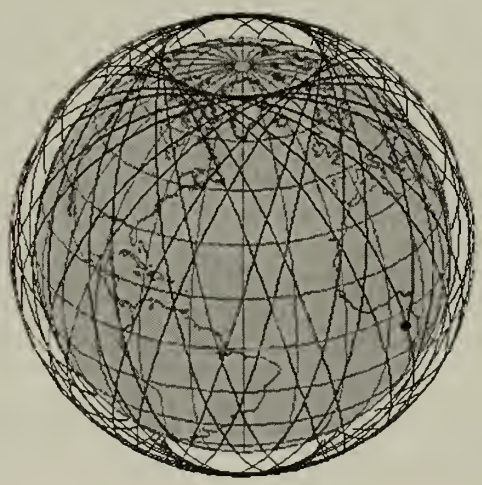

Figure B. 1 Representation of Baseline Orbit

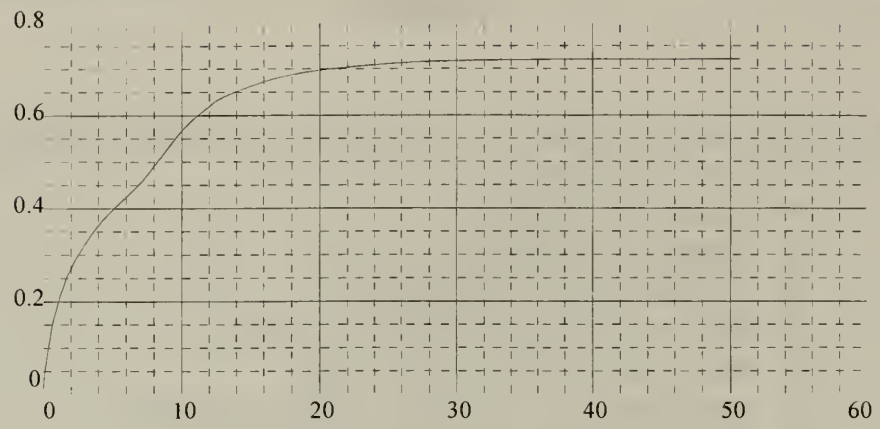

Figure B. 2 Geomagnetic Shielding at 400 nmi

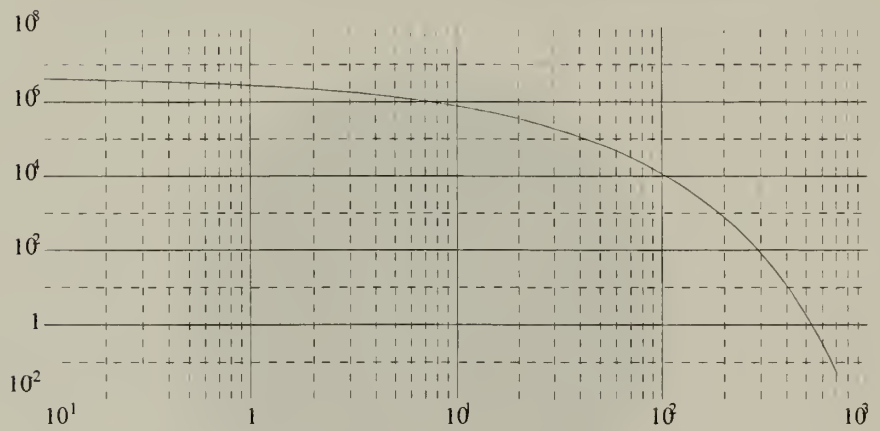

Figure B. 3 Solar Proton Environment (JPL1991 Model)

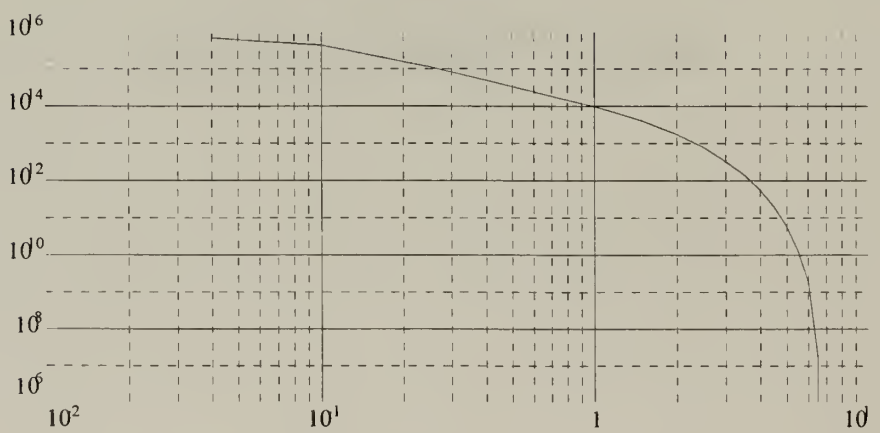

Figure B. 4 Trapped Electron Environment

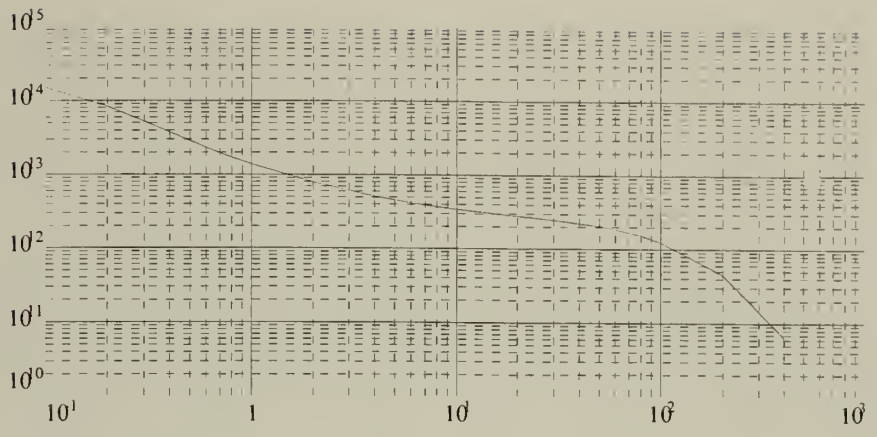

Figure B. 5 Trapped Proton Environment

DIFFERENTIAL RADIATION FLUX GRAPHS

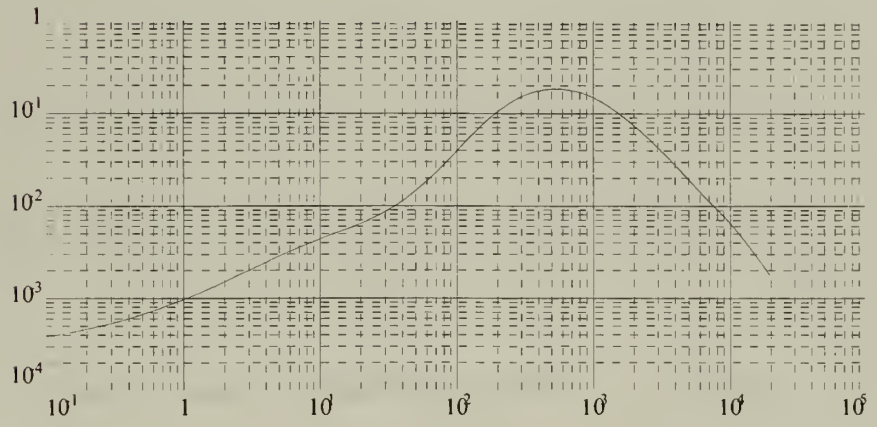

Figure B. 6 Galactic Cosmic Radiation : Slab : 50 mils

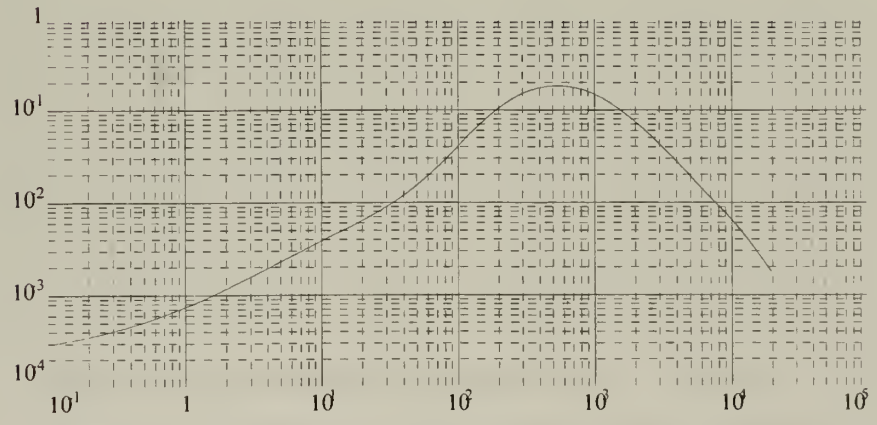

Figure B. 7 Galactic Cosmic Radiation : Slab : 100 mils

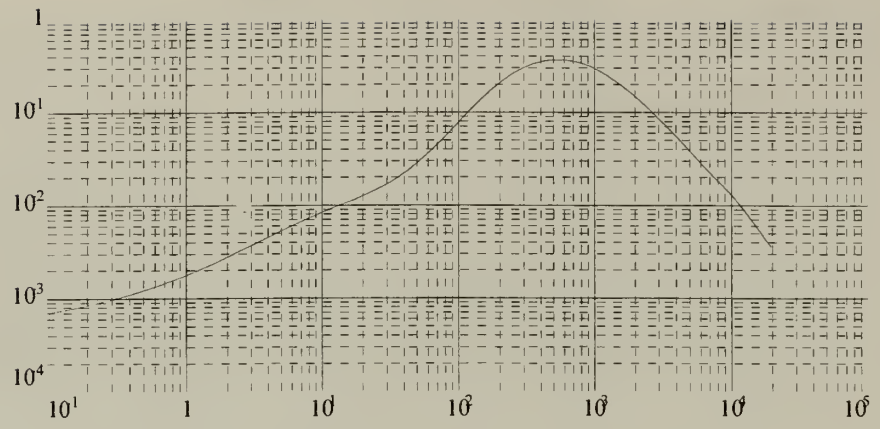

Figure B. 8 **Galactic Cosmic Radiation : Sphere : 100 mils**

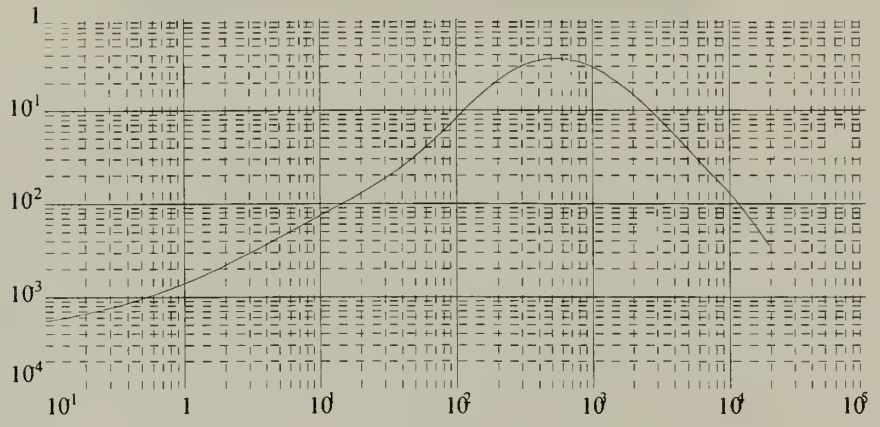

Figure B. 9 **Galactic Cosmic Radiation : Sphere : 300 mils**

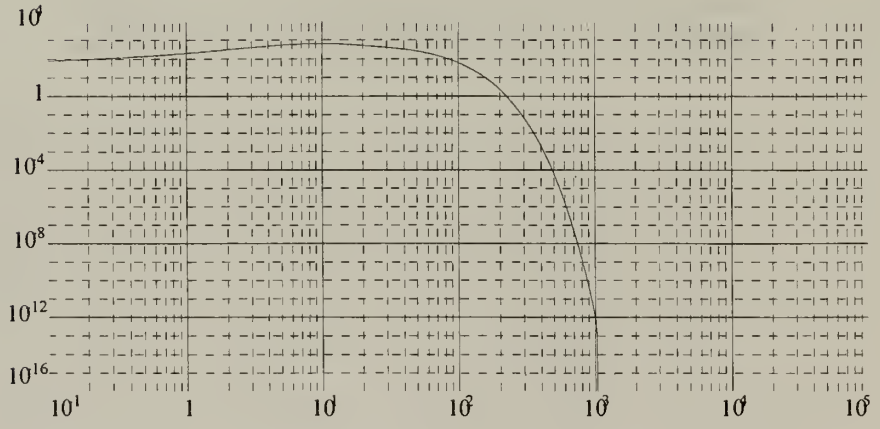

Figure B. 10 **Solar Energetic Particle Flux : Sphere : 100 mils**

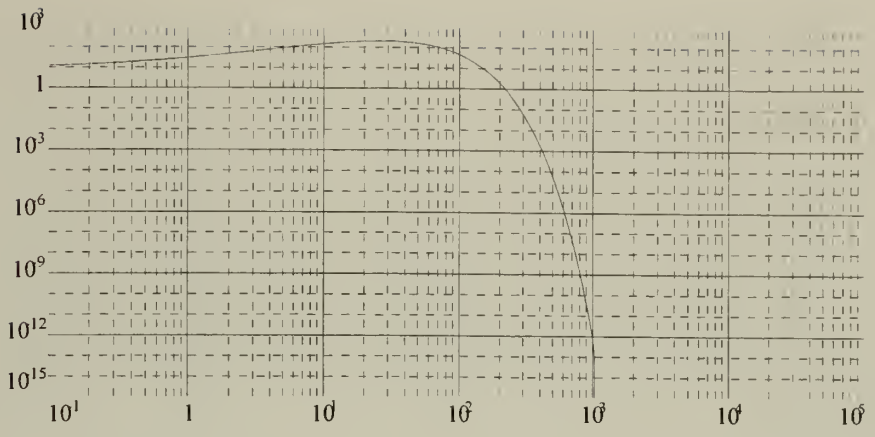

Figure B. 11 **Solar Energetic Particle Flux : Sphere : 300 mils**

PROTON ENERGY SPECTRUM GRAPHS

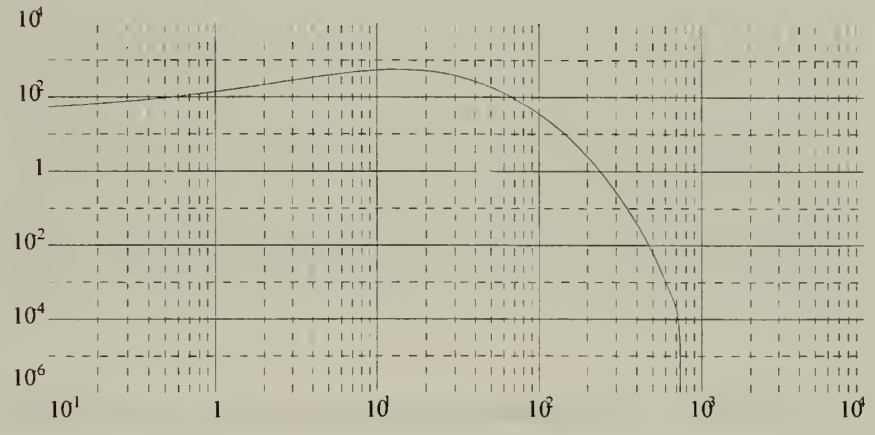

Figure B. 12 **Solar Proton Energy Spectrum : Sphere : 100 mils**

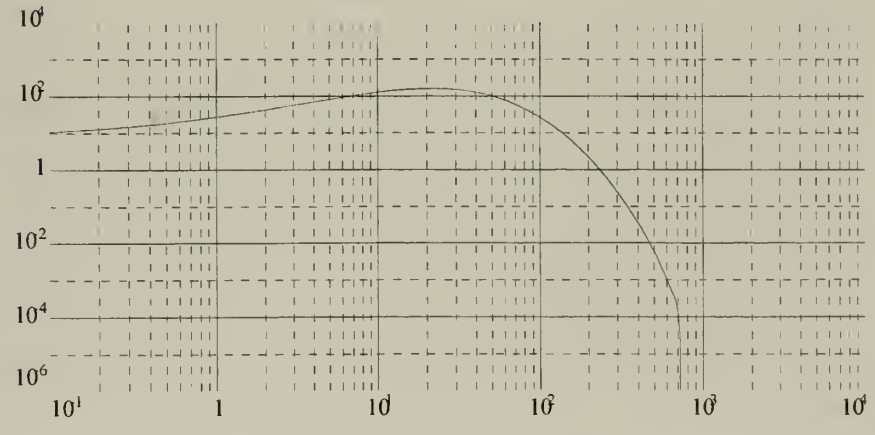

Figure B. 13 **Solar Proton Energy Spectrum : Sphere : 300 mils**

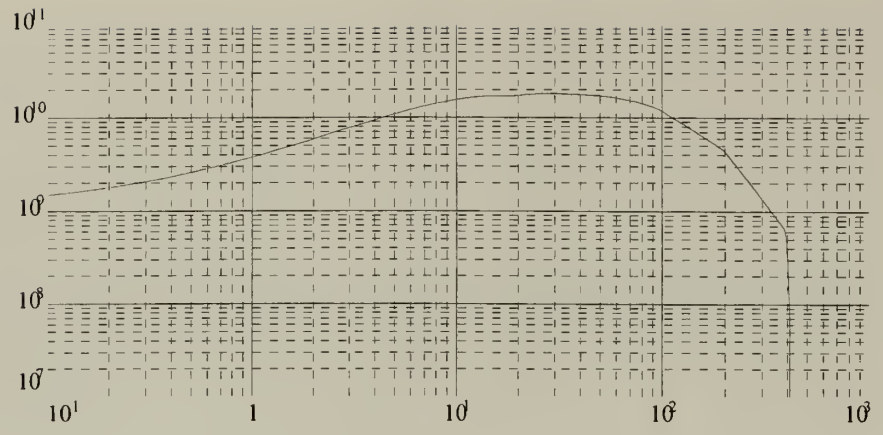

Figure B. 14 Trapped Proton Energy Spectrum : Sphere : 100 mils

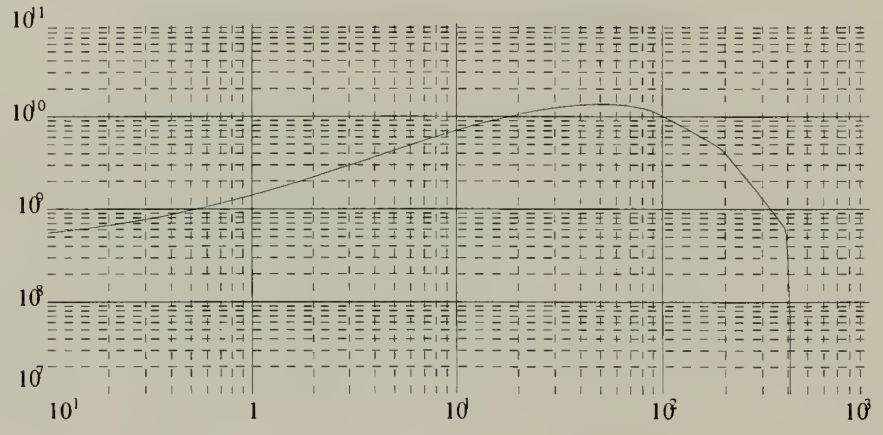

Figure B. 15 Trapped Proton Energy Spectrum : Sphere : 300 mils

DOSE DEPTH CURVES FOR SILICON

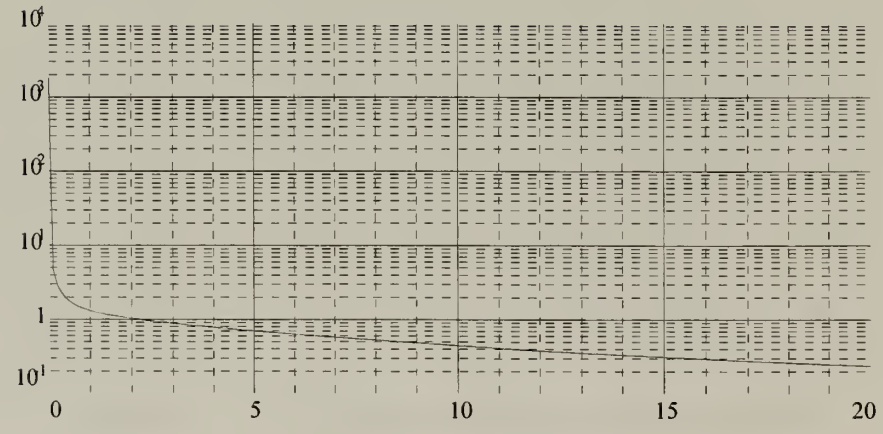

Figure B. 16 Trapped Protons

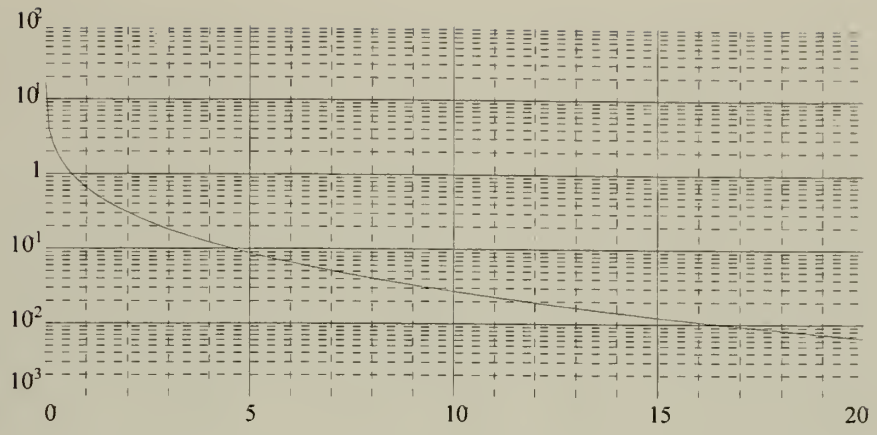

Figure B. 17 Solar Protons

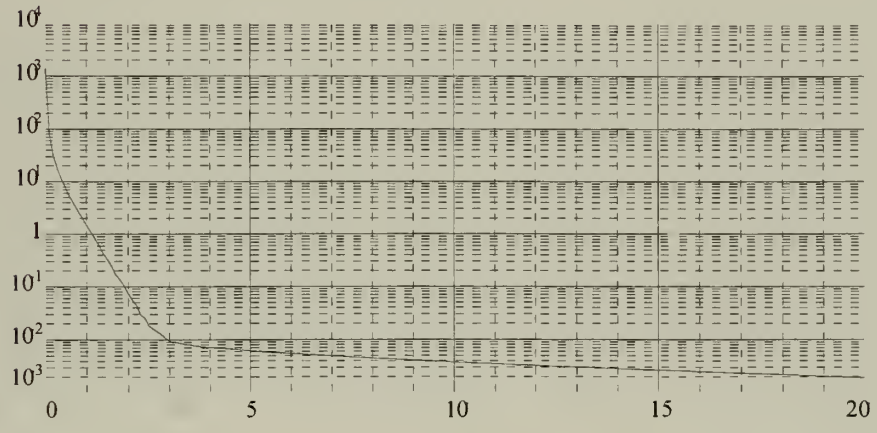

Figure B. 18 Trapped Electrons

LET Spectrum in Silicon Graphs

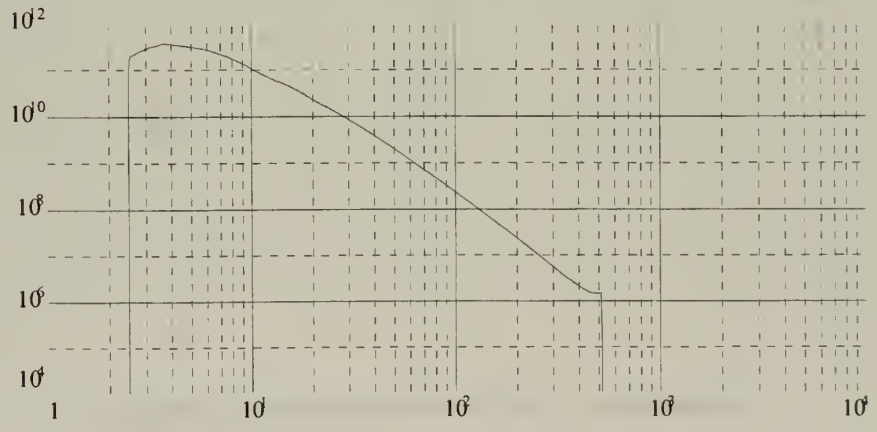

Figure B. 19 Trapped Proton LET : Sphere : 100 mils

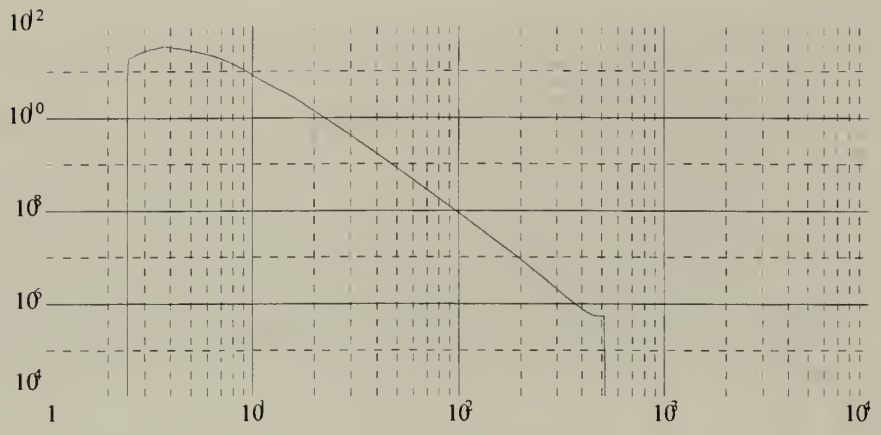

Figure B. 20 Trapped Proton LET : Sphere : 300 mils

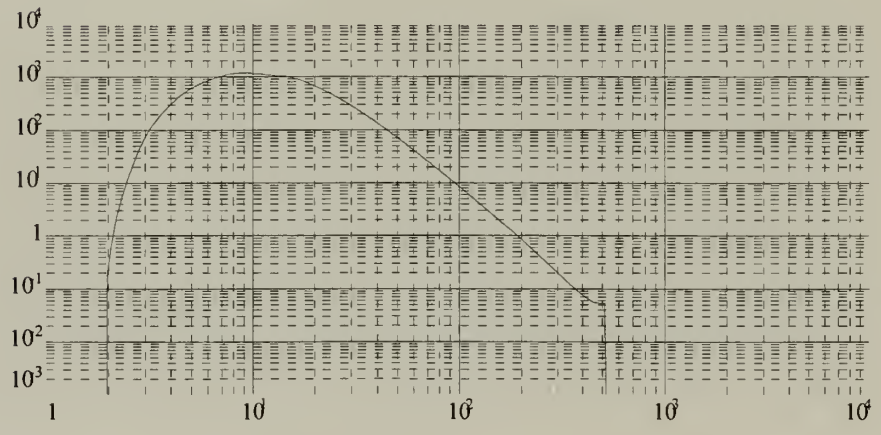

Figure B. 21 Solar Proton LET : Sphere : 100 mils

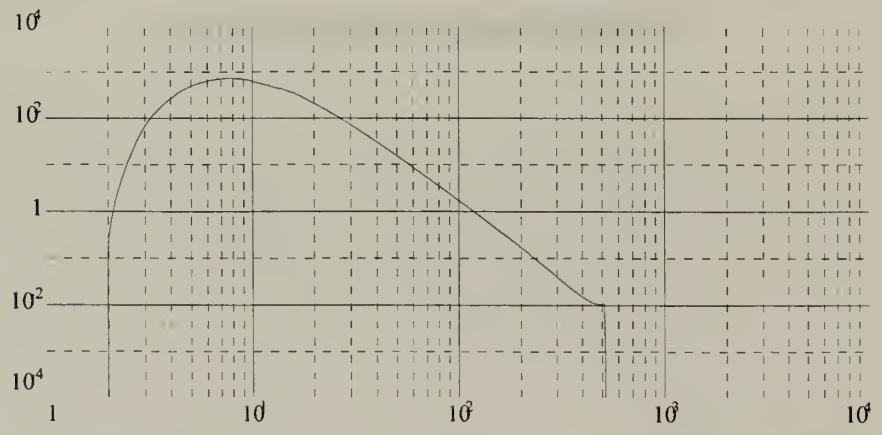

Figure B. 22 Solar Proton LET : Sphere : 300 mils

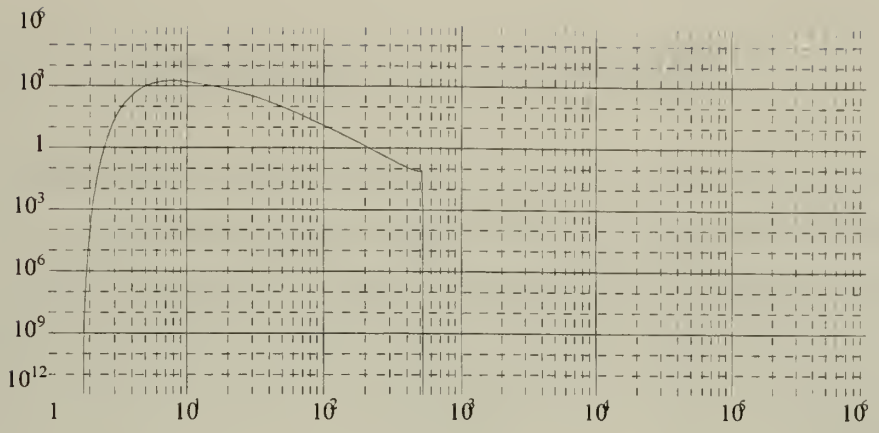

Figure B. 23 Solar Energetic Particle LET : Sphere : 100 mils

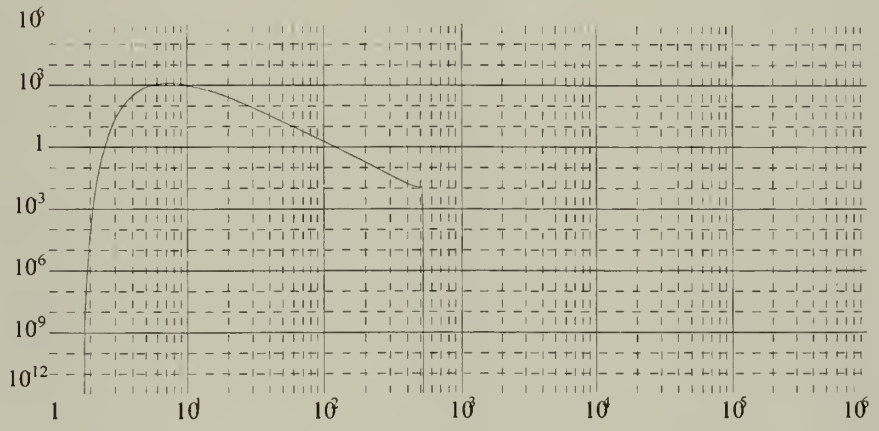

Figure B. 24 Solar Energetic Particle LET : Sphere : 300 mils

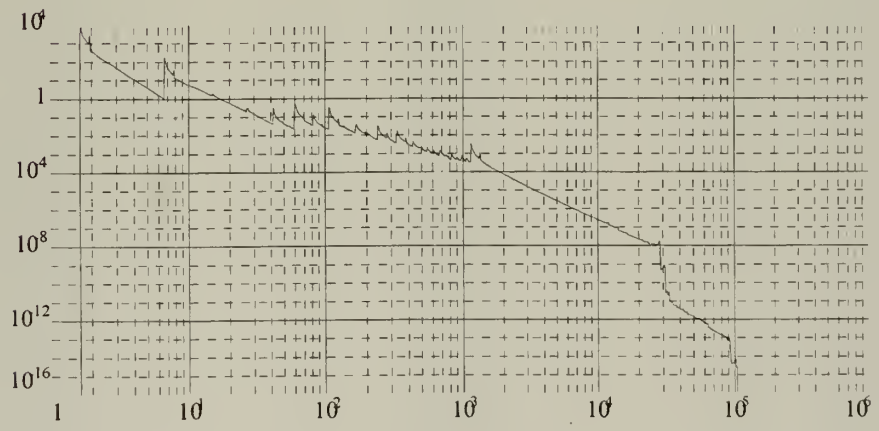

Figure B. 25 Galactic Cosmic LET : Sphere : 100 mils

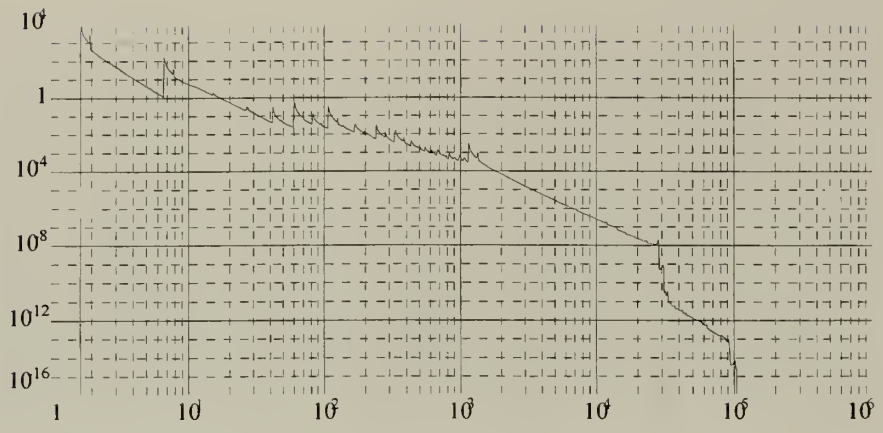

Figure B. 26 Galactic Cosmic LET : Sphere : 300 mils

APPENDIX C. DATA RESULTS

This Appendix includes the data files used in analysis of the Medium Earth Orbits (MEO) and baseline orbits, described in this thesis. This data formed the basis for many of the graphs in Chapter V through Chapter VII.

```
%Trapped Proton in
Silicon at 9k
(rads/day)
%1997-11-17  08:53:38
%Trapped Proton Dose-
Depth
%   201 = Number of
Depth Points
%Depth (g/cm² Al)
       Dose (rad/day)
tpdc9=[0
3.03e+006
0.1     3.65e+000
0.2     1.72e-001
0.3     1.55e-001
0.4     5.44e-009
0.5     2.10e-022
0.6     0.00e+000
0.7     0.00e+000
0.8     0.00e+000
0.9     0.00e+000
1       0.00e+000
1.1     0.00e+000
1.2     0.00e+000
1.3     0.00e+000
1.4     0.00e+000
1.5     0.00e+000
1.6     0.00e+000
1.7     0.00e+000
1.8     0.00e+000
1.9     0.00e+000
2       0.00e+000
2.1     0.00e+000
2.2     0.00e+000
2.3     0.00e+000
2.4     0.00e+000
2.5     0.00e+000
2.6     0.00e+000
2.7     0.00e+000
2.8     0.00e+000
2.9     0.00e+000
3       0.00e+000
3.1     0.00e+000
3.2     0.00e+000
3.3     0.00e+000
3.4     0.00e+000
3.5     0.00e+000
3.6     0.00e+000
3.7     0.00e+000
3.8     0.00e+000
3.9     0.00e+000
4       0.00e+000
4.1     0.00e+000
4.2     0.00e+000
4.3     0.00e+000
4.4     0.00e+000
4.5     0.00e+000
4.6     0.00e+000
4.7     0.00e+000
4.8     0.00e+000
4.9     0.00e+000
5       0.00e+000
5.1     0.00e+000
5.2     0.00e+000
5.3     0.00e+000
5.4     0.00e+000
5.5     0.00e+000
5.6     0.00e+000
5.7     0.00e+000
5.8     0.00e+000
5.9     0.00e+000
6       0.00e+000
6.1     0.00e+000
6.2     0.00e+000
6.3     0.00e+000
6.4     0.00e+000
6.5     0.00e+000
6.6     0.00e+000
6.7     0.00e+000
6.8     0.00e+000
6.9     0.00e+000
7       0.00e+000
7.1     0.00e+000
7.2     0.00e+000
7.3     0.00e+000
7.4     0.00e+000
7.5     0.00e+000
7.6     0.00e+000
7.7     0.00e+000
7.8     0.00e+000
7.9     0.00e+000
8       0.00e+000
8.1     0.00e+000
8.2     0.00e+000
8.3     0.00e+000
8.4     0.00e+000
8.5     0.00e+000
8.6     0.00e+000
8.7     0.00e+000
8.8     0.00e+000
8.9     0.00e+000
9       0.00e+000
9.1     0.00e+000
9.2     0.00e+000
9.3     0.00e+000
9.4     0.00e+000
9.5     0.00e+000
9.6     0.00e+000
9.7     0.00e+000
9.8     0.00e+000
9.9     0.00e+000
10      0.00e+000
10.1    0.00e+000
10.2    0.00e+000
10.3    0.00e+000
10.4    0.00e+000
10.5    0.00e+000
10.6    0.00e+000
10.7    0.00e+000
10.8    0.00e+000
10.9    0.00e+000
11      0.00e+000
11.1    0.00e+000
11.2    0.00e+000
11.3    0.00e+000
11.4    0.00e+000
11.5    0.00e+000
11.6    0.00e+000
11.7    0.00e+000
11.8    0.00e+000
11.9    0.00e+000
12      0.00e+000
12.1    0.00e+000
12.2    0.00e+000
12.3    0.00e+000
12.4    0.00e+000
12.5    0.00e+000
12.6    0.00e+000
12.7    0.00e+000
12.8    0.00e+000
12.9    0.00e+000
13      0.00e+000
13.1    0.00e+000
13.2    0.00e+000
13.3    0.00e+000
13.4    0.00e+000
13.5    0.00e+000
13.6    0.00e+000
13.7    0.00e+000
13.8    0.00e+000
13.9    0.00e+000
14      0.00e+000
14.1    0.00e+000
14.2    0.00e+000
14.3    0.00e+000
```

```
14.4    0.00e+000
14.5    0.00e+000
14.6    0.00e+000
14.7    0.00e+000
14.8    0.00e+000
14.9    0.00e+000
15      0.00e+000
15.1    0.00e+000
15.2    0.00e+000
15.3    0.00e+000
15.4    0.00e+000
15.5    0.00e+000
15.6    0.00e+000
15.7    0.00e+000
15.8    0.00e+000
15.9    0.00e+000
16      0.00e+000
16.1    0.00e+000
16.2    0.00e+000
16.3    0.00e+000
16.4    0.00e+000
16.5    0.00e+000
16.6    0.00e+000
16.7    0.00e+000
16.8    0.00e+000
16.9    0.00e+000
17      0.00e+000
17.1    0.00e+000
17.2    0.00e+000
17.3    0.00e+000
17.4    0.00e+000
17.5    0.00e+000
17.6    0.00e+000
17.7    0.00e+000
17.8    0.00e+000
17.9    0.00e+000
18      0.00e+000
18.1    0.00e+000
18.2    0.00e+000
18.3    0.00e+000
18.4    0.00e+000
18.5    0.00e+000
18.6    0.00e+000
18.7    0.00e+000
18.8    0.00e+000
18.9    0.00e+000
19      0.00e+000
19.1    0.00e+000
19.2    0.00e+000
19.3    0.00e+000
19.4    0.00e+000
19.5    0.00e+000
19.6    0.00e+000
19.7    0.00e+000
19.8    0.00e+000
19.9    0.00e+000
20      0.00e+000 ];
%Trapped Proton in
Silicon at 8k
(rads/day)
%1997-11-17  08:53:14
%Trapped Proton Dose-
Depth
%    201 = Number of
Depth Points
%Depth (g/cm² Al)
      Dose (rad/day)
tpdc8=[0
4.98e+006
0.1     6.57e+001
0.2     2.51e+000
0.3     3.77e-001
0.4     3.18e-001
0.5     3.01e-001
0.6     1.90e-002
0.7     3.70e-009
0.8     5.73e-015
0.9     4.40e-020
1       1.25e-024
1.1     1.03e-028
1.2     1.50e-033
1.3     0.00e+000
1.4     0.00e+000
1.5     0.00e+000
1.6     0.00e+000
1.7     0.00e+000
1.8     0.00e+000
1.9     0.00e+000
2       0.00e+000
2.1     0.00e+000
2.2     0.00e+000
2.3     0.00e+000
2.4     0.00e+000
2.5     0.00e+000
2.6     0.00e+000
2.7     0.00e+000
2.8     0.00e+000
2.9     0.00e+000
3       0.00e+000
3.1     0.00e+000
3.2     0.00e+000
3.3     0.00e+000
3.4     0.00e+000
3.5     0.00e+000
3.6     0.00e+000
3.7     0.00e+000
3.8     0.00e+000
3.9     0.00e+000
4       0.00e+000
4.1     0.00e+000
4.2     0.00e+000
4.3     0.00e+000
4.4     0.00e+000
4.5     0.00e+000
4.6     0.00e+000
4.7     0.00e+000
4.8     0.00e+000
4.9     0.00e+000
5       0.00e+000
5.1     0.00e+000
5.2     0.00e+000
5.3     0.00e+000
5.4     0.00e+000
5.5     0.00e+000
5.6     0.00e+000
5.7     0.00e+000
5.8     0.00e+000
5.9     0.00e+000
6       0.00e+000
6.1     0.00e+000
6.2     0.00e+000
6.3     0.00e+000
6.4     0.00e+000
6.5     0.00e+000
6.6     0.00e+000
6.7     0.00e+000
6.8     0.00e+000
6.9     0.00e+000
7       0.00e+000
7.1     0.00e+000
7.2     0.00e+000
7.3     0.00e+000
7.4     0.00e+000
7.5     0.00e+000
7.6     0.00e+000
7.7     0.00e+000
7.8     0.00e+000
7.9     0.00e+000
8       0.00e+000
8.1     0.00e+000
8.2     0.00e+000
8.3     0.00e+000
8.4     0.00e+000
8.5     0.00e+000
8.6     0.00e+000
8.7     0.00e+000
8.8     0.00e+000
8.9     0.00e+000
9       0.00e+000
9.1     0.00e+000
9.2     0.00e+000
9.3     0.00e+000
9.4     0.00e+000
9.5     0.00e+000
9.6     0.00e+000
9.7     0.00e+000
9.8     0.00e+000
9.9     0.00e+000
10      0.00e+000
10.1    0.00e+000
10.2    0.00e+000
10.3    0.00e+000
10.4    0.00e+000
10.5    0.00e+000
10.6    0.00e+000
10.7    0.00e+000
10.8    0.00e+000
10.9    0.00e+000
11      0.00e+000
11.1    0.00e+000
11.2    0.00e+000
11.3    0.00e+000
11.4    0.00e+000
11.5    0.00e+000
11.6    0.00e+000
11.7    0.00e+000
11.8    0.00e+000
11.9    0.00e+000
12      0.00e+000
12.1    0.00e+000
12.2    0.00e+000
12.3    0.00e+000
12.4    0.00e+000
12.5    0.00e+000
12.6    0.00e+000
12.7    0.00e+000
12.8    0.00e+000
12.9    0.00e+000
13      0.00e+000
13.1    0.00e+000
13.2    0.00e+000
```

```
13.3    0.00e+000
13.4    0.00e+000
13.5    0.00e+000
13.6    0.00e+000
13.7    0.00e+000
13.8    0.00e+000
13.9    0.00e+000
14      0.00e+000
14.1    0.00e+000
14.2    0.00e+000
14.3    0.00e+000
14.4    0.00e+000
14.5    0.00e+000
14.6    0.00e+000
14.7    0.00e+000
14.8    0.00e+000
14.9    0.00e+000
15      0.00e+000
15.1    0.00e+000
15.2    0.00e+000
15.3    0.00e+000
15.4    0.00e+000
15.5    0.00e+000
15.6    0.00e+000
15.7    0.00e+000
15.8    0.00e+000
15.9    0.00e+000
16      0.00e+000
16.1    0.00e+000
16.2    0.00e+000
16.3    0.00e+000
16.4    0.00e+000
16.5    0.00e+000
16.6    0.00e+000
16.7    0.00e+000
16.8    0.00e+000
16.9    0.00e+000
17      0.00e+000
17.1    0.00e+000
17.2    0.00e+000
17.3    0.00e+000
17.4    0.00e+000
17.5    0.00e+000
17.6    0.00e+000
17.7    0.00e+000
17.8    0.00e+000
17.9    0.00e+000
18      0.00e+000
18.1    0.00e+000
18.2    0.00e+000
18.3    0.00e+000
18.4    0.00e+000
18.5    0.00e+000
18.6    0.00e+000
18.7    0.00e+000
18.8    0.00e+000
18.9    0.00e+000
19      0.00e+000
19.1    0.00e+000
19.2    0.00e+000
19.3    0.00e+000
19.4    0.00e+000
19.5    0.00e+000
19.6    0.00e+000
19.7    0.00e+000
19.8    0.00e+000
19.9    0.00e+000
20      0.00e+000 ];
%Trapped Proton in
Silicon at 7k
(rads/day)
%1997-11-17  08:52:51
%Trapped Proton Dose-
Depth
%    201 = Number of
Depth Points
%Depth (g/cm² Al)
       Dose (rad/day)
tpdc7=[0
1.43e+007
0.1     5.41e+002
0.2     5.49e+001
0.3     1.37e+001
0.4     5.09e+000
0.5     2.38e+000
0.6     1.32e+000
0.7     8.39e-001
0.8     5.83e-001
0.9     4.43e-001
1       3.59e-001
1.1     3.11e-001
1.2     2.84e-001
1.3     2.72e-001
1.4     2.61e-001
1.5     2.50e-001
1.6     2.38e-001
1.7     2.27e-001
1.8     2.15e-001
1.9     2.04e-001
2       1.91e-001
2.1     1.79e-001
2.2     1.66e-001
2.3     1.52e-001
2.4     1.38e-001
2.5     1.24e-001
2.6     1.07e-001
2.7     8.97e-002
2.8     6.91e-002
2.9     4.26e-002
3       1.04e-003
3.1     8.79e-007
3.2     9.29e-010
3.3     1.21e-012
3.4     1.96e-015
3.5     3.80e-018
3.6     8.83e-021
3.7     2.42e-023
3.8     7.78e-026
3.9     2.90e-028
4       1.21e-030
4.1     0.00e+000
4.2     0.00e+000
4.3     0.00e+000
4.4     0.00e+000
4.5     0.00e+000
4.6     0.00e+000
4.7     0.00e+000
4.8     0.00e+000
4.9     0.00e+000
5       0.00e+000
5.1     0.00e+000
5.2     0.00e+000
5.3     0.00e+000
5.4     0.00e+000
5.5     0.00e+000
5.6     0.00e+000
5.7     0.00e+000
5.8     0.00e+000
5.9     0.00e+000
6       0.00e+000
6.1     0.00e+000
6.2     0.00e+000
6.3     0.00e+000
6.4     0.00e+000
6.5     0.00e+000
6.6     0.00e+000
6.7     0.00e+000
6.8     0.00e+000
6.9     0.00e+000
7       0.00e+000
7.1     0.00e+000
7.2     0.00e+000
7.3     0.00e+000
7.4     0.00e+000
7.5     0.00e+000
7.6     0.00e+000
7.7     0.00e+000
7.8     0.00e+000
7.9     0.00e+000
8       0.00e+000
8.1     0.00e+000
8.2     0.00e+000
8.3     0.00e+000
8.4     0.00e+000
8.5     0.00e+000
8.6     0.00e+000
8.7     0.00e+000
8.8     0.00e+000
8.9     0.00e+000
9       0.00e+000
9.1     0.00e+000
9.2     0.00e+000
9.3     0.00e+000
9.4     0.00e+000
9.5     0.00e+000
9.6     0.00e+000
9.7     0.00e+000
9.8     0.00e+000
9.9     0.00e+000
10      0.00e+000
10.1    0.00e+000
10.2    0.00e+000
10.3    0.00e+000
10.4    0.00e+000
10.5    0.00e+000
10.6    0.00e+000
10.7    0.00e+000
10.8    0.00e+000
10.9    0.00e+000
11      0.00e+000
11.1    0.00e+000
11.2    0.00e+000
11.3    0.00e+000
11.4    0.00e+000
11.5    0.00e+000
11.6    0.00e+000
11.7    0.00e+000
11.8    0.00e+000
11.9    0.00e+000
12      0.00e+000
12.1    0.00e+000
```

```
12.2    0.00e+000
12.3    0.00e+000
12.4    0.00e+000
12.5    0.00e+000
12.6    0.00e+000
12.7    0.00e+000
12.8    0.00e+000
12.9    0.00e+000
13      0.00e+000
13.1    0.00e+000
13.2    0.00e+000
13.3    0.00e+000
13.4    0.00e+000
13.5    0.00e+000
13.6    0.00e+000
13.7    0.00e+000
13.8    0.00e+000
13.9    0.00e+000
14      0.00e+000
14.1    0.00e+000
14.2    0.00e+000
14.3    0.00e+000
14.4    0.00e+000
14.5    0.00e+000
14.6    0.00e+000
14.7    0.00e+000
14.8    0.00e+000
14.9    0.00e+000
15      0.00e+000
15.1    0.00e+000
15.2    0.00e+000
15.3    0.00e+000
15.4    0.00e+000
15.5    0.00e+000
15.6    0.00e+000
15.7    0.00e+000
15.8    0.00e+000
15.9    0.00e+000
16      0.00e+000
16.1    0.00e+000
16.2    0.00e+000
16.3    0.00e+000
16.4    0.00e+000
16.5    0.00e+000
16.6    0.00e+000
16.7    0.00e+000
16.8    0.00e+000
16.9    0.00e+000
17      0.00e+000
17.1    0.00e+000
17.2    0.00e+000
17.3    0.00e+000
17.4    0.00e+000
17.5    0.00e+000
17.6    0.00e+000
17.7    0.00e+000
17.8    0.00e+000
17.9    0.00e+000
18      0.00e+000
18.1    0.00e+000
18.2    0.00e+000
18.3    0.00e+000
18.4    0.00e+000
18.5    0.00e+000
18.6    0.00e+000
18.7    0.00e+000
18.8    0.00e+000
18.9    0.00e+000
19      0.00e+000
19.1    0.00e+000
19.2    0.00e+000
19.3    0.00e+000
19.4    0.00e+000
19.5    0.00e+000
19.6    0.00e+000
19.7    0.00e+000
19.8    0.00e+000
19.9    0.00e+000
20      0.00e+000
%Trapped Proton in
Silicon at 6k
(rads/day) corrected
%1997-11-20  18:39:49
%Trapped Proton Dose-
Depth
%    201 = Number of
Depth Points
%Depth (g/cm² Al)
      Dose (rad/day)
tpdc6=[0
1.29e+007
0.1     2.61e+003
0.2     3.84e+002
0.3     1.22e+002
0.4     5.22e+001
0.5     2.64e+001
0.6     1.51e+001
0.7     9.43e+000
0.8     6.26e+000
0.9     4.37e+000
1       3.17e+000
1.1     2.36e+000
1.2     1.80e+000
1.3     1.40e+000
1.4     1.10e+000
1.5     8.86e-001
1.6     7.21e-001
1.7     5.94e-001
1.8     4.95e-001
1.9     4.16e-001
2       3.53e-001
2.1     3.02e-001
2.2     2.60e-001
2.3     2.26e-001
2.4     1.97e-001
2.5     1.73e-001
2.6     1.53e-001
2.7     1.36e-001
2.8     1.21e-001
2.9     1.09e-001
3       9.80e-002
3.1     8.86e-002
3.2     8.03e-002
3.3     7.32e-002
3.4     6.68e-002
3.5     6.13e-002
3.6     5.64e-002
3.7     5.20e-002
3.8     4.81e-002
3.9     4.47e-002
4       4.16e-002
4.1     3.90e-002
4.2     3.66e-002
4.3     3.44e-002
4.4     3.24e-002
4.5     3.05e-002
4.6     2.88e-002
4.7     2.71e-002
4.8     2.57e-002
4.9     2.43e-002
5       2.30e-002
5.1     2.18e-002
5.2     2.06e-002
5.3     1.96e-002
5.4     1.86e-002
5.5     1.76e-002
5.6     1.68e-002
5.7     1.59e-002
5.8     1.52e-002
5.9     1.44e-002
6       1.37e-002
6.1     1.31e-002
6.2     1.24e-002
6.3     1.19e-002
6.4     1.13e-002
6.5     1.08e-002
6.6     1.03e-002
6.7     9.78e-003
6.8     9.31e-003
6.9     8.87e-003
7       8.45e-003
7.1     8.05e-003
7.2     7.67e-003
7.3     7.31e-003
7.4     6.96e-003
7.5     6.63e-003
7.6     6.31e-003
7.7     6.00e-003
7.8     5.71e-003
7.9     5.43e-003
8       5.15e-003
8.1     4.89e-003
8.2     4.64e-003
8.3     4.40e-003
8.4     4.16e-003
8.5     3.94e-003
8.6     3.72e-003
8.7     3.50e-003
8.8     3.29e-003
8.9     3.09e-003
9       2.89e-003
9.1     2.70e-003
9.2     2.51e-003
9.3     2.32e-003
9.4     2.13e-003
9.5     1.94e-003
9.6     1.75e-003
9.7     1.56e-003
9.8     1.37e-003
9.9     1.16e-003
10      9.33e-004
10.1    6.39e-004
10.2    3.78e-004
10.3    2.24e-004
10.4    1.34e-004
10.5    8.04e-005
10.6    4.85e-005
10.7    2.93e-005
10.8    1.78e-005
10.9    1.09e-005
11      6.69e-006
```

```
11.1    4.12e-006
11.2    2.55e-006
11.3    1.58e-006
11.4    9.86e-007
11.5    6.16e-007
11.6    3.87e-007
11.7    2.44e-007
11.8    1.54e-007
11.9    9.78e-008
12      6.23e-008
12.1    3.98e-008
12.2    2.56e-008
12.3    1.65e-008
12.4    1.06e-008
12.5    6.90e-009
12.6    4.49e-009
12.7    2.93e-009
12.8    1.92e-009
12.9    1.26e-009
13      8.31e-010
13.1    5.50e-010
13.2    3.64e-010
13.3    2.42e-010
13.4    1.62e-010
13.5    1.08e-010
13.6    7.26e-011
13.7    4.89e-011
13.8    3.30e-011
13.9    2.23e-011
14      1.52e-011
14.1    1.03e-011
14.2    7.04e-012
14.3    4.82e-012
14.4    3.30e-012
14.5    2.27e-012
14.6    1.57e-012
14.7    1.08e-012
14.8    7.50e-013
14.9    5.21e-013
15      3.63e-013
15.1    2.53e-013
15.2    1.77e-013
15.3    1.24e-013
15.4    8.72e-014
15.5    6.14e-014
15.6    4.34e-014
15.7    3.07e-014
15.8    2.17e-014
15.9    1.54e-014
16      1.10e-014
16.1    7.85e-015
16.2    5.61e-015
16.3    4.02e-015
16.4    2.88e-015
16.5    2.07e-015
16.6    1.49e-015
16.7    1.08e-015
16.8    7.80e-016
16.9    5.66e-016
17      4.11e-016
17.1    2.99e-016
17.2    2.18e-016
17.3    1.59e-016
17.4    1.16e-016
17.5    8.52e-017
17.6    6.25e-017
17.7    4.60e-017
17.8    3.38e-017
17.9    2.50e-017
18      1.84e-017
18.1    1.37e-017
18.2    1.01e-017
18.3    7.52e-018
18.4    5.59e-018
18.5    4.16e-018
18.6    3.11e-018
18.7    2.32e-018
18.8    1.74e-018
18.9    1.30e-018
19      9.78e-019
19.1    7.35e-019
19.2    5.54e-019
19.3    4.17e-019
19.4    3.15e-019
19.5    2.38e-019
19.6    1.80e-019
19.7    1.37e-019
19.8    1.04e-019
19.9    7.90e-020
20      6.02e-020 ];
%Trapped Proton in
Silicon at 5k
(rads/day)
%1997-11-17  08:51:55
%Trapped Proton Dose-
Depth
%    201 = Number of
Depth Points
%Depth (g/cm² Al)
      Dose (rad/day)
tpdc5=[0
8.06e+006
0.1     9.36e+003
0.2     1.67e+003
0.3     6.00e+002
0.4     2.86e+002
0.5     1.59e+002
0.6     9.70e+001
0.7     6.33e+001
0.8     4.38e+001
0.9     3.17e+001
1       2.37e+001
1.1     1.82e+001
1.2     1.43e+001
1.3     1.14e+001
1.4     9.28e+000
1.5     7.64e+000
1.6     6.37e+000
1.7     5.37e+000
1.8     4.57e+000
1.9     3.93e+000
2       3.41e+000
2.1     2.97e+000
2.2     2.61e+000
2.3     2.31e+000
2.4     2.06e+000
2.5     1.84e+000
2.6     1.66e+000
2.7     1.50e+000
2.8     1.36e+000
2.9     1.24e+000
3       1.14e+000
3.1     1.05e+000
3.2     9.71e-001
3.3     9.00e-001
3.4     8.36e-001
3.5     7.78e-001
3.6     7.26e-001
3.7     6.79e-001
3.8     6.37e-001
3.9     5.98e-001
4       5.62e-001
4.1     5.30e-001
4.2     5.01e-001
4.3     4.74e-001
4.4     4.49e-001
4.5     4.25e-001
4.6     4.04e-001
4.7     3.84e-001
4.8     3.65e-001
4.9     3.48e-001
5       3.31e-001
5.1     3.16e-001
5.2     3.02e-001
5.3     2.88e-001
5.4     2.76e-001
5.5     2.64e-001
5.6     2.53e-001
5.7     2.42e-001
5.8     2.33e-001
5.9     2.23e-001
6       2.14e-001
6.1     2.06e-001
6.2     1.98e-001
6.3     1.91e-001
6.4     1.83e-001
6.5     1.77e-001
6.6     1.70e-001
6.7     1.64e-001
6.8     1.58e-001
6.9     1.53e-001
7       1.47e-001
7.1     1.42e-001
7.2     1.37e-001
7.3     1.33e-001
7.4     1.28e-001
7.5     1.24e-001
7.6     1.20e-001
7.7     1.16e-001
7.8     1.13e-001
7.9     1.09e-001
8       1.06e-001
8.1     1.02e-001
8.2     9.92e-002
8.3     9.62e-002
8.4     9.34e-002
8.5     9.06e-002
8.6     8.79e-002
8.7     8.53e-002
8.8     8.29e-002
8.9     8.05e-002
9       7.82e-002
9.1     7.60e-002
9.2     7.39e-002
9.3     7.18e-002
9.4     6.98e-002
9.5     6.79e-002
9.6     6.60e-002
9.7     6.42e-002
9.8     6.25e-002
9.9     6.08e-002
```

```
10      5.92e-002
10.1    5.76e-002
10.2    5.60e-002
10.3    5.45e-002
10.4    5.31e-002
10.5    5.17e-002
10.6    5.03e-002
10.7    4.90e-002
10.8    4.78e-002
10.9    4.66e-002
11      4.54e-002
11.1    4.43e-002
11.2    4.32e-002
11.3    4.21e-002
11.4    4.11e-002
11.5    4.01e-002
11.6    3.91e-002
11.7    3.82e-002
11.8    3.73e-002
11.9    3.64e-002
12      3.56e-002
12.1    3.47e-002
12.2    3.39e-002
12.3    3.32e-002
12.4    3.24e-002
12.5    3.17e-002
12.6    3.10e-002
12.7    3.03e-002
12.8    2.96e-002
12.9    2.90e-002
13      2.84e-002
13.1    2.78e-002
13.2    2.72e-002
13.3    2.66e-002
13.4    2.60e-002
13.5    2.55e-002
13.6    2.50e-002
13.7    2.44e-002
13.8    2.39e-002
13.9    2.35e-002
14      2.30e-002
14.1    2.25e-002
14.2    2.21e-002
14.3    2.16e-002
14.4    2.12e-002
14.5    2.08e-002
14.6    2.04e-002
14.7    2.00e-002
14.8    1.96e-002
14.9    1.92e-002
15      1.89e-002
15.1    1.85e-002
15.2    1.82e-002
15.3    1.78e-002
15.4    1.75e-002
15.5    1.72e-002
15.6    1.68e-002
15.7    1.65e-002
15.8    1.62e-002
15.9    1.59e-002
16      1.56e-002
16.1    1.54e-002
16.2    1.51e-002
16.3    1.48e-002
16.4    1.46e-002
16.5    1.43e-002
16.6    1.40e-002
16.7    1.38e-002
16.8    1.36e-002
16.9    1.33e-002
17      1.31e-002
17.1    1.29e-002
17.2    1.26e-002
17.3    1.24e-002
17.4    1.22e-002
17.5    1.20e-002
17.6    1.18e-002
17.7    1.16e-002
17.8    1.14e-002
17.9    1.12e-002
18      1.10e-002
18.1    1.09e-002
18.2    1.07e-002
18.3    1.05e-002
18.4    1.03e-002
18.5    1.02e-002
18.6    1.00e-002
18.7    9.84e-003
18.8    9.68e-003
18.9    9.52e-003
19      9.37e-003
19.1    9.22e-003
19.2    9.08e-003
19.3    8.93e-003
19.4    8.79e-003
19.5    8.65e-003
19.6    8.51e-003
19.7    8.38e-003
19.8    8.25e-003
19.9    8.12e-003
20      7.99e-003 ];
%Trapped Proton in
Silicon at 4k
(rads/day)
%1997-11-17  08:51:30
%Trapped Proton Dose-
Depth
%    201 = Number of
Depth Points
%Depth (g/cm² Al)
       Dose (rad/day)
tpdc4=[0
1.24e+007
0.1     2.34e+004
0.2     5.19e+003
0.3     2.04e+003
0.4     1.02e+003
0.5     5.87e+002
0.6     3.71e+002
0.7     2.52e+002
0.8     1.80e+002
0.9     1.34e+002
1       1.04e+002
1.1     8.24e+001
1.2     6.69e+001
1.3     5.53e+001
1.4     4.64e+001
1.5     3.94e+001
1.6     3.38e+001
1.7     2.93e+001
1.8     2.56e+001
1.9     2.26e+001
2       2.00e+001
2.1     1.79e+001
2.2     1.60e+001
2.3     1.45e+001
2.4     1.32e+001
2.5     1.20e+001
2.6     1.10e+001
2.7     1.01e+001
2.8     9.35e+000
2.9     8.68e+000
3       8.09e+000
3.1     7.56e+000
3.2     7.09e+000
3.3     6.66e+000
3.4     6.27e+000
3.5     5.92e+000
3.6     5.59e+000
3.7     5.30e+000
3.8     5.02e+000
3.9     4.77e+000
4       4.54e+000
4.1     4.33e+000
4.2     4.14e+000
4.3     3.96e+000
4.4     3.79e+000
4.5     3.63e+000
4.6     3.48e+000
4.7     3.34e+000
4.8     3.21e+000
4.9     3.09e+000
5       2.97e+000
5.1     2.86e+000
5.2     2.76e+000
5.3     2.66e+000
5.4     2.57e+000
5.5     2.48e+000
5.6     2.40e+000
5.7     2.32e+000
5.8     2.25e+000
5.9     2.17e+000
6       2.11e+000
6.1     2.04e+000
6.2     1.98e+000
6.3     1.92e+000
6.4     1.86e+000
6.5     1.81e+000
6.6     1.76e+000
6.7     1.71e+000
6.8     1.66e+000
6.9     1.62e+000
7       1.58e+000
7.1     1.54e+000
7.2     1.50e+000
7.3     1.46e+000
7.4     1.42e+000
7.5     1.39e+000
7.6     1.35e+000
7.7     1.32e+000
7.8     1.29e+000
7.9     1.26e+000
8       1.23e+000
8.1     1.20e+000
8.2     1.17e+000
8.3     1.14e+000
8.4     1.12e+000
8.5     1.09e+000
8.6     1.07e+000
8.7     1.04e+000
8.8     1.02e+000
```

```
8.9     1.00e+000
9       9.79e-001
9.1     9.58e-001
9.2     9.38e-001
9.3     9.19e-001
9.4     9.00e-001
9.5     8.82e-001
9.6     8.64e-001
9.7     8.47e-001
9.8     8.30e-001
9.9     8.14e-001
10      7.98e-001
10.1    7.82e-001
10.2    7.67e-001
10.3    7.52e-001
10.4    7.38e-001
10.5    7.24e-001
10.6    7.11e-001
10.7    6.97e-001
10.8    6.85e-001
10.9    6.72e-001
11      6.60e-001
11.1    6.48e-001
11.2    6.37e-001
11.3    6.26e-001
11.4    6.15e-001
11.5    6.04e-001
11.6    5.94e-001
11.7    5.83e-001
11.8    5.74e-001
11.9    5.64e-001
12      5.54e-001
12.1    5.45e-001
12.2    5.36e-001
12.3    5.28e-001
12.4    5.19e-001
12.5    5.11e-001
12.6    5.03e-001
12.7    4.95e-001
12.8    4.87e-001
12.9    4.79e-001
13      4.72e-001
13.1    4.65e-001
13.2    4.58e-001
13.3    4.51e-001
13.4    4.44e-001
13.5    4.37e-001
13.6    4.31e-001
13.7    4.24e-001
13.8    4.18e-001
13.9    4.12e-001
14      4.06e-001
14.1    4.00e-001
14.2    3.94e-001
14.3    3.89e-001
14.4    3.83e-001
14.5    3.78e-001
14.6    3.73e-001
14.7    3.68e-001
14.8    3.63e-001
14.9    3.58e-001
15      3.53e-001
15.1    3.48e-001
15.2    3.43e-001
15.3    3.39e-001
15.4    3.34e-001
15.5    3.30e-001
15.6    3.25e-001
15.7    3.21e-001
15.8    3.17e-001
15.9    3.13e-001
16      3.09e-001
16.1    3.05e-001
16.2    3.01e-001
16.3    2.97e-001
16.4    2.93e-001
16.5    2.90e-001
16.6    2.86e-001
16.7    2.82e-001
16.8    2.79e-001
16.9    2.75e-001
17      2.72e-001
17.1    2.69e-001
17.2    2.65e-001
17.3    2.62e-001
17.4    2.59e-001
17.5    2.56e-001
17.6    2.53e-001
17.7    2.50e-001
17.8    2.47e-001
17.9    2.44e-001
18      2.41e-001
18.1    2.38e-001
18.2    2.35e-001
18.3    2.33e-001
18.4    2.30e-001
18.5    2.27e-001
18.6    2.25e-001
18.7    2.22e-001
18.8    2.20e-001
18.9    2.17e-001
19      2.15e-001
19.1    2.12e-001
19.2    2.10e-001
19.3    2.08e-001
19.4    2.05e-001
19.5    2.03e-001
19.6    2.01e-001
19.7    1.98e-001
19.8    1.96e-001
19.9    1.94e-001
20      1.92e-001];
Trapped Proton in
Silicon at 3k
(rads/day)
%1997-11-17  08:51:02
%Trapped Proton Dose-
Depth
%    201 = Number of
Depth Points
%Depth (g/cm² Al)
       Dose (rad/day)
tpdc3=[0
1.74e+006
0.1     4.14e+004
0.2     1.09e+004
0.3     4.50e+003
0.4     2.33e+003
0.5     1.39e+003
0.6     9.18e+002
0.7     6.53e+002
0.8     4.88e+002
0.9     3.80e+002
1       3.06e+002
1.1     2.53e+002
1.2     2.14e+002
1.3     1.85e+002
1.4     1.62e+002
1.5     1.43e+002
1.6     1.27e+002
1.7     1.14e+002
1.8     1.03e+002
1.9     9.37e+001
2       8.57e+001
2.1     7.87e+001
2.2     7.27e+001
2.3     6.74e+001
2.4     6.28e+001
2.5     5.87e+001
2.6     5.51e+001
2.7     5.19e+001
2.8     4.90e+001
2.9     4.64e+001
3       4.42e+001
3.1     4.22e+001
3.2     4.03e+001
3.3     3.86e+001
3.4     3.70e+001
3.5     3.55e+001
3.6     3.41e+001
3.7     3.28e+001
3.8     3.16e+001
3.9     3.05e+001
4       2.95e+001
4.1     2.85e+001
4.2     2.76e+001
4.3     2.68e+001
4.4     2.60e+001
4.5     2.52e+001
4.6     2.45e+001
4.7     2.38e+001
4.8     2.31e+001
4.9     2.25e+001
5       2.19e+001
5.1     2.13e+001
5.2     2.08e+001
5.3     2.02e+001
5.4     1.97e+001
5.5     1.93e+001
5.6     1.88e+001
5.7     1.84e+001
5.8     1.79e+001
5.9     1.75e+001
6       1.71e+001
6.1     1.68e+001
6.2     1.64e+001
6.3     1.60e+001
6.4     1.57e+001
6.5     1.54e+001
6.6     1.51e+001
6.7     1.48e+001
6.8     1.45e+001
6.9     1.42e+001
7       1.39e+001
7.1     1.37e+001
7.2     1.34e+001
7.3     1.32e+001
7.4     1.29e+001
7.5     1.27e+001
7.6     1.25e+001
7.7     1.22e+001
```

```
7.8     1.20e+001
7.9     1.18e+001
8       1.16e+001
8.1     1.14e+001
8.2     1.12e+001
8.3     1.10e+001
8.4     1.09e+001
8.5     1.07e+001
8.6     1.05e+001
8.7     1.03e+001
8.8     1.02e+001
8.9     1.00e+001
9       9.85e+000
9.1     9.69e+000
9.2     9.54e+000
9.3     9.40e+000
9.4     9.25e+000
9.5     9.11e+000
9.6     8.97e+000
9.7     8.84e+000
9.8     8.70e+000
9.9     8.57e+000
10      8.45e+000
10.1    8.32e+000
10.2    8.20e+000
10.3    8.08e+000
10.4    7.96e+000
10.5    7.84e+000
10.6    7.73e+000
10.7    7.62e+000
10.8    7.51e+000
10.9    7.41e+000
11      7.30e+000
11.1    7.20e+000
11.2    7.11e+000
11.3    7.01e+000
11.4    6.91e+000
11.5    6.82e+000
11.6    6.73e+000
11.7    6.64e+000
11.8    6.56e+000
11.9    6.47e+000
12      6.39e+000
12.1    6.31e+000
12.2    6.23e+000
12.3    6.15e+000
12.4    6.07e+000
12.5    6.00e+000
12.6    5.93e+000
12.7    5.85e+000
12.8    5.78e+000
12.9    5.71e+000
13      5.65e+000
13.1    5.58e+000
13.2    5.51e+000
13.3    5.45e+000
13.4    5.39e+000
13.5    5.33e+000
13.6    5.26e+000
13.7    5.21e+000
13.8    5.15e+000
13.9    5.09e+000
14      5.03e+000
14.1    4.98e+000
14.2    4.92e+000
14.3    4.87e+000
14.4    4.82e+000
14.5    4.76e+000
14.6    4.71e+000
14.7    4.66e+000
14.8    4.61e+000
14.9    4.57e+000
15      4.52e+000
15.1    4.47e+000
15.2    4.43e+000
15.3    4.38e+000
15.4    4.34e+000
15.5    4.29e+000
15.6    4.25e+000
15.7    4.21e+000
15.8    4.16e+000
15.9    4.12e+000
16      4.08e+000
16.1    4.04e+000
16.2    4.00e+000
16.3    3.96e+000
16.4    3.93e+000
16.5    3.89e+000
16.6    3.85e+000
16.7    3.81e+000
16.8    3.78e+000
16.9    3.74e+000
17      3.71e+000
17.1    3.67e+000
17.2    3.64e+000
17.3    3.60e+000
17.4    3.57e+000
17.5    3.54e+000
17.6    3.51e+000
17.7    3.47e+000
17.8    3.44e+000
17.9    3.41e+000
18      3.38e+000
18.1    3.35e+000
18.2    3.32e+000
18.3    3.29e+000
18.4    3.26e+000
18.5    3.24e+000
18.6    3.21e+000
18.7    3.18e+000
18.8    3.15e+000
18.9    3.13e+000
19      3.10e+000
19.1    3.07e+000
19.2    3.05e+000
19.3    3.02e+000
19.4    3.00e+000
19.5    2.97e+000
19.6    2.94e+000
19.7    2.92e+000
19.8    2.90e+000
19.9    2.87e+000
20      2.85e+000];
%Trapped Electron Dose
Depth in Silicon at 9k
(rads/day)
%1997-11-17  08:47:48
%Trapped Electron
Dose-Depth
%    201 = Number of
Depth Points
%Depth (g/cm² Al)
       Dose (rad/day)
tedc9=[0
1.31e+005
0.1     1.17e+004
0.2     6.24e+003
0.3     4.16e+003
0.4     2.97e+003
0.5     2.17e+003
0.6     1.61e+003
0.7     1.21e+003
0.8     9.08e+002
0.9     6.97e+002
1       5.35e+002
1.1     4.11e+002
1.2     3.16e+002
1.3     2.45e+002
1.4     1.81e+002
1.5     1.43e+002
1.6     1.08e+002
1.7     7.72e+001
1.8     6.12e+001
1.9     4.61e+001
2       3.17e+001
2.1     2.28e+001
2.2     1.80e+001
2.3     1.34e+001
2.4     9.01e+000
2.5     5.60e+000
2.6     4.83e+000
2.7     4.10e+000
2.8     3.39e+000
2.9     2.71e+000
3       2.05e+000
3.1     1.98e+000
3.2     1.91e+000
3.3     1.84e+000
3.4     1.77e+000
3.5     1.71e+000
3.6     1.65e+000
3.7     1.61e+000
3.8     1.59e+000
3.9     1.57e+000
4       1.55e+000
4.1     1.53e+000
4.2     1.51e+000
4.3     1.49e+000
4.4     1.47e+000
4.5     1.45e+000
4.6     1.43e+000
4.7     1.42e+000
4.8     1.40e+000
4.9     1.38e+000
5       1.37e+000
5.1     1.35e+000
5.2     1.34e+000
5.3     1.33e+000
5.4     1.31e+000
5.5     1.30e+000
5.6     1.29e+000
5.7     1.27e+000
5.8     1.26e+000
5.9     1.25e+000
6       1.24e+000
6.1     1.22e+000
6.2     1.21e+000
6.3     1.20e+000
6.4     1.19e+000
6.5     1.18e+000
```

6.6	1.17e+000
6.7	1.16e+000
6.8	1.15e+000
6.9	1.14e+000
7	1.13e+000
7.1	1.12e+000
7.2	1.11e+000
7.3	1.10e+000
7.4	1.09e+000
7.5	1.08e+000
7.6	1.07e+000
7.7	1.06e+000
7.8	1.05e+000
7.9	1.04e+000
8	1.04e+000
8.1	1.03e+000
8.2	1.02e+000
8.3	1.01e+000
8.4	1.00e+000
8.5	9.97e-001
8.6	9.89e-001
8.7	9.82e-001
8.8	9.74e-001
8.9	9.67e-001
9	9.60e-001
9.1	9.53e-001
9.2	9.45e-001
9.3	9.38e-001
9.4	9.31e-001
9.5	9.25e-001
9.6	9.18e-001
9.7	9.12e-001
9.8	9.06e-001
9.9	9.00e-001
10	8.94e-001
10.1	8.88e-001
10.2	8.82e-001
10.3	8.76e-001
10.4	8.70e-001
10.5	8.65e-001
10.6	8.59e-001
10.7	8.53e-001
10.8	8.48e-001
10.9	8.42e-001
11	8.37e-001
11.1	8.31e-001
11.2	8.26e-001
11.3	8.21e-001
11.4	8.15e-001
11.5	8.10e-001
11.6	8.05e-001
11.7	8.01e-001
11.8	7.96e-001
11.9	7.91e-001
12	7.86e-001
12.1	7.82e-001
12.2	7.77e-001
12.3	7.73e-001
12.4	7.68e-001
12.5	7.64e-001
12.6	7.59e-001
12.7	7.55e-001
12.8	7.50e-001
12.9	7.46e-001
13	7.42e-001
13.1	7.37e-001
13.2	7.33e-001
13.3	7.29e-001
13.4	7.25e-001
13.5	7.21e-001
13.6	7.17e-001
13.7	7.12e-001
13.8	7.08e-001
13.9	7.04e-001
14	7.00e-001
14.1	6.96e-001
14.2	6.93e-001
14.3	6.89e-001
14.4	6.85e-001
14.5	6.81e-001
14.6	6.77e-001
14.7	6.73e-001
14.8	6.70e-001
14.9	6.66e-001
15	6.62e-001
15.1	6.58e-001
15.2	6.55e-001
15.3	6.51e-001
15.4	6.47e-001
15.5	6.44e-001
15.6	6.40e-001
15.7	6.37e-001
15.8	6.33e-001
15.9	6.30e-001
16	6.26e-001
16.1	6.23e-001
16.2	6.19e-001
16.3	6.16e-001
16.4	6.12e-001
16.5	6.09e-001
16.6	6.06e-001
16.7	6.02e-001
16.8	5.99e-001
16.9	5.96e-001
17	5.92e-001
17.1	5.89e-001
17.2	5.85e-001
17.3	5.82e-001
17.4	5.79e-001
17.5	5.75e-001
17.6	5.72e-001
17.7	5.69e-001
17.8	5.65e-001
17.9	5.62e-001
18	5.59e-001
18.1	5.56e-001
18.2	5.53e-001
18.3	5.49e-001
18.4	5.46e-001
18.5	5.43e-001
18.6	5.40e-001
18.7	5.37e-001
18.8	5.34e-001
18.9	5.31e-001
19	5.27e-001
19.1	5.24e-001
19.2	5.21e-001
19.3	5.18e-001
19.4	5.15e-001
19.5	5.12e-001
19.6	5.09e-001
19.7	5.06e-001
19.8	5.03e-001
19.9	5.00e-001

```
20      4.98e-001];
%Trapped Electron Dose
Depth in Silicon at 8k
(rads/day)
%1997-11-17  08:47:31
%Trapped Electron
Dose-Depth
%    201 = Number of
Depth Points
%Depth (g/cm² Al)
       Dose (rad/day)
tedc8=[0
1.15e+005
0.1     7.63e+003
0.2     3.90e+003
0.3     2.59e+003
0.4     1.87e+003
0.5     1.38e+003
0.6     1.03e+003
0.7     7.82e+002
0.8     5.91e+002
0.9     4.56e+002
1       3.52e+002
1.1     2.74e+002
1.2     2.14e+002
1.3     1.70e+002
1.4     1.30e+002
1.5     1.06e+002
1.6     8.33e+001
1.7     6.32e+001
1.8     5.13e+001
1.9     4.00e+001
2       2.93e+001
2.1     2.22e+001
2.2     1.77e+001
2.3     1.34e+001
2.4     9.29e+000
2.5     6.04e+000
2.6     5.10e+000
2.7     4.20e+000
2.8     3.32e+000
2.9     2.48e+000
3       1.67e+000
3.1     1.57e+000
3.2     1.47e+000
3.3     1.38e+000
3.4     1.29e+000
3.5     1.20e+000
3.6     1.12e+000
3.7     1.08e+000
3.8     1.06e+000
3.9     1.04e+000
4       1.03e+000
4.1     1.01e+000
4.2     1.00e+000
4.3     9.86e-001
4.4     9.73e-001
4.5     9.61e-001
4.6     9.50e-001
4.7     9.39e-001
4.8     9.29e-001
4.9     9.18e-001
5       9.08e-001
5.1     8.98e-001
5.2     8.88e-001
5.3     8.79e-001
5.4     8.70e-001
```

```
5.5     8.61e-001
5.6     8.52e-001
5.7     8.44e-001
5.8     8.36e-001
5.9     8.27e-001
6       8.19e-001
6.1     8.11e-001
6.2     8.04e-001
6.3     7.96e-001
6.4     7.89e-001
6.5     7.81e-001
6.6     7.74e-001
6.7     7.68e-001
6.8     7.61e-001
6.9     7.54e-001
7       7.48e-001
7.1     7.41e-001
7.2     7.35e-001
7.3     7.29e-001
7.4     7.22e-001
7.5     7.16e-001
7.6     7.10e-001
7.7     7.04e-001
7.8     6.99e-001
7.9     6.93e-001
8       6.88e-001
8.1     6.82e-001
8.2     6.77e-001
8.3     6.72e-001
8.4     6.67e-001
8.5     6.62e-001
8.6     6.57e-001
8.7     6.52e-001
8.8     6.47e-001
8.9     6.42e-001
9       6.37e-001
9.1     6.32e-001
9.2     6.28e-001
9.3     6.23e-001
9.4     6.18e-001
9.5     6.14e-001
9.6     6.10e-001
9.7     6.06e-001
9.8     6.02e-001
9.9     5.98e-001
10      5.94e-001
10.1    5.90e-001
10.2    5.86e-001
10.3    5.82e-001
10.4    5.78e-001
10.5    5.74e-001
10.6    5.70e-001
10.7    5.67e-001
10.8    5.63e-001
10.9    5.59e-001
11      5.56e-001
11.1    5.52e-001
11.2    5.49e-001
11.3    5.45e-001
11.4    5.41e-001
11.5    5.38e-001
11.6    5.35e-001
11.7    5.32e-001
11.8    5.29e-001
11.9    5.25e-001
12      5.22e-001
12.1    5.19e-001
12.2    5.16e-001
12.3    5.13e-001
12.4    5.10e-001
12.5    5.07e-001
12.6    5.04e-001
12.7    5.01e-001
12.8    4.99e-001
12.9    4.96e-001
13      4.93e-001
13.1    4.90e-001
13.2    4.87e-001
13.3    4.84e-001
13.4    4.82e-001
13.5    4.79e-001
13.6    4.76e-001
13.7    4.73e-001
13.8    4.71e-001
13.9    4.68e-001
14      4.66e-001
14.1    4.63e-001
14.2    4.60e-001
14.3    4.58e-001
14.4    4.55e-001
14.5    4.53e-001
14.6    4.50e-001
14.7    4.48e-001
14.8    4.45e-001
14.9    4.43e-001
15      4.40e-001
15.1    4.38e-001
15.2    4.35e-001
15.3    4.33e-001
15.4    4.31e-001
15.5    4.28e-001
15.6    4.26e-001
15.7    4.24e-001
15.8    4.21e-001
15.9    4.19e-001
16      4.17e-001
16.1    4.14e-001
16.2    4.12e-001
16.3    4.10e-001
16.4    4.08e-001
16.5    4.05e-001
16.6    4.03e-001
16.7    4.01e-001
16.8    3.99e-001
16.9    3.97e-001
17      3.94e-001
17.1    3.92e-001
17.2    3.90e-001
17.3    3.88e-001
17.4    3.85e-001
17.5    3.83e-001
17.6    3.81e-001
17.7    3.79e-001
17.8    3.77e-001
17.9    3.75e-001
18      3.72e-001
18.1    3.70e-001
18.2    3.68e-001
18.3    3.66e-001
18.4    3.64e-001
18.5    3.62e-001
18.6    3.60e-001
18.7    3.58e-001
18.8    3.56e-001
18.9    3.54e-001
19      3.52e-001
19.1    3.50e-001
19.2    3.48e-001
19.3    3.46e-001
19.4    3.44e-001
19.5    3.42e-001
19.6    3.40e-001
19.7    3.38e-001
19.8    3.36e-001
19.9    3.34e-001
20      3.32e-001];
%Trapped Electron Dose
Depth in Silicon at 7k
(rads/day)
%1997-11-17  08:47:10
%Trapped Electron
Dose-Depth
%    201 = Number of
Depth Points
%Depth (g/cm² Al)
       Dose (rad/day)
tedc7=[0
1.40e+005
0.1     5.38e+003
0.2     2.48e+003
0.3     1.58e+003
0.4     1.11e+003
0.5     8.03e+002
0.6     5.96e+002
0.7     4.48e+002
0.8     3.36e+002
0.9     2.57e+002
1       1.97e+002
1.1     1.52e+002
1.2     1.19e+002
1.3     9.48e+001
1.4     7.32e+001
1.5     6.05e+001
1.6     4.86e+001
1.7     3.80e+001
1.8     3.16e+001
1.9     2.55e+001
2       1.97e+001
2.1     1.55e+001
2.2     1.27e+001
2.3     9.93e+000
2.4     7.31e+000
2.5     5.18e+000
2.6     4.39e+000
2.7     3.62e+000
2.8     2.88e+000
2.9     2.16e+000
3       1.47e+000
3.1     1.34e+000
3.2     1.22e+000
3.3     1.09e+000
3.4     9.74e-001
3.5     8.59e-001
3.6     7.46e-001
3.7     6.99e-001
3.8     6.87e-001
3.9     6.74e-001
4       6.62e-001
4.1     6.50e-001
4.2     6.39e-001
4.3     6.27e-001
```

```
4.4     6.16e-001
4.5     6.09e-001
4.6     6.01e-001
4.7     5.94e-001
4.8     5.87e-001
4.9     5.80e-001
5       5.73e-001
5.1     5.67e-001
5.2     5.60e-001
5.3     5.54e-001
5.4     5.48e-001
5.5     5.42e-001
5.6     5.36e-001
5.7     5.31e-001
5.8     5.25e-001
5.9     5.20e-001
6       5.15e-001
6.1     5.09e-001
6.2     5.04e-001
6.3     4.99e-001
6.4     4.94e-001
6.5     4.90e-001
6.6     4.85e-001
6.7     4.81e-001
6.8     4.76e-001
6.9     4.72e-001
7       4.68e-001
7.1     4.63e-001
7.2     4.59e-001
7.3     4.55e-001
7.4     4.51e-001
7.5     4.47e-001
7.6     4.43e-001
7.7     4.39e-001
7.8     4.36e-001
7.9     4.32e-001
8       4.29e-001
8.1     4.25e-001
8.2     4.22e-001
8.3     4.18e-001
8.4     4.15e-001
8.5     4.12e-001
8.6     4.08e-001
8.7     4.05e-001
8.8     4.02e-001
8.9     3.99e-001
9       3.96e-001
9.1     3.93e-001
9.2     3.90e-001
9.3     3.87e-001
9.4     3.84e-001
9.5     3.81e-001
9.6     3.78e-001
9.7     3.76e-001
9.8     3.73e-001
9.9     3.70e-001
10      3.68e-001
10.1    3.65e-001
10.2    3.63e-001
10.3    3.60e-001
10.4    3.58e-001
10.5    3.55e-001
10.6    3.53e-001
10.7    3.51e-001
10.8    3.48e-001
10.9    3.46e-001
11      3.44e-001
11.1    3.41e-001
11.2    3.39e-001
11.3    3.37e-001
11.4    3.34e-001
11.5    3.32e-001
11.6    3.30e-001
11.7    3.28e-001
11.8    3.26e-001
11.9    3.24e-001
12      3.22e-001
12.1    3.20e-001
12.2    3.18e-001
12.3    3.16e-001
12.4    3.14e-001
12.5    3.13e-001
12.6    3.11e-001
12.7    3.09e-001
12.8    3.07e-001
12.9    3.05e-001
13      3.03e-001
13.1    3.01e-001
13.2    3.00e-001
13.3    2.98e-001
13.4    2.96e-001
13.5    2.94e-001
13.6    2.93e-001
13.7    2.91e-001
13.8    2.89e-001
13.9    2.87e-001
14      2.86e-001
14.1    2.84e-001
14.2    2.83e-001
14.3    2.81e-001
14.4    2.79e-001
14.5    2.78e-001
14.6    2.76e-001
14.7    2.75e-001
14.8    2.73e-001
14.9    2.71e-001
15      2.70e-001
15.1    2.68e-001
15.2    2.67e-001
15.3    2.65e-001
15.4    2.64e-001
15.5    2.62e-001
15.6    2.61e-001
15.7    2.59e-001
15.8    2.58e-001
15.9    2.56e-001
16      2.55e-001
16.1    2.53e-001
16.2    2.52e-001
16.3    2.51e-001
16.4    2.49e-001
16.5    2.48e-001
16.6    2.46e-001
16.7    2.45e-001
16.8    2.44e-001
16.9    2.42e-001
17      2.41e-001
17.1    2.39e-001
17.2    2.38e-001
17.3    2.37e-001
17.4    2.35e-001
17.5    2.34e-001
17.6    2.33e-001
17.7    2.31e-001
17.8    2.30e-001
17.9    2.29e-001
18      2.27e-001
18.1    2.26e-001
18.2    2.25e-001
18.3    2.23e-001
18.4    2.22e-001
18.5    2.21e-001
18.6    2.19e-001
18.7    2.18e-001
18.8    2.17e-001
18.9    2.16e-001
19      2.14e-001
19.1    2.13e-001
19.2    2.12e-001
19.3    2.11e-001
19.4    2.09e-001
19.5    2.08e-001
19.6    2.07e-001
19.7    2.06e-001
19.8    2.04e-001
19.9    2.03e-001
20      2.02e-001];
%Trapped Electron Dose
Depth in Silicon at 6k
(rads/day) corrected
%1997-11-18  17:07:00
%Trapped Electron
Dose-Depth
%    201 = Number of
Depth Points
%Depth (g/cm² Al)
      Dose (rad/day)
tedc6=[0
2.15e+005
0.1     4.53e+003
0.2     1.66e+003
0.3     9.53e+002
0.4     6.31e+002
0.5     4.35e+002
0.6     3.06e+002
0.7     2.16e+002
0.8     1.52e+002
0.9     1.09e+002
1       7.86e+001
1.1     5.75e+001
1.2     4.26e+001
1.3     3.29e+001
1.4     2.43e+001
1.5     1.99e+001
1.6     1.58e+001
1.7     1.22e+001
1.8     1.01e+001
1.9     8.23e+000
2       6.42e+000
2.1     5.13e+000
2.2     4.25e+000
2.3     3.41e+000
2.4     2.60e+000
2.5     1.95e+000
2.6     1.69e+000
2.7     1.45e+000
2.8     1.21e+000
2.9     9.81e-001
3       7.60e-001
3.1     7.11e-001
3.2     6.63e-001
```

```
3.3     6.17e-001
3.4     5.73e-001
3.5     5.29e-001
3.6     4.87e-001
3.7     4.67e-001
3.8     4.58e-001
3.9     4.49e-001
4       4.41e-001
4.1     4.33e-001
4.2     4.24e-001
4.3     4.17e-001
4.4     4.09e-001
4.5     4.03e-001
4.6     3.97e-001
4.7     3.91e-001
4.8     3.86e-001
4.9     3.80e-001
5       3.75e-001
5.1     3.70e-001
5.2     3.64e-001
5.3     3.59e-001
5.4     3.55e-001
5.5     3.50e-001
5.6     3.46e-001
5.7     3.42e-001
5.8     3.38e-001
5.9     3.33e-001
6       3.29e-001
6.1     3.25e-001
6.2     3.21e-001
6.3     3.18e-001
6.4     3.14e-001
6.5     3.10e-001
6.6     3.07e-001
6.7     3.04e-001
6.8     3.00e-001
6.9     2.97e-001
7       2.94e-001
7.1     2.91e-001
7.2     2.88e-001
7.3     2.85e-001
7.4     2.82e-001
7.5     2.79e-001
7.6     2.76e-001
7.7     2.73e-001
7.8     2.70e-001
7.9     2.68e-001
8       2.65e-001
8.1     2.63e-001
8.2     2.60e-001
8.3     2.58e-001
8.4     2.55e-001
8.5     2.53e-001
8.6     2.51e-001
8.7     2.48e-001
8.8     2.46e-001
8.9     2.44e-001
9       2.42e-001
9.1     2.39e-001
9.2     2.37e-001
9.3     2.35e-001
9.4     2.33e-001
9.5     2.31e-001
9.6     2.29e-001
9.7     2.27e-001
9.8     2.25e-001
9.9     2.23e-001
10      2.22e-001
10.1    2.20e-001
10.2    2.18e-001
10.3    2.16e-001
10.4    2.15e-001
10.5    2.13e-001
10.6    2.11e-001
10.7    2.10e-001
10.8    2.08e-001
10.9    2.06e-001
11      2.05e-001
11.1    2.03e-001
11.2    2.01e-001
11.3    2.00e-001
11.4    1.98e-001
11.5    1.97e-001
11.6    1.95e-001
11.7    1.94e-001
11.8    1.92e-001
11.9    1.91e-001
12      1.90e-001
12.1    1.88e-001
12.2    1.87e-001
12.3    1.86e-001
12.4    1.84e-001
12.5    1.83e-001
12.6    1.82e-001
12.7    1.81e-001
12.8    1.79e-001
12.9    1.78e-001
13      1.77e-001
13.1    1.75e-001
13.2    1.74e-001
13.3    1.73e-001
13.4    1.72e-001
13.5    1.71e-001
13.6    1.69e-001
13.7    1.68e-001
13.8    1.67e-001
13.9    1.66e-001
14      1.65e-001
14.1    1.64e-001
14.2    1.63e-001
14.3    1.61e-001
14.4    1.60e-001
14.5    1.59e-001
14.6    1.58e-001
14.7    1.57e-001
14.8    1.56e-001
14.9    1.55e-001
15      1.54e-001
15.1    1.53e-001
15.2    1.52e-001
15.3    1.51e-001
15.4    1.50e-001
15.5    1.49e-001
15.6    1.48e-001
15.7    1.47e-001
15.8    1.46e-001
15.9    1.45e-001
16      1.44e-001
16.1    1.43e-001
16.2    1.42e-001
16.3    1.41e-001
16.4    1.40e-001
16.5    1.40e-001
16.6    1.39e-001
16.7    1.38e-001
16.8    1.37e-001
16.9    1.36e-001
17      1.35e-001
17.1    1.34e-001
17.2    1.33e-001
17.3    1.32e-001
17.4    1.31e-001
17.5    1.31e-001
17.6    1.30e-001
17.7    1.29e-001
17.8    1.28e-001
17.9    1.27e-001
18      1.26e-001
18.1    1.25e-001
18.2    1.25e-001
18.3    1.24e-001
18.4    1.23e-001
18.5    1.22e-001
18.6    1.21e-001
18.7    1.21e-001
18.8    1.20e-001
18.9    1.19e-001
19      1.18e-001
19.1    1.17e-001
19.2    1.17e-001
19.3    1.16e-001
19.4    1.15e-001
19.5    1.14e-001
19.6    1.13e-001
19.7    1.13e-001
19.8    1.12e-001
19.9    1.11e-001
20      1.10e-001];
%Trapped Electron Dose
Depth in Silicon at 5k
(rads/day)
%1997-11-17  08:46:24
%Trapped Electron
Dose-Depth
%    201 = Number of
Depth Points
%Depth (g/cm² Al)
       Dose (rad/day)
tedc5=[0
2.90e+005
0.1     5.58e+003
0.2     1.42e+003
0.3     5.88e+002
0.4     3.08e+002
0.5     1.76e+002
0.6     1.07e+002
0.7     6.67e+001
0.8     4.14e+001
0.9     2.76e+001
1       1.82e+001
1.1     1.24e+001
1.2     8.54e+000
1.3     6.34e+000
1.4     4.38e+000
1.5     3.58e+000
1.6     2.84e+000
1.7     2.18e+000
1.8     1.89e+000
1.9     1.61e+000
2       1.35e+000
2.1     1.16e+000
```

```
2.2     1.04e+000
2.3     9.27e-001
2.4     8.16e-001
2.5     7.24e-001
2.6     6.80e-001
2.7     6.37e-001
2.8     5.96e-001
2.9     5.57e-001
3       5.18e-001
3.1     5.01e-001
3.2     4.84e-001
3.3     4.68e-001
3.4     4.52e-001
3.5     4.37e-001
3.6     4.22e-001
3.7     4.12e-001
3.8     4.03e-001
3.9     3.95e-001
4       3.86e-001
4.1     3.78e-001
4.2     3.71e-001
4.3     3.63e-001
4.4     3.56e-001
4.5     3.49e-001
4.6     3.43e-001
4.7     3.37e-001
4.8     3.32e-001
4.9     3.26e-001
5       3.20e-001
5.1     3.15e-001
5.2     3.10e-001
5.3     3.04e-001
5.4     3.00e-001
5.5     2.95e-001
5.6     2.91e-001
5.7     2.87e-001
5.8     2.82e-001
5.9     2.78e-001
6       2.74e-001
6.1     2.70e-001
6.2     2.66e-001
6.3     2.62e-001
6.4     2.59e-001
6.5     2.55e-001
6.6     2.52e-001
6.7     2.49e-001
6.8     2.45e-001
6.9     2.42e-001
7       2.39e-001
7.1     2.36e-001
7.2     2.33e-001
7.3     2.30e-001
7.4     2.27e-001
7.5     2.24e-001
7.6     2.22e-001
7.7     2.19e-001
7.8     2.16e-001
7.9     2.13e-001
8       2.11e-001
8.1     2.09e-001
8.2     2.06e-001
8.3     2.04e-001
8.4     2.02e-001
8.5     2.00e-001
8.6     1.97e-001
8.7     1.95e-001
8.8     1.93e-001
8.9     1.91e-001
9       1.89e-001
9.1     1.87e-001
9.2     1.85e-001
9.3     1.83e-001
9.4     1.81e-001
9.5     1.79e-001
9.6     1.77e-001
9.7     1.75e-001
9.8     1.73e-001
9.9     1.72e-001
10      1.70e-001
10.1    1.68e-001
10.2    1.67e-001
10.3    1.65e-001
10.4    1.63e-001
10.5    1.62e-001
10.6    1.60e-001
10.7    1.59e-001
10.8    1.57e-001
10.9    1.56e-001
11      1.54e-001
11.1    1.53e-001
11.2    1.51e-001
11.3    1.50e-001
11.4    1.48e-001
11.5    1.47e-001
11.6    1.45e-001
11.7    1.44e-001
11.8    1.43e-001
11.9    1.42e-001
12      1.40e-001
12.1    1.39e-001
12.2    1.38e-001
12.3    1.37e-001
12.4    1.35e-001
12.5    1.34e-001
12.6    1.33e-001
12.7    1.32e-001
12.8    1.31e-001
12.9    1.30e-001
13      1.28e-001
13.1    1.27e-001
13.2    1.26e-001
13.3    1.25e-001
13.4    1.24e-001
13.5    1.23e-001
13.6    1.22e-001
13.7    1.21e-001
13.8    1.19e-001
13.9    1.18e-001
14      1.17e-001
14.1    1.16e-001
14.2    1.15e-001
14.3    1.14e-001
14.4    1.14e-001
14.5    1.13e-001
14.6    1.12e-001
14.7    1.11e-001
14.8    1.10e-001
14.9    1.09e-001
15      1.08e-001
15.1    1.07e-001
15.2    1.06e-001
15.3    1.05e-001
15.4    1.04e-001
15.5    1.03e-001
15.6    1.03e-001
15.7    1.02e-001
15.8    1.01e-001
15.9    1.00e-001
16      9.91e-002
16.1    9.83e-002
16.2    9.74e-002
16.3    9.66e-002
16.4    9.58e-002
16.5    9.49e-002
16.6    9.41e-002
16.7    9.33e-002
16.8    9.25e-002
16.9    9.17e-002
17      9.10e-002
17.1    9.02e-002
17.2    8.95e-002
17.3    8.88e-002
17.4    8.80e-002
17.5    8.73e-002
17.6    8.66e-002
17.7    8.59e-002
17.8    8.52e-002
17.9    8.45e-002
18      8.38e-002
18.1    8.31e-002
18.2    8.24e-002
18.3    8.17e-002
18.4    8.10e-002
18.5    8.04e-002
18.6    7.97e-002
18.7    7.90e-002
18.8    7.83e-002
18.9    7.77e-002
19      7.70e-002
19.1    7.64e-002
19.2    7.57e-002
19.3    7.51e-002
19.4    7.44e-002
19.5    7.38e-002
19.6    7.31e-002
19.7    7.25e-002
19.8    7.19e-002
19.9    7.12e-002
20      7.06e-002 ];
%Trapped Electron Dose
Depth in Silicon at 4k
(rads/day)
%1997-11-21  20:25:24
%Trapped Electron
Dose-Depth
%    201 = Number of
Depth Points
%Depth (g/cm² Al)
       Dose (rad/day)
tedc4=[0
4.61e+005
0.1     9.15e+003
0.2     1.34e+003
0.3     3.92e+002
0.4     1.56e+002
0.5     7.02e+001
0.6     3.61e+001
0.7     2.02e+001
0.8     1.18e+001
0.9     7.94e+000
1       5.41e+000
```

```
1.1     3.96e+000
1.2     3.00e+000
1.3     2.47e+000
1.4     2.00e+000
1.5     1.82e+000
1.6     1.66e+000
1.7     1.51e+000
1.8     1.43e+000
1.9     1.35e+000
2       1.28e+000
2.1     1.22e+000
2.2     1.17e+000
2.3     1.13e+000
2.4     1.08e+000
2.5     1.04e+000
2.6     1.00e+000
2.7     9.72e-001
2.8     9.40e-001
2.9     9.09e-001
3       8.80e-001
3.1     8.56e-001
3.2     8.33e-001
3.3     8.10e-001
3.4     7.89e-001
3.5     7.67e-001
3.6     7.47e-001
3.7     7.29e-001
3.8     7.13e-001
3.9     6.97e-001
4       6.82e-001
4.1     6.66e-001
4.2     6.52e-001
4.3     6.37e-001
4.4     6.23e-001
4.5     6.12e-001
4.6     6.00e-001
4.7     5.89e-001
4.8     5.78e-001
4.9     5.67e-001
5       5.57e-001
5.1     5.46e-001
5.2     5.36e-001
5.3     5.26e-001
5.4     5.17e-001
5.5     5.09e-001
5.6     5.01e-001
5.7     4.93e-001
5.8     4.85e-001
5.9     4.77e-001
6       4.69e-001
6.1     4.62e-001
6.2     4.54e-001
6.3     4.47e-001
6.4     4.40e-001
6.5     4.33e-001
6.6     4.27e-001
6.7     4.21e-001
6.8     4.15e-001
6.9     4.09e-001
7       4.04e-001
7.1     3.98e-001
7.2     3.92e-001
7.3     3.87e-001
7.4     3.82e-001
7.5     3.76e-001
7.6     3.71e-001
7.7     3.66e-001
7.8     3.61e-001
7.9     3.56e-001
8       3.52e-001
8.1     3.47e-001
8.2     3.43e-001
8.3     3.39e-001
8.4     3.34e-001
8.5     3.30e-001
8.6     3.26e-001
8.7     3.22e-001
8.8     3.18e-001
8.9     3.14e-001
9       3.10e-001
9.1     3.06e-001
9.2     3.03e-001
9.3     2.99e-001
9.4     2.95e-001
9.5     2.91e-001
9.6     2.88e-001
9.7     2.85e-001
9.8     2.82e-001
9.9     2.79e-001
10      2.75e-001
10.1    2.72e-001
10.2    2.69e-001
10.3    2.66e-001
10.4    2.63e-001
10.5    2.60e-001
10.6    2.57e-001
10.7    2.54e-001
10.8    2.52e-001
10.9    2.49e-001
11      2.46e-001
11.1    2.43e-001
11.2    2.40e-001
11.3    2.37e-001
11.4    2.35e-001
11.5    2.32e-001
11.6    2.30e-001
11.7    2.27e-001
11.8    2.25e-001
11.9    2.23e-001
12      2.20e-001
12.1    2.18e-001
12.2    2.16e-001
12.3    2.13e-001
12.4    2.11e-001
12.5    2.09e-001
12.6    2.07e-001
12.7    2.05e-001
12.8    2.02e-001
12.9    2.00e-001
13      1.98e-001
13.1    1.96e-001
13.2    1.94e-001
13.3    1.92e-001
13.4    1.90e-001
13.5    1.88e-001
13.6    1.86e-001
13.7    1.84e-001
13.8    1.82e-001
13.9    1.80e-001
14      1.78e-001
14.1    1.76e-001
14.2    1.74e-001
14.3    1.73e-001
14.4    1.71e-001
14.5    1.69e-001
14.6    1.68e-001
14.7    1.66e-001
14.8    1.64e-001
14.9    1.63e-001
15      1.61e-001
15.1    1.59e-001
15.2    1.58e-001
15.3    1.56e-001
15.4    1.55e-001
15.5    1.53e-001
15.6    1.51e-001
15.7    1.50e-001
15.8    1.48e-001
15.9    1.47e-001
16      1.45e-001
16.1    1.44e-001
16.2    1.42e-001
16.3    1.41e-001
16.4    1.39e-001
16.5    1.38e-001
16.6    1.36e-001
16.7    1.35e-001
16.8    1.33e-001
16.9    1.32e-001
17      1.31e-001
17.1    1.29e-001
17.2    1.28e-001
17.3    1.27e-001
17.4    1.26e-001
17.5    1.24e-001
17.6    1.23e-001
17.7    1.22e-001
17.8    1.21e-001
17.9    1.20e-001
18      1.19e-001
18.1    1.17e-001
18.2    1.16e-001
18.3    1.15e-001
18.4    1.14e-001
18.5    1.13e-001
18.6    1.12e-001
18.7    1.10e-001
18.8    1.09e-001
18.9    1.08e-001
19      1.07e-001
19.1    1.06e-001
19.2    1.05e-001
19.3    1.04e-001
19.4    1.03e-001
19.5    1.02e-001
19.6    1.01e-001
19.7    9.95e-002
19.8    9.84e-002
19.9    9.74e-002
20      9.63e-002 ];
%Trapped Electron Dose
Depth in Silicon at 3k
(rads/day)
%1997-11-17  08:45:42
%Trapped Electron
Dose-Depth
%   201 = Number of
Depth Points
%Depth (g/cm² Al)
       Dose (rad/day)
```

```
tedc3=[0
5.15e+005
0.1     1.23e+004
0.2     2.06e+003
0.3     6.66e+002
0.4     3.12e+002
0.5     1.66e+002
0.6     9.40e+001
0.7     5.49e+001
0.8     3.19e+001
0.9     2.08e+001
1       1.34e+001
1.1     9.00e+000
1.2     6.10e+000
1.3     4.49e+000
1.4     3.07e+000
1.5     2.61e+000
1.6     2.19e+000
1.7     1.82e+000
1.8     1.70e+000
1.9     1.59e+000
2       1.48e+000
2.1     1.40e+000
2.2     1.35e+000
2.3     1.29e+000
2.4     1.24e+000
2.5     1.19e+000
2.6     1.15e+000
2.7     1.12e+000
2.8     1.08e+000
2.9     1.05e+000
3       1.02e+000
3.1     9.89e-001
3.2     9.63e-001
3.3     9.37e-001
3.4     9.13e-001
3.5     8.89e-001
3.6     8.66e-001
3.7     8.46e-001
3.8     8.28e-001
3.9     8.10e-001
4       7.92e-001
4.1     7.75e-001
4.2     7.59e-001
4.3     7.43e-001
4.4     7.27e-001
4.5     7.13e-001
4.6     7.00e-001
4.7     6.88e-001
4.8     6.75e-001
4.9     6.63e-001
5       6.51e-001
5.1     6.40e-001
5.2     6.28e-001
5.3     6.17e-001
5.4     6.07e-001
5.5     5.97e-001
5.6     5.88e-001
5.7     5.79e-001
5.8     5.70e-001
5.9     5.61e-001
6       5.52e-001
6.1     5.44e-001
6.2     5.36e-001
6.3     5.27e-001
6.4     5.19e-001
6.5     5.12e-001
6.6     5.05e-001
6.7     4.98e-001
6.8     4.91e-001
6.9     4.85e-001
7       4.78e-001
7.1     4.72e-001
7.2     4.65e-001
7.3     4.59e-001
7.4     4.53e-001
7.5     4.47e-001
7.6     4.41e-001
7.7     4.35e-001
7.8     4.29e-001
7.9     4.24e-001
8       4.19e-001
8.1     4.14e-001
8.2     4.09e-001
8.3     4.04e-001
8.4     3.99e-001
8.5     3.95e-001
8.6     3.90e-001
8.7     3.85e-001
8.8     3.81e-001
8.9     3.76e-001
9       3.72e-001
9.1     3.67e-001
9.2     3.63e-001
9.3     3.59e-001
9.4     3.54e-001
9.5     3.50e-001
9.6     3.46e-001
9.7     3.43e-001
9.8     3.39e-001
9.9     3.36e-001
10      3.32e-001
10.1    3.28e-001
10.2    3.25e-001
10.3    3.21e-001
10.4    3.18e-001
10.5    3.15e-001
10.6    3.11e-001
10.7    3.08e-001
10.8    3.05e-001
10.9    3.01e-001
11      2.98e-001
11.1    2.95e-001
11.2    2.92e-001
11.3    2.88e-001
11.4    2.85e-001
11.5    2.82e-001
11.6    2.80e-001
11.7    2.77e-001
11.8    2.74e-001
11.9    2.71e-001
12      2.69e-001
12.1    2.66e-001
12.2    2.63e-001
12.3    2.61e-001
12.4    2.58e-001
12.5    2.56e-001
12.6    2.53e-001
12.7    2.51e-001
12.8    2.48e-001
12.9    2.46e-001
13      2.43e-001
13.1    2.41e-001
13.2    2.38e-001
13.3    2.36e-001
13.4    2.34e-001
13.5    2.31e-001
13.6    2.29e-001
13.7    2.27e-001
13.8    2.24e-001
13.9    2.22e-001
14      2.20e-001
14.1    2.18e-001
14.2    2.16e-001
14.3    2.14e-001
14.4    2.12e-001
14.5    2.10e-001
14.6    2.08e-001
14.7    2.06e-001
14.8    2.04e-001
14.9    2.02e-001
15      2.00e-001
15.1    1.98e-001
15.2    1.96e-001
15.3    1.94e-001
15.4    1.93e-001
15.5    1.91e-001
15.6    1.89e-001
15.7    1.87e-001
15.8    1.85e-001
15.9    1.83e-001
16      1.82e-001
16.1    1.80e-001
16.2    1.78e-001
16.3    1.76e-001
16.4    1.75e-001
16.5    1.73e-001
16.6    1.71e-001
16.7    1.69e-001
16.8    1.68e-001
16.9    1.66e-001
17      1.65e-001
17.1    1.63e-001
17.2    1.62e-001
17.3    1.60e-001
17.4    1.59e-001
17.5    1.57e-001
17.6    1.56e-001
17.7    1.54e-001
17.8    1.53e-001
17.9    1.52e-001
18      1.50e-001
18.1    1.49e-001
18.2    1.47e-001
18.3    1.46e-001
18.4    1.45e-001
18.5    1.43e-001
18.6    1.42e-001
18.7    1.41e-001
18.8    1.39e-001
18.9    1.38e-001
19      1.37e-001
19.1    1.35e-001
19.2    1.34e-001
19.3    1.33e-001
19.4    1.31e-001
19.5    1.30e-001
19.6    1.29e-001
19.7    1.27e-001
19.8    1.26e-001
19.9    1.25e-001
```

```
20      1.24e-001 ];
%Solar Proton Dose
Depth in Silicon at 9k
quiet (JPL1991)
%1997-11-17  15:06:57
%Solar Proton Dose-
Depth
%    201 = Number of
Depth Points
%Depth (g/cm² A1)
       Dose (rad/day)
spdc9=[0      2.43e-
004
0.1     2.43e-004
0.2     2.44e-004
0.3     2.44e-004
0.4     2.44e-004
0.5     2.44e-004
0.6     2.45e-004
0.7     2.45e-004
0.8     2.45e-004
0.9     2.45e-004
1       2.45e-004
1.1     2.45e-004
1.2     2.46e-004
1.3     2.46e-004
1.4     2.46e-004
1.5     2.46e-004
1.6     2.47e-004
1.7     2.47e-004
1.8     2.47e-004
1.9     2.47e-004
2       2.48e-004
2.1     2.48e-004
2.2     2.48e-004
2.3     2.48e-004
2.4     2.48e-004
2.5     2.49e-004
2.6     2.49e-004
2.7     2.49e-004
2.8     2.49e-004
2.9     2.49e-004
3       2.50e-004
3.1     2.50e-004
3.2     2.50e-004
3.3     2.50e-004
3.4     2.51e-004
3.5     2.51e-004
3.6     2.51e-004
3.7     2.52e-004
3.8     2.52e-004
3.9     2.52e-004
4       2.52e-004
4.1     2.53e-004
4.2     2.53e-004
4.3     2.53e-004
4.4     2.53e-004
4.5     2.53e-004
4.6     2.54e-004
4.7     2.54e-004
4.8     2.54e-004
4.9     2.55e-004
5       2.55e-004
5.1     2.55e-004
5.2     2.55e-004
5.3     2.56e-004
5.4     2.56e-004
5.5     2.56e-004
5.6     2.56e-004
5.7     2.57e-004
5.8     2.57e-004
5.9     2.57e-004
6       2.57e-004
6.1     2.58e-004
6.2     2.58e-004
6.3     2.58e-004
6.4     2.59e-004
6.5     2.59e-004
6.6     2.59e-004
6.7     2.60e-004
6.8     2.60e-004
6.9     2.60e-004
7       2.60e-004
7.1     2.61e-004
7.2     2.61e-004
7.3     2.61e-004
7.4     2.62e-004
7.5     2.62e-004
7.6     2.62e-004
7.7     2.62e-004
7.8     2.63e-004
7.9     2.63e-004
8       2.63e-004
8.1     2.64e-004
8.2     2.64e-004
8.3     2.65e-004
8.4     2.65e-004
8.5     2.65e-004
8.6     2.66e-004
8.7     2.66e-004
8.8     2.66e-004
8.9     2.66e-004
9       2.67e-004
9.1     2.67e-004
9.2     2.67e-004
9.3     2.68e-004
9.4     2.68e-004
9.5     2.69e-004
9.6     2.69e-004
9.7     2.69e-004
9.8     2.70e-004
9.9     2.70e-004
10      2.71e-004
10.1    2.71e-004
10.2    2.71e-004
10.3    2.72e-004
10.4    2.72e-004
10.5    2.72e-004
10.6    2.73e-004
10.7    2.73e-004
10.8    2.74e-004
10.9    2.74e-004
11      2.75e-004
11.1    2.75e-004
11.2    2.76e-004
11.3    2.76e-004
11.4    2.76e-004
11.5    2.77e-004
11.6    2.77e-004
11.7    2.78e-004
11.8    2.78e-004
11.9    2.79e-004
12      2.79e-004
12.1    2.80e-004
12.2    2.80e-004
12.3    2.81e-004
12.4    2.81e-004
12.5    2.82e-004
12.6    2.82e-004
12.7    2.83e-004
12.8    2.84e-004
12.9    2.84e-004
13      2.85e-004
13.1    2.85e-004
13.2    2.86e-004
13.3    2.87e-004
13.4    2.87e-004
13.5    2.88e-004
13.6    2.89e-004
13.7    2.89e-004
13.8    2.90e-004
13.9    2.91e-004
14      2.92e-004
14.1    2.92e-004
14.2    2.93e-004
14.3    2.94e-004
14.4    2.95e-004
14.5    2.95e-004
14.6    2.96e-004
14.7    2.97e-004
14.8    2.98e-004
14.9    2.99e-004
15      3.00e-004
15.1    3.02e-004
15.2    3.03e-004
15.3    3.04e-004
15.4    3.05e-004
15.5    3.06e-004
15.6    3.07e-004
15.7    3.08e-004
15.8    3.09e-004
15.9    3.10e-004
16      3.11e-004
16.1    3.11e-004
16.2    3.12e-004
16.3    3.13e-004
16.4    3.13e-004
16.5    3.14e-004
16.6    3.14e-004
16.7    3.15e-004
16.8    3.15e-004
16.9    3.16e-004
17      3.16e-004
17.1    3.16e-004
17.2    3.17e-004
17.3    3.17e-004
17.4    3.17e-004
17.5    3.18e-004
17.6    3.18e-004
17.7    3.18e-004
17.8    3.18e-004
17.9    3.18e-004
18      3.18e-004
18.1    3.18e-004
18.2    3.18e-004
18.3    3.19e-004
18.4    3.19e-004
18.5    3.19e-004
18.6    3.19e-004
18.7    3.19e-004
18.8    3.19e-004
```

```
18.9    3.19e-004
19      3.18e-004
19.1    3.18e-004
19.2    3.18e-004
19.3    3.18e-004
19.4    3.18e-004
19.5    3.18e-004
19.6    3.18e-004
19.7    3.18e-004
19.8    3.18e-004
19.9    3.17e-004
20      3.17e-004];
%Solar Proton Dose
Depth in Silicon at 8k
quiet (JPL1991)
%1997-11-21  20:24:17
%Solar Proton Dose-
Depth
%    201 = Number of
Depth Points
%Depth (g/cm² A1)
       Dose (rad/day)
spdc8=[0       3.74e-
005
0.1     3.74e-005
0.2     3.75e-005
0.3     3.75e-005
0.4     3.75e-005
0.5     3.75e-005
0.6     3.75e-005
0.7     3.76e-005
0.8     3.76e-005
0.9     3.76e-005
1       3.76e-005
1.1     3.76e-005
1.2     3.76e-005
1.3     3.76e-005
1.4     3.77e-005
1.5     3.77e-005
1.6     3.77e-005
1.7     3.78e-005
1.8     3.78e-005
1.9     3.78e-005
2       3.78e-005
2.1     3.79e-005
2.2     3.79e-005
2.3     3.79e-005
2.4     3.79e-005
2.5     3.79e-005
2.6     3.79e-005
2.7     3.80e-005
2.8     3.80e-005
2.9     3.80e-005
3       3.80e-005
3.1     3.80e-005
3.2     3.81e-005
3.3     3.81e-005
3.4     3.81e-005
3.5     3.81e-005
3.6     3.81e-005
3.7     3.82e-005
3.8     3.82e-005
3.9     3.82e-005
4       3.82e-005
4.1     3.83e-005
4.2     3.83e-005
4.3     3.83e-005
4.4     3.83e-005
4.5     3.83e-005
4.6     3.84e-005
4.7     3.84e-005
4.8     3.84e-005
4.9     3.85e-005
5       3.85e-005
5.1     3.85e-005
5.2     3.85e-005
5.3     3.85e-005
5.4     3.85e-005
5.5     3.86e-005
5.6     3.86e-005
5.7     3.86e-005
5.8     3.86e-005
5.9     3.86e-005
6       3.87e-005
6.1     3.87e-005
6.2     3.87e-005
6.3     3.87e-005
6.4     3.87e-005
6.5     3.88e-005
6.6     3.88e-005
6.7     3.88e-005
6.8     3.89e-005
6.9     3.89e-005
7       3.89e-005
7.1     3.90e-005
7.2     3.90e-005
7.3     3.90e-005
7.4     3.90e-005
7.5     3.91e-005
7.6     3.91e-005
7.7     3.91e-005
7.8     3.91e-005
7.9     3.91e-005
8       3.92e-005
8.1     3.92e-005
8.2     3.92e-005
8.3     3.93e-005
8.4     3.93e-005
8.5     3.93e-005
8.6     3.93e-005
8.7     3.94e-005
8.8     3.94e-005
8.9     3.94e-005
9       3.95e-005
9.1     3.95e-005
9.2     3.95e-005
9.3     3.95e-005
9.4     3.96e-005
9.5     3.96e-005
9.6     3.96e-005
9.7     3.96e-005
9.8     3.97e-005
9.9     3.97e-005
10      3.97e-005
10.1    3.98e-005
10.2    3.98e-005
10.3    3.98e-005
10.4    3.98e-005
10.5    3.99e-005
10.6    3.99e-005
10.7    3.99e-005
10.8    4.00e-005
10.9    4.00e-005
11      4.00e-005
11.1    4.01e-005
11.2    4.01e-005
11.3    4.01e-005
11.4    4.02e-005
11.5    4.02e-005
11.6    4.02e-005
11.7    4.02e-005
11.8    4.03e-005
11.9    4.03e-005
12      4.03e-005
12.1    4.04e-005
12.2    4.04e-005
12.3    4.04e-005
12.4    4.05e-005
12.5    4.05e-005
12.6    4.05e-005
12.7    4.05e-005
12.8    4.06e-005
12.9    4.06e-005
13      4.06e-005
13.1    4.07e-005
13.2    4.07e-005
13.3    4.08e-005
13.4    4.08e-005
13.5    4.08e-005
13.6    4.09e-005
13.7    4.09e-005
13.8    4.09e-005
13.9    4.10e-005
14      4.10e-005
14.1    4.10e-005
14.2    4.11e-005
14.3    4.11e-005
14.4    4.11e-005
14.5    4.11e-005
14.6    4.12e-005
14.7    4.12e-005
14.8    4.13e-005
14.9    4.13e-005
15      4.13e-005
15.1    4.14e-005
15.2    4.14e-005
15.3    4.15e-005
15.4    4.15e-005
15.5    4.15e-005
15.6    4.16e-005
15.7    4.16e-005
15.8    4.16e-005
15.9    4.17e-005
16      4.17e-005
16.1    4.18e-005
16.2    4.18e-005
16.3    4.18e-005
16.4    4.19e-005
16.5    4.19e-005
16.6    4.19e-005
16.7    4.20e-005
16.8    4.20e-005
16.9    4.21e-005
17      4.21e-005
17.1    4.22e-005
17.2    4.22e-005
17.3    4.23e-005
17.4    4.23e-005
17.5    4.23e-005
17.6    4.24e-005
17.7    4.24e-005
```

```
17.8    4.25e-005
17.9    4.25e-005
18      4.25e-005
18.1    4.26e-005
18.2    4.26e-005
18.3    4.27e-005
18.4    4.27e-005
18.5    4.28e-005
18.6    4.28e-005
18.7    4.28e-005
18.8    4.29e-005
18.9    4.29e-005
19      4.30e-005
19.1    4.30e-005
19.2    4.31e-005
19.3    4.31e-005
19.4    4.32e-005
19.5    4.32e-005
19.6    4.33e-005
19.7    4.33e-005
19.8    4.34e-005
19.9    4.34e-005
20      4.35e-005};
%Solar Proton Dose
Depth in Silicon at 7k
quiet (JPL1991)
%1997-11-17  15:06:04
%Solar Proton Dose-
Depth
%    201 = Number of
Depth Points
%Depth (g/cm² Al)
      Dose (rad/day)
spdc7=[0      3.92e-
006
0.1     3.92e-006
0.2     3.92e-006
0.3     3.92e-006
0.4     3.92e-006
0.5     3.92e-006
0.6     3.92e-006
0.7     3.92e-006
0.8     3.93e-006
0.9     3.93e-006
1       3.93e-006
1.1     3.93e-006
1.2     3.93e-006
1.3     3.93e-006
1.4     3.93e-006
1.5     3.94e-006
1.6     3.94e-006
1.7     3.94e-006
1.8     3.94e-006
1.9     3.95e-006
2       3.95e-006
2.1     3.95e-006
2.2     3.95e-006
2.3     3.95e-006
2.4     3.95e-006
2.5     3.96e-006
2.6     3.96e-006
2.7     3.96e-006
2.8     3.96e-006
2.9     3.96e-006
3       3.96e-006
3.1     3.96e-006
3.2     3.96e-006
3.3     3.97e-006
3.4     3.97e-006
3.5     3.97e-006
3.6     3.97e-006
3.7     3.97e-006
3.8     3.97e-006
3.9     3.98e-006
4       3.98e-006
4.1     3.98e-006
4.2     3.98e-006
4.3     3.98e-006
4.4     3.98e-006
4.5     3.98e-006
4.6     3.99e-006
4.7     3.99e-006
4.8     3.99e-006
4.9     3.99e-006
5       3.99e-006
5.1     3.98e-006
5.2     3.98e-006
5.3     3.98e-006
5.4     3.99e-006
5.5     3.99e-006
5.6     3.99e-006
5.7     3.99e-006
5.8     3.99e-006
5.9     3.99e-006
6       3.99e-006
6.1     3.99e-006
6.2     4.00e-006
6.3     4.00e-006
6.4     4.00e-006
6.5     4.00e-006
6.6     4.01e-006
6.7     4.01e-006
6.8     4.01e-006
6.9     4.01e-006
7       4.02e-006
7.1     4.02e-006
7.2     4.02e-006
7.3     4.02e-006
7.4     4.02e-006
7.5     4.02e-006
7.6     4.03e-006
7.7     4.03e-006
7.8     4.03e-006
7.9     4.03e-006
8       4.03e-006
8.1     4.03e-006
8.2     4.04e-006
8.3     4.04e-006
8.4     4.04e-006
8.5     4.04e-006
8.6     4.04e-006
8.7     4.04e-006
8.8     4.05e-006
8.9     4.05e-006
9       4.05e-006
9.1     4.05e-006
9.2     4.05e-006
9.3     4.05e-006
9.4     4.05e-006
9.5     4.05e-006
9.6     4.06e-006
9.7     4.06e-006
9.8     4.06e-006
9.9     4.06e-006
10      4.06e-006
10.1    4.07e-006
10.2    4.07e-006
10.3    4.07e-006
10.4    4.07e-006
10.5    4.07e-006
10.6    4.07e-006
10.7    4.08e-006
10.8    4.08e-006
10.9    4.08e-006
11      4.09e-006
11.1    4.09e-006
11.2    4.09e-006
11.3    4.09e-006
11.4    4.09e-006
11.5    4.10e-006
11.6    4.10e-006
11.7    4.10e-006
11.8    4.10e-006
11.9    4.10e-006
12      4.10e-006
12.1    4.11e-006
12.2    4.11e-006
12.3    4.11e-006
12.4    4.11e-006
12.5    4.11e-006
12.6    4.11e-006
12.7    4.12e-006
12.8    4.12e-006
12.9    4.12e-006
13      4.12e-006
13.1    4.12e-006
13.2    4.12e-006
13.3    4.13e-006
13.4    4.13e-006
13.5    4.13e-006
13.6    4.13e-006
13.7    4.13e-006
13.8    4.14e-006
13.9    4.12e-006
14      4.13e-006
14.1    4.13e-006
14.2    4.13e-006
14.3    4.13e-006
14.4    4.13e-006
14.5    4.13e-006
14.6    4.14e-006
14.7    4.14e-006
14.8    4.14e-006
14.9    4.14e-006
15      4.15e-006
15.1    4.15e-006
15.2    4.15e-006
15.3    4.15e-006
15.4    4.16e-006
15.5    4.16e-006
15.6    4.16e-006
15.7    4.16e-006
15.8    4.16e-006
15.9    4.17e-006
16      4.17e-006
16.1    4.17e-006
16.2    4.17e-006
16.3    4.17e-006
16.4    4.18e-006
16.5    4.18e-006
16.6    4.18e-006
```

```
16.7    4.18e-006
16.8    4.18e-006
16.9    4.18e-006
17      4.19e-006
17.1    4.19e-006
17.2    4.19e-006
17.3    4.20e-006
17.4    4.20e-006
17.5    4.20e-006
17.6    4.20e-006
17.7    4.20e-006
17.8    4.20e-006
17.9    4.21e-006
18      4.21e-006
18.1    4.21e-006
18.2    4.21e-006
18.3    4.22e-006
18.4    4.22e-006
18.5    4.22e-006
18.6    4.22e-006
18.7    4.22e-006
18.8    4.23e-006
18.9    4.23e-006
19      4.23e-006
19.1    4.23e-006
19.2    4.24e-006
19.3    4.24e-006
19.4    4.24e-006
19.5    4.24e-006
19.6    4.25e-006
19.7    4.25e-006
19.8    4.25e-006
19.9    4.25e-006
20      4.25e-006];
%Solar Proton Dose
Depth in Silicon at 6k
quiet (JPL1991)
corrected
%1997-11-21  20:23:36
%Solar Proton Dose-
Depth
%    201 = Number of
Depth Points
%Depth (g/cm² Al)
      Dose (rad/day)
spdc=[0       2.09e-
007
0.1     2.09e-007
0.2     2.09e-007
0.3     2.10e-007
0.4     2.10e-007
0.5     2.10e-007
0.6     2.10e-007
0.7     2.10e-007
0.8     2.10e-007
0.9     2.10e-007
1       2.10e-007
1.1     2.10e-007
1.2     2.11e-007
1.3     2.11e-007
1.4     2.11e-007
1.5     2.11e-007
1.6     2.11e-007
1.7     2.11e-007
1.8     2.11e-007
1.9     2.11e-007
2       2.11e-007
2.1     2.11e-007
2.2     2.11e-007
2.3     2.11e-007
2.4     2.11e-007
2.5     2.11e-007
2.6     2.11e-007
2.7     2.12e-007
2.8     2.12e-007
2.9     2.12e-007
3       2.12e-007
3.1     2.12e-007
3.2     2.12e-007
3.3     2.12e-007
3.4     2.12e-007
3.5     2.12e-007
3.6     2.12e-007
3.7     2.12e-007
3.8     2.12e-007
3.9     2.13e-007
4       2.13e-007
4.1     2.13e-007
4.2     2.13e-007
4.3     2.13e-007
4.4     2.13e-007
4.5     2.13e-007
4.6     2.13e-007
4.7     2.13e-007
4.8     2.14e-007
4.9     2.14e-007
5       2.14e-007
5.1     2.10e-007
5.2     2.10e-007
5.3     2.10e-007
5.4     2.10e-007
5.5     2.10e-007
5.6     2.10e-007
5.7     2.10e-007
5.8     2.10e-007
5.9     2.10e-007
6       2.11e-007
6.1     2.11e-007
6.2     2.11e-007
6.3     2.11e-007
6.4     2.11e-007
6.5     2.11e-007
6.6     2.11e-007
6.7     2.11e-007
6.8     2.11e-007
6.9     2.12e-007
7       2.12e-007
7.1     2.12e-007
7.2     2.12e-007
7.3     2.12e-007
7.4     2.12e-007
7.5     2.12e-007
7.6     2.12e-007
7.7     2.13e-007
7.8     2.13e-007
7.9     2.13e-007
8       2.13e-007
8.1     2.13e-007
8.2     2.13e-007
8.3     2.13e-007
8.4     2.13e-007
8.5     2.13e-007
8.6     2.13e-007
8.7     2.13e-007
8.8     2.13e-007
8.9     2.13e-007
9       2.13e-007
9.1     2.13e-007
9.2     2.14e-007
9.3     2.14e-007
9.4     2.14e-007
9.5     2.14e-007
9.6     2.14e-007
9.7     2.14e-007
9.8     2.14e-007
9.9     2.14e-007
10      2.14e-007
10.1    2.14e-007
10.2    2.14e-007
10.3    2.15e-007
10.4    2.15e-007
10.5    2.15e-007
10.6    2.15e-007
10.7    2.15e-007
10.8    2.15e-007
10.9    2.15e-007
11      2.15e-007
11.1    2.15e-007
11.2    2.16e-007
11.3    2.16e-007
11.4    2.16e-007
11.5    2.16e-007
11.6    2.16e-007
11.7    2.16e-007
11.8    2.16e-007
11.9    2.16e-007
12      2.16e-007
12.1    2.16e-007
12.2    2.17e-007
12.3    2.17e-007
12.4    2.17e-007
12.5    2.17e-007
12.6    2.17e-007
12.7    2.17e-007
12.8    2.17e-007
12.9    2.17e-007
13      2.17e-007
13.1    2.17e-007
13.2    2.17e-007
13.3    2.17e-007
13.4    2.17e-007
13.5    2.18e-007
13.6    2.18e-007
13.7    2.18e-007
13.8    2.18e-007
13.9    2.14e-007
14      2.14e-007
14.1    2.14e-007
14.2    2.15e-007
14.3    2.15e-007
14.4    2.15e-007
14.5    2.15e-007
14.6    2.15e-007
14.7    2.15e-007
14.8    2.15e-007
14.9    2.15e-007
15      2.15e-007
15.1    2.15e-007
15.2    2.16e-007
15.3    2.16e-007
15.4    2.16e-007
```

```
15.5    2.16e-007
15.6    2.16e-007
15.7    2.16e-007
15.8    2.16e-007
15.9    2.16e-007
16      2.16e-007
16.1    2.16e-007
16.2    2.16e-007
16.3    2.17e-007
16.4    2.17e-007
16.5    2.17e-007
16.6    2.17e-007
16.7    2.17e-007
16.8    2.17e-007
16.9    2.17e-007
17      2.17e-007
17.1    2.18e-007
17.2    2.18e-007
17.3    2.18e-007
17.4    2.18e-007
17.5    2.18e-007
17.6    2.18e-007
17.7    2.18e-007
17.8    2.18e-007
17.9    2.18e-007
18      2.18e-007
18.1    2.18e-007
18.2    2.18e-007
18.3    2.19e-007
18.4    2.19e-007
18.5    2.19e-007
18.6    2.19e-007
18.7    2.19e-007
18.8    2.19e-007
18.9    2.19e-007
19      2.19e-007
19.1    2.19e-007
19.2    2.20e-007
19.3    2.20e-007
19.4    2.20e-007
19.5    2.20e-007
19.6    2.20e-007
19.7    2.20e-007
19.8    2.20e-007
19.9    2.20e-007
20      2.20e-007 ];
%Solar Proton Dose
Depth in Silicon at 5k
quiet (JPL1991)
%1997-11-21  20:20:55
%Solar Proton Dose-
Depth
%    201 = Number of
Depth Points
%Depth (g/cm² Al)
       Dose (rad/day)
spdc5=[0       4.75e-
009
0.1     4.75e-009
0.2     4.76e-009
0.3     4.76e-009
0.4     4.76e-009
0.5     4.77e-009
0.6     4.77e-009
0.7     4.77e-009
0.8     4.78e-009
0.9     4.78e-009
1       4.78e-009
1.1     4.79e-009
1.2     4.79e-009
1.3     4.79e-009
1.4     4.79e-009
1.5     4.80e-009
1.6     4.80e-009
1.7     4.80e-009
1.8     4.80e-009
1.9     4.80e-009
2       4.81e-009
2.1     4.81e-009
2.2     4.81e-009
2.3     4.81e-009
2.4     4.81e-009
2.5     4.82e-009
2.6     4.82e-009
2.7     4.82e-009
2.8     4.82e-009
2.9     4.82e-009
3       4.83e-009
3.1     4.83e-009
3.2     4.83e-009
3.3     4.83e-009
3.4     4.83e-009
3.5     4.84e-009
3.6     4.84e-009
3.7     4.84e-009
3.8     4.84e-009
3.9     4.85e-009
4       4.85e-009
4.1     4.85e-009
4.2     4.86e-009
4.3     4.86e-009
4.4     4.87e-009
4.5     4.87e-009
4.6     4.88e-009
4.7     4.88e-009
4.8     4.89e-009
4.9     4.89e-009
5       4.89e-009
5.1     4.67e-009
5.2     4.68e-009
5.3     4.68e-009
5.4     4.68e-009
5.5     4.69e-009
5.6     4.69e-009
5.7     4.70e-009
5.8     4.70e-009
5.9     4.70e-009
6       4.71e-009
6.1     4.71e-009
6.2     4.71e-009
6.3     4.72e-009
6.4     4.72e-009
6.5     4.72e-009
6.6     4.73e-009
6.7     4.73e-009
6.8     4.73e-009
6.9     4.74e-009
7       4.74e-009
7.1     4.74e-009
7.2     4.74e-009
7.3     4.75e-009
7.4     4.75e-009
7.5     4.75e-009
7.6     4.76e-009
7.7     4.76e-009
7.8     4.76e-009
7.9     4.76e-009
8       4.77e-009
8.1     4.77e-009
8.2     4.77e-009
8.3     4.78e-009
8.4     4.78e-009
8.5     4.78e-009
8.6     4.78e-009
8.7     4.79e-009
8.8     4.79e-009
8.9     4.79e-009
9       4.79e-009
9.1     4.79e-009
9.2     4.80e-009
9.3     4.80e-009
9.4     4.80e-009
9.5     4.80e-009
9.6     4.80e-009
9.7     4.81e-009
9.8     4.81e-009
9.9     4.82e-009
10      4.82e-009
10.1    4.83e-009
10.2    4.83e-009
10.3    4.83e-009
10.4    4.84e-009
10.5    4.84e-009
10.6    4.85e-009
10.7    4.85e-009
10.8    4.85e-009
10.9    4.86e-009
11      4.86e-009
11.1    4.87e-009
11.2    4.87e-009
11.3    4.87e-009
11.4    4.88e-009
11.5    4.88e-009
11.6    4.88e-009
11.7    4.89e-009
11.8    4.89e-009
11.9    4.89e-009
12      4.90e-009
12.1    4.90e-009
12.2    4.90e-009
12.3    4.91e-009
12.4    4.91e-009
12.5    4.91e-009
12.6    4.92e-009
12.7    4.92e-009
12.8    4.92e-009
12.9    4.93e-009
13      4.93e-009
13.1    4.93e-009
13.2    4.94e-009
13.3    4.94e-009
13.4    4.94e-009
13.5    4.94e-009
13.6    4.94e-009
13.7    4.95e-009
13.8    4.95e-009
13.9    4.73e-009
14      4.73e-009
14.1    4.73e-009
14.2    4.74e-009
14.3    4.74e-009
```

```
14.4    4.74e-009
14.5    4.74e-009
14.6    4.74e-009
14.7    4.75e-009
14.8    4.75e-009
14.9    4.75e-009
15      4.76e-009
15.1    4.76e-009
15.2    4.77e-009
15.3    4.77e-009
15.4    4.77e-009
15.5    4.78e-009
15.6    4.78e-009
15.7    4.79e-009
15.8    4.79e-009
15.9    4.79e-009
16      4.80e-009
16.1    4.80e-009
16.2    4.80e-009
16.3    4.81e-009
16.4    4.81e-009
16.5    4.81e-009
16.6    4.82e-009
16.7    4.82e-009
16.8    4.82e-009
16.9    4.83e-009
17      4.83e-009
17.1    4.84e-009
17.2    4.84e-009
17.3    4.84e-009
17.4    4.85e-009
17.5    4.85e-009
17.6    4.86e-009
17.7    4.86e-009
17.8    4.86e-009
17.9    4.87e-009
18      4.87e-009
18.1    4.88e-009
18.2    4.88e-009
18.3    4.88e-009
18.4    4.89e-009
18.5    4.89e-009
18.6    4.89e-009
18.7    4.89e-009
18.8    4.90e-009
18.9    4.90e-009
19      4.90e-009
19.1    4.91e-009
19.2    4.91e-009
19.3    4.91e-009
19.4    4.91e-009
19.5    4.91e-009
19.6    4.92e-009
19.7    4.92e-009
19.8    4.92e-009
19.9    4.92e-009
20      4.92e-009];
%Solar Proton Dose
Depth in Silicon at 4k
quiet (JPL1991)
%1997-11-17  08:57:17
%Solar Proton Dose-
Depth
%    201 = Number of
Depth Points
%Depth (g/cm² Al)
      Dose (rad/day)
```

```
spdc4=[0
0.00e+000
0.1     0.00e+000
0.2     0.00e+000
0.3     0.00e+000
0.4     0.00e+000
0.5     0.00e+000
0.6     0.00e+000
0.7     0.00e+000
0.8     0.00e+000
0.9     0.00e+000
1       0.00e+000
1.1     0.00e+000
1.2     0.00e+000
1.3     0.00e+000
1.4     1.01e-014
1.5     2.10e-014
1.6     3.18e-014
1.7     4.26e-014
1.8     5.33e-014
1.9     6.39e-014
2       7.45e-014
2.1     8.50e-014
2.2     9.54e-014
2.3     1.06e-013
2.4     1.16e-013
2.5     1.26e-013
2.6     1.36e-013
2.7     1.46e-013
2.8     1.56e-013
2.9     1.66e-013
3       1.76e-013
3.1     1.86e-013
3.2     1.96e-013
3.3     2.06e-013
3.4     2.15e-013
3.5     2.25e-013
3.6     2.34e-013
3.7     2.44e-013
3.8     2.53e-013
3.9     2.62e-013
4       2.72e-013
4.1     2.81e-013
4.2     2.90e-013
4.3     2.99e-013
4.4     3.08e-013
4.5     3.17e-013
4.6     3.26e-013
4.7     3.34e-013
4.8     3.43e-013
4.9     3.52e-013
5       3.61e-013
5.1     0.00e+000
5.2     0.00e+000
5.3     0.00e+000
5.4     0.00e+000
5.5     0.00e+000
5.6     0.00e+000
5.7     0.00e+000
5.8     0.00e+000
5.9     0.00e+000
6       0.00e+000
6.1     0.00e+000
6.2     0.00e+000
6.3     0.00e+000
6.4     0.00e+000
6.5     0.00e+000
```

```
6.6     0.00e+000
6.7     0.00e+000
6.8     0.00e+000
6.9     0.00e+000
7       0.00e+000
7.1     0.00e+000
7.2     0.00e+000
7.3     0.00e+000
7.4     0.00e+000
7.5     0.00e+000
7.6     0.00e+000
7.7     0.00e+000
7.8     0.00e+000
7.9     0.00e+000
8       0.00e+000
8.1     0.00e+000
8.2     0.00e+000
8.3     0.00e+000
8.4     0.00e+000
8.5     0.00e+000
8.6     0.00e+000
8.7     0.00e+000
8.8     0.00e+000
8.9     0.00e+000
9       0.00e+000
9.1     0.00e+000
9.2     0.00e+000
9.3     0.00e+000
9.4     0.00e+000
9.5     0.00e+000
9.6     0.00e+000
9.7     0.00e+000
9.8     0.00e+000
9.9     0.00e+000
10      0.00e+000
10.1    0.00e+000
10.2    7.16e-015
10.3    1.78e-014
10.4    2.84e-014
10.5    3.89e-014
10.6    4.94e-014
10.7    5.98e-014
10.8    7.01e-014
10.9    8.04e-014
11      9.06e-014
11.1    1.01e-013
11.2    1.11e-013
11.3    1.21e-013
11.4    1.31e-013
11.5    1.40e-013
11.6    1.50e-013
11.7    1.60e-013
11.8    1.70e-013
11.9    1.79e-013
12      1.89e-013
12.1    1.98e-013
12.2    2.08e-013
12.3    2.17e-013
12.4    2.26e-013
12.5    2.35e-013
12.6    2.45e-013
12.7    2.54e-013
12.8    2.63e-013
12.9    2.72e-013
13      2.81e-013
13.1    2.89e-013
13.2    2.98e-013
```

```
13.3    3.07e-013
13.4    3.16e-013
13.5    3.24e-013
13.6    3.33e-013
13.7    3.41e-013
13.8    3.50e-013
13.9    0.00e+000
14      0.00e+000
14.1    0.00e+000
14.2    0.00e+000
14.3    0.00e+000
14.4    0.00e+000
14.5    0.00e+000
14.6    0.00e+000
14.7    0.00e+000
14.8    0.00e+000
14.9    0.00e+000
15      0.00e+000
15.1    0.00e+000
15.2    0.00e+000
15.3    0.00e+000
15.4    0.00e+000
15.5    0.00e+000
15.6    0.00e+000
15.7    0.00e+000
15.8    0.00e+000
15.9    0.00e+000
16      0.00e+000
16.1    0.00e+000
16.2    0.00e+000
16.3    0.00e+000
16.4    0.00e+000
16.5    0.00e+000
16.6    0.00e+000
16.7    0.00e+000
16.8    0.00e+000
16.9    0.00e+000
17      0.00e+000
17.1    0.00e+000
17.2    0.00e+000
17.3    0.00e+000
17.4    0.00e+000
17.5    0.00e+000
17.6    0.00e+000
17.7    0.00e+000
17.8    0.00e+000
17.9    0.00e+000
18      0.00e+000
18.1    0.00e+000
18.2    0.00e+000
18.3    0.00e+000
18.4    0.00e+000
18.5    0.00e+000
18.6    0.00e+000
18.7    2.40e-015
18.8    1.28e-014
18.9    2.32e-014
19      3.35e-014
19.1    4.38e-014
19.2    5.39e-014
19.3    6.40e-014
19.4    7.41e-014
19.5    8.40e-014
19.6    9.39e-014
19.7    1.04e-013
19.8    1.14e-013
19.9    1.23e-013
20      1.33e-013 ];
%Solar Proton Dose
Depth in Silicon at 3k
quiet (JPL1991)
%1997-11-17  08:56:40
%Solar Proton Dose-
Depth
%    201 = Number of
Depth Points
%Depth (g/cm² Al)
       Dose (rad/day)
spdc3=[0
0.00e+000
0.1     0.00e+000
0.2     0.00e+000
0.3     0.00e+000
0.4     0.00e+000
0.5     0.00e+000
0.6     0.00e+000
0.7     0.00e+000
0.8     0.00e+000
0.9     0.00e+000
1       0.00e+000
1.1     0.00e+000
1.2     0.00e+000
1.3     0.00e+000
1.4     0.00e+000
1.5     0.00e+000
1.6     0.00e+000
1.7     0.00e+000
1.8     0.00e+000
1.9     0.00e+000
2       0.00e+000
2.1     0.00e+000
2.2     0.00e+000
2.3     0.00e+000
2.4     0.00e+000
2.5     0.00e+000
2.6     0.00e+000
2.7     0.00e+000
2.8     0.00e+000
2.9     0.00e+000
3       0.00e+000
3.1     0.00e+000
3.2     0.00e+000
3.3     0.00e+000
3.4     0.00e+000
3.5     0.00e+000
3.6     0.00e+000
3.7     0.00e+000
3.8     0.00e+000
3.9     0.00e+000
4       0.00e+000
4.1     0.00e+000
4.2     0.00e+000
4.3     0.00e+000
4.4     0.00e+000
4.5     0.00e+000
4.6     0.00e+000
4.7     0.00e+000
4.8     0.00e+000
4.9     0.00e+000
5       0.00e+000
5.1     0.00e+000
5.2     0.00e+000
5.3     0.00e+000
5.4     0.00e+000
5.5     0.00e+000
5.6     0.00e+000
5.7     0.00e+000
5.8     0.00e+000
5.9     0.00e+000
6       0.00e+000
6.1     0.00e+000
6.2     0.00e+000
6.3     0.00e+000
6.4     0.00e+000
6.5     0.00e+000
6.6     0.00e+000
6.7     0.00e+000
6.8     0.00e+000
6.9     0.00e+000
7       0.00e+000
7.1     0.00e+000
7.2     0.00e+000
7.3     0.00e+000
7.4     0.00e+000
7.5     0.00e+000
7.6     0.00e+000
7.7     0.00e+000
7.8     0.00e+000
7.9     0.00e+000
8       0.00e+000
8.1     0.00e+000
8.2     0.00e+000
8.3     0.00e+000
8.4     0.00e+000
8.5     0.00e+000
8.6     0.00e+000
8.7     0.00e+000
8.8     0.00e+000
8.9     0.00e+000
9       0.00e+000
9.1     0.00e+000
9.2     0.00e+000
9.3     0.00e+000
9.4     0.00e+000
9.5     0.00e+000
9.6     0.00e+000
9.7     0.00e+000
9.8     0.00e+000
9.9     0.00e+000
10      0.00e+000
10.1    0.00e+000
10.2    0.00e+000
10.3    0.00e+000
10.4    0.00e+000
10.5    0.00e+000
10.6    0.00e+000
10.7    0.00e+000
10.8    0.00e+000
10.9    0.00e+000
11      0.00e+000
11.1    0.00e+000
11.2    0.00e+000
11.3    0.00e+000
11.4    0.00e+000
11.5    0.00e+000
11.6    0.00e+000
11.7    0.00e+000
11.8    0.00e+000
11.9    0.00e+000
12      0.00e+000
12.1    0.00e+000
```

```
12.2    0.00e+000
12.3    0.00e+000
12.4    0.00e+000
12.5    0.00e+000
12.6    0.00e+000
12.7    0.00e+000
12.8    0.00e+000
12.9    0.00e+000
13      0.00e+000
13.1    0.00e+000
13.2    0.00e+000
13.3    0.00e+000
13.4    0.00e+000
13.5    0.00e+000
13.6    0.00e+000
13.7    0.00e+000
13.8    0.00e+000
13.9    0.00e+000
14      0.00e+000
14.1    0.00e+000
14.2    0.00e+000
14.3    0.00e+000
14.4    0.00e+000
14.5    0.00e+000
14.6    0.00e+000
14.7    0.00e+000
14.8    0.00e+000
14.9    0.00e+000
15      0.00e+000
15.1    0.00e+000
15.2    0.00e+000
15.3    0.00e+000
15.4    0.00e+000
15.5    0.00e+000
15.6    0.00e+000
15.7    0.00e+000
15.8    0.00e+000
15.9    0.00e+000
16      0.00e+000
16.1    0.00e+000
16.2    0.00e+000
16.3    0.00e+000
16.4    0.00e+000
16.5    0.00e+000
16.6    0.00e+000
16.7    0.00e+000
16.8    0.00e+000
16.9    0.00e+000
17      0.00e+000
17.1    0.00e+000
17.2    0.00e+000
17.3    0.00e+000
17.4    0.00e+000
17.5    0.00e+000
17.6    0.00e+000
17.7    0.00e+000
17.8    0.00e+000
17.9    0.00e+000
18      0.00e+000
18.1    0.00e+000
18.2    0.00e+000
18.3    0.00e+000
18.4    0.00e+000
18.5    0.00e+000
18.6    0.00e+000
18.7    0.00e+000
18.8    0.00e+000
18.9    0.00e+000
19      0.00e+000
19.1    0.00e+000
19.2    0.00e+000
19.3    0.00e+000
19.4    0.00e+000
19.5    0.00e+000
19.6    0.00e+000
19.7    0.00e+000
19.8    0.00e+000
19.9    0.00e+000
20      0.00e+000
```

%Damage.dat

0.00E+00	0.000E+00
1.00E-05	0.000E+00
5.00E-05	0.000E+00
6.00E-05	7.270E-08
1.00E-04	7.811E-08
2.00E-04	8.628E-08
5.00E-04	8.853E-08
1.00E-03	8.188E-08
2.00E-03	6.889E-08
5.00E-03	4.751E-08
1.00E-02	3.272E-08
2.00E-02	2.121E-08
5.00E-02	1.116E-08
1.00E-01	6.615E-09
2.00E-01	3.826E-09
5.00E-01	1.805E-09
1.00E+00	9.912E-10
1.50E+00	7.548E-10
2.00E+00	5.183E-10
3.00E+00	3.528E-10
5.00E+00	2.165E-10
7.00E+00	1.565E-10
1.00E+01	1.110E-10
1.50E+01	8.588E-11
2.00E+01	7.579E-11
3.00E+01	6.842E-11
5.00E+01	5.913E-11
7.00E+01	5.336E-11
1.00E+02	4.754E-11
1.50E+02	4.073E-11
2.00E+02	3.793E-11
3.00E+02	3.485E-11
4.00E+02	3.302E-11
5.00E+02	3.168E-11
1.00E+03	2.724E-11
1.00E+05	2.724E-11

```
%Solar Cell Damage
from Trapped Protons
quiet 9K GaAs, no cg
tpg0=[4.19E+15,
5.87E+15, 2.11E+15 ;
6.30E+15, 8.83E+15,
3.17E+15;
2.03E+16, 2.84E+16,
1.01E+16;
1.79E+16, 2.50E+16,
8.94E+15;
1.09E+16, 1.53E+16,
5.46E+15;
2.09E+16, 2.93E+16,
1.25E+16;
2.75E+15, 3.85E+15,
1.58E+15];

%Solar Cell Damage
from Trapped Protons
quiet 9K GaAs, 3 mil
cg      {PMAX}
tpg3=[5.12E+12,
7.17E+12, 2.91E+12 ;
2.33E+13, 3.26E+13,
1.30E+13;
7.63E+13, 1.07E+14,
4.18E+13;
1.67E+14, 2.33E+14,
8.98E+13 ;
2.59E+14, 3.63E+14,
1.37E+14;
2.89E+14, 4.05E+14,
1.50E+14;
1.93E+14, 2.71E+14,
9.70E+13];

%Solar Cell Damage
from Trapped Protons
quiet 3K GaAs, 6mil cg
        {PMAX}
tpg6=[9.29E+13,
1.30E+14, 4.48E+13 ;
8.73E+13, 1.22E+14,
4.29E+13;
5.26E+13, 7.37E+13,
2.61E+13;
2.26E+13, 3.16E+13,
1.13E+13;
6.99E+12, 9.79E+12,
3.53E+12;
1.45E+12, 2.04E+12,
7.39E+11;
1.88E+11, 2.63E+11,
9.63E+10];

%Solar Cell Damage
from Trapped Protons
quiet 3K silicon, no
cg
tps0=[2.66E+15,
8.42E+14 ;
1.19E+16, 2.79E+15;
1.67E+16, 5.15E+15;
2.40E+16, 6.90E+15 ;
2.44E+16, 6.51E+15;
1.01E+16, 3.17E+15;
5.42E+15, 1.57E+15 ];
```

```
%Solar Cell Damage
from Trapped Protons
quiet 9K silicon, 3
mil cg {PMAX,VOC}
tps3=[6.51E+12,
2.06E+12;
3.52E+13, 1.17E+13;
1.32E+14,  4.56E+13;
3.34E+14,1.19E+14;
6.08E+14, 2.25E+14;
7.99E+14, 3.08E+14;
6.39E+14, 2.65E+14 ];

%Solar Cell Damage
from Trapped Protons
quiet 9K silicon 6mil
cg     {PMAX,VOC}
tps6=[3.83E+11,
1.35E+11;
3.34E+12, 1.21E+12;
1.74E+13, 6.45E+12;
6.07E+13, 2.30E+13;
1.56E+14, 6.07E+13;
2.79E+14, 1.13E+14;
3.29E+14, 1.42E+14];

%Solar Cell Damage
from Trapped Electron
quiet, silicon, no cg,
9k
tes0=[1.49E+11
9.60E+10
5.97E+10
3.76E+10
1.85E+10
4.26E+10
2.45E+10];

%Solar Cell Damage
from Trapped Electron
quiet, silicon, 3 mil
cg, 3k
tes3=[1.85E+10
2.00E+10
1.46E+10
2.81E+10
4.84E+10
7.96E+10
1.24E+11];

% olar Cell Damage
from Trapped Electron
quiet, silicon, 6 mil
cg, 9k
tes6=[1.09E+11
7.01E+10
4.22E+10
2.35E+10
1.22E+10
1.27E+10
1.49E+10 ];

% Solar Cell Damage
from Trapped Electron
quiet, GaAs, 6 mil cg,
3k
teg6=[1.60E+10
1.24E+10
1.24E+10
2.13E+10
3.64E+10
5.99E+10
9.36E+10];

% Solar Cell Damage
from Trapped Electron
quiet, GaAs, 3 mil cg,
9k
teg3=[1.07E+11
6.83E+10
4.20E+10
2.54E+10
1.48E+10
1.87E+10
1.98E+10];

%Solar Cell Damage
from Trapped Electron
quiet, GaAs, no cg, 3k

teg0=[2.60E+10
3.74E+10
1.87E+10
3.41E+10
5.23E+10
8.31E+10
1.30E+11];

%Solar Cell Damage
from Solar Proton
Event JPL1991 quiet 3k
silicon no cg
      {PMAX,VOC}
spes0=[0.00E+00,
0.00E+00;
0.00E+00, 0.00E+00;
1.09E+01, 1.09E+01;
5.86E+02, 5.86E+02 ;
1.28E+04, 1.28E+04;
1.38E+05, 1.38E+05;
1.01E+06, 1.01E+06];

%Solar Cell Damage
from Solar Proton
Event JPL1991 quiet 9k
silicon 3 mil cg
%{PMAX,VOC}
spes3=[1.02E+06,
1.02E+06;
1.39E+05, 1.39E+05;
1.28E+04, 1.28E+04;
5.87E+02, 5.87E+02 ;
1.09E+01, 1.09E+01;
0.00E+00, 0.00E+00;
0.00E+00, 0.00E+00];

%Solar Cell Damage
from Solar Proton
Event JPL1991 quiet 3k
silicon 6 mil cg
spes6=[0.00E+00,
0.00E+00;
0.00E+00, 0.00E+00;
1.09E+01, 1.09E+01;
5.85E+02, 5.85E+02 ;
1.28E+04, 1.28E+04;
1.38E+05, 1.38E+05;
1.02E+06, 1.02E+06];

%Solar Cell Damage
from Solar Proton
Event JPL1991 quiet 9k
GaAs 6 mil cg
speg6=[1.21E+06,
1.69E+06, 1.18E+05;
2.03E+05, 2.84E+05,
1.92E+04;
2.28E+04, 3.19E+04,
2.09E+03;
1.29E+03, 1.80E+03,
1.14E+02 ;
2.99E+01, 4.19E+01,
2.56E+00;
0.00E+00, 0.00E+00,
0.00E+00;
0.00E+00, 0.00E+00,
0.00E+00];

% Solar Cell Damage
from Solar Proton
Event JPL1991 quiet 3k
GaAs 3 mil cg
speg3=[0.00E+00,
0.00E+00, 0.00E+00;
0.00E+00, 0.00E+00,
0.00E+00;
2.98E+01, 4.18E+01,
2.57E+00;
1.29E+03, 1.80E+03,
1.14E+02;
2.27E+04, 3.18E+04,
2.09E+03;
2.03E+05, 2.84E+05,
1.92E+04;
1.20E+06, 1.69E+06,
1.18E+05];

% Solar Cell Damage
from Solar Proton
Event JPL1991 quiet 9k
GaAs no cg
%{PMAX} {VOC} {ISC} 1-
MeV e/day

pspego= [1.20E+06,
2.03E+05, 2.27E+04,
1.29E+03, 2.98E+01, 0,
0];
vspego=[1.69E+06,
2.84E+05, 3.18E+04,
1.80E+03, 4.18E+01, 0,
0];
ispego=[1.19E+05,
1.92E+04, 2.10E+03,
1.15E+02, 2.57E+00, 0,
0];

%Solar Cell Damage
from Trapped Protons
no cg GaAs {PMAX}
{VOC}{ISC}
```

```
btpg=[5.06E+12,7.09E+1
2, 3.45E+12  ;
1.65E+10,
2.31E+10,7.39E+09 ;
8.80E+09,
1.23E+10,3.36E+09 ];

%Solar Cell Damage
from Solar Protons JPL
1991 no cg GaAs {PMAX}
{VOC}{ISC}
bspg=[2.55E+10,3.57E+1
0, 1.31E+10 ;
7.37E+09,1.03E+10,3.27
E+09 ;
5.23E+09,
7.32E+09,2.19E+09];

%Solar Cell Damage
from Trapped Electrons
no cg GaAs
bteg0=6.20E+08 ;
bteg3=4.63E+08 ;
bteg6=3.85E+08 ;

%Solar Cell Damage
from Trapped Protons
no cg  {PMAX,VOC}
{Isc}
btps=[1.34E+12,
1.43E+11;
4.91E+10, 2.48E+10 ;
2.82E+10, 1.67E+10] ;

%Solar Cell Damage
from Trapped Electrons
no cg
btes0 = [6.72E+08];
btes3 = [5.06E+08];
btes6 = [4.23E+08];

%Solar Cell Damage
from Solar Protons JPL
1991 no cg
       {PMAX,VOC}
{Isc}
bsps=[5.14E+10,
2.34E+10 ;
2.60E+10, 1.43E+10 ;
1.90E+10,1.13E+10 ];
Proton Displacement
Data/graphs

%Baseline Data
%Proton Displacement
from Galactic
g3=2.80E-06 ;
%Proton Displacement
from Galactic 100
g1=2.80E-06 ;
%Proton Displacement
from solar energetic
100
se1=3.35E-04 ;
%Proton Displacement
from solar energetic
300
se3=1.17E-04 ;
%Proton Displacement
from solar proton
xport 100
sp1=2.63E-04 ;
%Proton Displacement
from solar proton
xport 300
sp3=8.74E-05 ;
%Proton Displacement
from trapped proton
xport 100
tp1=5.46E-04 ;
%Proton Displacement
from trapped proton
xport 300
tp3=3.98E-04 ;

%MEO Data
%Proton Displacement
from galactic/thin
shell/3k
g1k=[1.54E-06
2.33E-06
3.26E-06
4.22E-06
5.17E-06
6.08E-06
6.91E-06 ];

%Proton Displacement
from Solar
Energetic(CREME)/thin
shell/3k
se1k=[0.00E+00
9.48E-19
1.11E-14
5.22E-12
4.16E-10
8.35E-09
9.16E-08];

%Proton Displacement
from Solar Proton/thin
shell/3k
sp1k=[0.00E+00
2.75E-16
4.44E-12
1.84E-10
3.21E-09
2.88E-08
1.75E-07 ];

%  Proton Displacement
Effect from Trapped
Protons/300mils/3k
tp3k=[2.42E-02
5.20E-03
8.49E-04
8.53E-05
4.53E-05
0.00E+00
0.00E+00  ];

%Proton Displacement
Effect from Trapped
Protons/100 mils/3k
tp1k=[1.84E-01
7.05E-02
1.78E-02
2.68E-03
2.43E-04
1.36E-11
0.00E+00 ];

%Proton Displacement
from Solar
Proton/thickshell/3k

sp3k=[0.00E+00
0.00E+00
4.29E-12
1.81E-10
3.21E-09
2.89E-08
1.76E-07 ];

%Proton Displacement
from galactic/thick
shell/3k
g3k=[1.54E-06
2.33E-06
3.26E-06
4.22E-06
5.18E-06
6.08E-06
6.91E-06];

%Proton Displacement
from Solar
Energetic(CREME)/thick
shell/3k
se3k=[0.00E+00
9.48E-19
1.10E-14
5.23E-12
4.18E-10
8.38E-09
9.24E-08 ];

%Comparisons
gthin=g1k/g1;
gthick=g3k/g3;
sethin=se1k/se1;
sethick=se3k/se3;
spthin=sp1k/sp1;
spthick=sp3k/sp3;
tpthin=tp1k/tp1;
tpthick=tp3k/tp3;
tot1k=g1k+se1k+tp1k+sp
1k;
tot1=g1+se1+tp1+sp1;
totthin=tot1k/tot1;
tot3k=g3k+se3k+tp3k;
tot3=g3+se3+tp3+sp3;
totthick=tot3k/tot3;
tot1ka=g1k+se1k+tp1k;
tot1a=g1+se1+tp1;
totthina=tot1k/tot1;
tot3ka=g3k+se3k+tp3k;
tot3a=g3+se3+tp3;
totthicka=tot3k/tot3;
```

INITIAL DISTRIBUTION LIST

1. Defense Technical Information Center 2
   8725 John J. Kingman Rd., Ste 0944
   Fort Belvoir, VA 22060-6218

2. Dudley Knox Library, Code 013 2
   Naval Postgraduate School
   411 Dyer Rd.
   Monterey, CA 93943-5101

3. Prof. Vicente Garcia, Code EC/Ha 1
   Department of Electrical and Computer Engineering
   Naval Postgraduate School
   Monterey, CA 93943-5101

4. Prof. Brij Agrawal, Code AA/Ag 1
   Department of Aeronautical and Astronautical Engineering
   Naval Postgraduate School
   Monterey, CA 93943-5101

5. Chariman, Code AA 1
   Department of Aeronautical and Astronautical Engineering
   Naval Postgraduate School
   Monterey, CA 93943-5101

6. LT Jennifer Bolin 5
   1713 Sturbridge Dr.
   Sewickley, PA 15143

7. Dr. D. Joe Anderson 1
   University of Santa Cruz, Sinsheimer Laboratory
   Santa Cruz, CA 95064

DUDLEY KNOX LIBRARY
NAVAL POSTGRADUATE SCHOOL
MONTEREY CA 93943-5101

DUDLEY KNOX LIBRARY
3 2768 00342056 3